THE UNIVERSITY OF CHICAGO

LOW LATITUDE ANDEAN GLACIERS: CLIMATE DRIVERS OF PAST, PRESENT, AND FUTURE CHANGES

A DISSERTATION SUBMITTED TO
THE FACULTY OF THE DIVISION OF THE PHYSICAL SCIENCES
IN CANDIDACY FOR THE DEGREE OF
DOCTOR OF PHILOSOPHY

DEPARTMENT OF THE GEOPHYSICAL SCIENCES

BY
ANDREW GRADY OROS MALONE

CHICAGO, ILLINOIS
JUNE 2017

TABLE OF CONTENTS

LIST OF FIGURES

LIST OF TABLES

ACKNOWLEDGMENTS

I would like to thank my committee members for their support, insight, and assistance in this dissertation: Douglas MacAyeal (the University of Chicago), Ray Pierrehumbert (formerly the University of Chicago; now Oxford University), Dorian Abbot (the University of Chicago), and Edwin Kite (the University of Chicago). Ray, my former primary advisor, thank you for introducing me to tropical glaciers as a way to think about past and present climate change. Doug, my primary advisor, thank you for the support these last three years, challenging me to think deeper and helping me to move from big and interesting problems to tangible solutions.

I would also like to acknowledge the wonderful faculty, graduate students, and staff in the Department of the Geophysical Sciences. Special thanks to Daniel Koll, a great friend and keen editor of manuscripts and poster drafts, and to Lei Wang, an awesome officemate with profound knowledge about all things dealing with fluid dynamics and climate. Also to Miquela, Bethany, and Lily, for helping me keep my focus and sanity, in part though the marvels of dark chocolate.

Beyond the University of Chicago community, I am deeply grateful for the support of the greater geological and climatological communities. Thomas Lowell (University of Cincinnati), thank you for helping me think deeply about the glacial world and climate change and for actively supporting collaborations between the glacial modeling and geology communities. Also, Meredith Kelly (Dartmouth College) and Yarrow Axford (Northwestern University), thank you for encouragement and insight into how we know what we know about past climates; I look forward to future collaborations! Also to the support from the National Science Foundation in funding a portion of this research through EAR-1003686.

Finally, my utmost gratitude to my wife, Rachel Daley, for being so supportive and loving as I worked for many months on this dissertation. And many thanks to my parents for their unwavering encouragement and support.

ABSTRACT

Tropical Andean glaciers are an essential component of the alpine Earth system providing vital water resources for life in their vicinity. Glaciers are also archives of past climate change and barometers of present climate change, and tropical glaciers can provide a much-needed additional low-latitude terrestrial paleoclimate proxy. Despite their societal and scientific importance, the study of tropical glaciers is nascent. This dissertation provides new perspectives on the climate components most important for tropical glacier change, illustrates that records of past tropical glacier changes can be used as a quantitive paleoclimate proxy, and provides a framework for a more rigorous interpretation of tropical glacier advances and retreats as a climate proxy.

A regional-scale surface energy and mass balance model is developed and implemented to quantify tropical glacier response to different types of climate change. The mass balance evolution from thermal year (July - June) 1980 - 2009 CE is simulated, and the dominant input climate variables are determined. The dominant climate drivers of glacier change at tropical Andean glaciers vary, depending on the regional climate setting and in particular the amount of annual precipitation. For both wet inner tropical glaciers and wet outer tropical glaciers, interannual temperature variability is the dominant climate forcing mechanism for equilibrium line altitude (ELA) or mass balance variability. For dry tropical glaciers, precipitation variability is the dominant variable for mass balance and ELA variability. For tropical glaciers, all-wave radiation (i.e. net shortwave and longwave radiation) is the dominant source of available melt energy, and at wet tropical glaciers, which is the classification type of the majority of Andean glaciers, temperature is able to modulate the all-wave radiation from year-to-year. By dictating the phase of precipitation, temperature determines the surface albedo and absorbed shortwave radiation at the lowest extents of the glacier, and this relationship is so strong that it can define the glacier-wide mass balance. Thus, for wet tropical glaciers, observations of mass balance or length changes primarily reflect temperature change.

A coupled ice flow and surface mass balance model is implemented at the world's largest tropical ice mass, the Quelccaya Ice Cap, Peru, to invert the Little Ice Age and Younger Dryas aged moraines into quantitive paleoclimate proxies. Temperature is shown to be the dominant climate driver for changes in extent for the Huancané Valley outlet glacier. Temperature coolings at the ice cap of between 0.7°C and 1.1°C could advance the glacier to the position of the Little Ice Age moraines. Temperature coolings at the ice cap of between 0.9°C and 2.6°C could advance the glacier to the position of the Younger Dryas moraines. These ice cap coolings are extrapolated along the moist adiabat curve to sea surface temperature (SST) coolings and correspond to tropical SST coolings of between 0.4°C and 0.6°C during the Little Ice Age and between 0.5°C and 1.5°C for the Younger Dryas. These coolings are compared to tropical SST coolings realized in paleoclimate general climate model simulations. They agree well with simulations that include climate forcing mechanisms thought to be important during each respective centennial/millennial-scale climate change event.

An ice flow model and idealized representation of how glacier mass balance responds to interannual climate variability are implemented to determine the long-term impact of interannual climate variability on the long-term glacier mass balance and length. Changes in the magnitude of temperature variability drive changes in the net mass balance and the mean glacier length, due to a mass balance asymmetry between anomalously warm years and anomalously cold years. A warm year ablates more anomalous mass than can be compensated by anomalous accumulation on an similarly cold year, producing a mass balance nonlinearity. The nonlinearity stems from a nonlinear vertical mass balance profile, with steeper mass balance gradients in the ablation zone than the accumulation zone. The size of the nonlinearity reflects the difference in mass balance gradients between the accumulation and ablation zones as well as the size of the temperature variability. For the same magnitude of temperature variability, glaciers with very steep ablation zone mass balance gradients and shallow accumulation zone mass balance gradients, such as tropical glaciers, will experience

larger mass balance nonlinearities as compared to glaciers with a smaller difference between their mass balance gradients, such as mid latitude glaciers. Since the mass balance nonlinearity stemming from interannual temperature variability is greater for tropical glaciers, consideration of length changes due to changes in the statistics of interannual temperature variability should be taken into account for tropical glaciers when interpreting the climate signal embedded in length changes.

The key findings of this dissertation indicate that the vast majority of tropical Andean glaciers are highly sensitive to temperature change and variability. These highly sensitive glaciers are wet tropical glaciers in regions that receive at least 0.75 meters water equivalent per year of precipitation. This strong linkage between temperature and mass balance or length changes indicates that tropical glaciers can provide good paleo-thermometers and that their longterm evolution will primarily reflect temperature changes. A portion of past length changes and future length changes may also reflect changes in the amount of interannual temperature variability, which stems from a universal mass balance nonlinearity that is especially acute for tropical glaciers. In closing, the strong relationship between temperature and glacier variability for the vast majority of the world's tropical glaciers highlights their continued and perhaps accelerated disappearance in an anthropogenic warming world.

CHAPTER 1

INTRODUCTION

Contemporary and projected climate change presents many human risks and hazards (Pachauri et al. (2015)). To fully comprehend and prepare for future climate, a deep understanding of past climate changes is required (Bradley and Eddy (1991); Bradley (1999)). Paleoclimate records provide insight into the magnitude and scope of past climate changes and a benchmark from which to test models used to predict future changes (Schmidt (2010); Braconnot et al. (2012)). The density of coverage (both spatial and temporal) of existing paleoclimate records, however, is heterogenous, and is especially lacking in the tropics. The sparsity of records impedes our understanding of decadal and centennial climate change events and ultimately general climate dynamics (Seager and Battisti (2007)). The IPCC AR5 report highlights the sparsity of tropical paleoclimate records as part of the 'fundamental limitation' for quantifying past climate variability at global and hemispheric scales (Masson-Delmotte et al. (2013)).

The cryosphere, the realm of frozen water, has long offered clues about past climates. Glaciers and ice sheets, key components of the cryosphere, are sculptors of landscapes, archiving their waxings and wanings. The relics of the great Northern Hemisphere ice sheets led to the profound late-19th century realization of drastically different past climates (Imbrie and Imbrie (1986)) and ultimately an understanding of the drivers of multi-millennial climate change (Milankovič (1998); Hays et al. (1976)). At an even longer timescale, diamictites and ice-rafted debris at low latitudes led to the discovery of arguably the Earth's most profound climate change – Snowball Earth (Sumner et al. (1987); Hoffman et al. (1998)). The study of such an extreme climate change has profoundly enhanced our understanding of key components of the climate system, such as the carbon cycle (Pierrehumbert et al. (2011)). At decadal, centennial, and millennial time-scales, glaciers and small ice caps record their waxings and wanings in the geologic record, which can be inverted into a signal of past climate change, i.e. a paleoclimate proxy (e.g. Oerlemans (2005); Anderson and Mackintosh

(2006); Leclercq and Oerlemans (2012); Doughty et al. (2013)).

At first glance, 'tropical' and 'glacier' may seem oxymoronic, but there are nearly 3,000 glaciated basins in the tropics, accounting for ∼2,300 km^2 and spanning four continents (see Figure 1.1). Tropical glaciers have long been viewed as highly sensitive indicators of environmental change (Kaser et al. (1996)), and they can provide a much-need additional terrestrial tropical paleoclimate proxy.

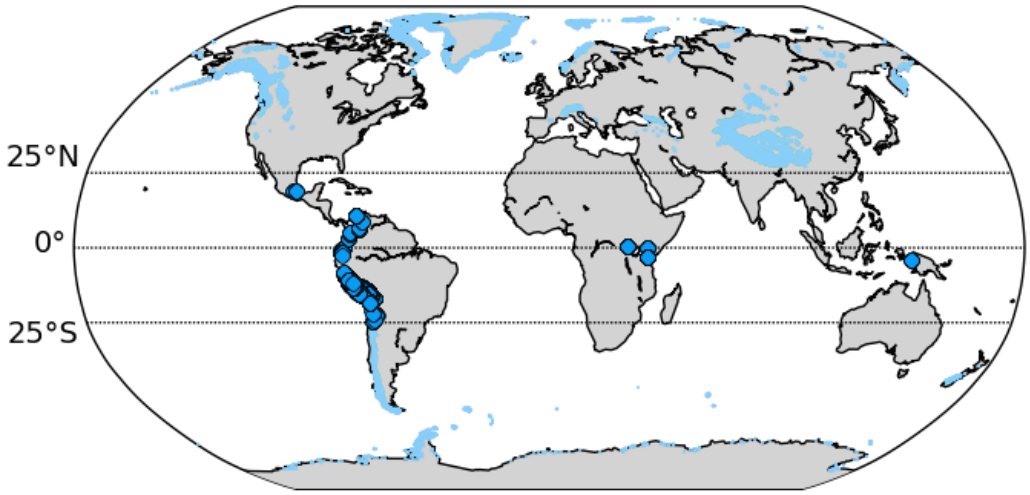

Figure 1.1: Location of world glaciers (not associated with the two ice sheets). Tropical glaciers are the larger and darker blue circles; all other glaciers are the small light blue dots. Data: Randolph Glacier Inventory (Pfeffer et al. (2014)).

In addition to being simply a scientific tool, tropical glaciers also provide a vital societal and spiritual dimension for communities in their sight. Mountains are often referred to as the *water towers of the world* (Liniger et al. (1998)), providing essential fresh water resources to regions with high precipitation seasonality or regional water scarcity (Viviroli et al. (2007)). In the tropics there is minimal seasonal snowpack due to low thermal seasonality, and glaciers provide much of the water tower function. The vast majority of tropical glaciers are found in the South American Andes (see Figure 1.1), and many communities in the region depend heavily on meltwater from glaciers. In the Rio Santa, in central Peru, ∼40% of the dry season water resources originate from glacier melt (Mark et al. (2005)). In La Paz city, Bolivia, ∼15% of annual water resources originate from glacier melt, and in the

dry season, glacier melt accounts for nearly 30% of the water resources (Soruco et al. (2015)). The observed extensive retreat and thinning of tropical Andean glaciers is alarming for the longterm security of regional water resources (Bradley et al. (2006); Casassa et al. (2007); Kaser et al. (2010)). In the short term, increased melt on tropical glaciers produces larger water resources for communities, but in the longer term as the glaciers recede a threshold is passed (i.e. *peak water*) and the net meltwater discharge decreases while variability increases (Bury et al. (2013)). For the Rio Santa in central Peru this threshold appears to have been passed (Bury et al. (2013)), posing challenges for local communities and regional agriculture and hydroelectric electricity production.

Glaciers also provide a vital spiritual dimension for indigenous tropical Andean communities. Many Pre-Columbian Andean religious beliefs attribute their deities' powers to the presence of snow and ice fields. In response to the the alarming retreat of tropical glaciers, some communities have altered spiritual practices to reduce associated impacts on the glaciers (Bolin et al. (2009)). The ability to understand the mechanisms and forecast the rate of tropical glacier change provides vital perspective for the societal and spiritual significance of tropical glaciers.

Despite the scientific and societal importance of tropical glaciers, their study is still in its adolescence. Field expeditions and glacier monitoring only began in the 1960s and 1970s, and have been at best sporadic (Mercer et al. (1975); Mercer and Palacios (1977); Hastenrath (1978); Hastenrath (1984)). The longest mass balance record for any tropical glacier, Lewis Glacier in Kenya, spans from 1978 to 2014 but only contains data on 22 years (data retrieved from the World Glacier Monitoring Service). In the tropical Andes, the longest record only has data for 22 years, beginning in the early 1990s (data retrieved from the World Glacier Monitoring Service). For comparison, Storglaciären in Sweden is the longest continuous mass balance record, starting in 1945 (Huang et al. (2015)), and many mid and high latitude countries maintain long-term mass balance measurement programs (e.g. Norway (Andreassen et al. (2005)) and the United State *Benchmark Glacier Network*

program (Fountain et al. (1997))). Compounding the problems stemming from a lack of field studies is the general recognition that many of the paradigms developed for mid high latitude glaciers regarding how glaciers interact with the climate system are inapplicable at lower latitudes (see Chapter 1.1). Adding to the sense of urgency, tropical glaciers are retreating and thinning at an alarming rate (Vuille et al. (2008a); Rabatel et al. (2013)) and may be experiencing the highest rate of mass loss globally (Gardner et al. (2013)). As such, additional studies focused on how tropical glaciers interact with the climate system and respond to climate change are vital.

1.1 Glacier-Climate Interactions

Glaciers wax and wane as mass is lost, gained, and transported along the glacier. These processes are governed by fundamental physical laws, providing a universality of these processes from place-to-place (Kaser et al. (2005)). The processes of mass loss and gain along the glacier, i.e the mass balance, are linked with local meteorology and are augmented by local topography, which drive glacier fluctuations (Oerlemans and Fortuin (1992); Oerlemans (2001)). Fluctuations in glacier extent scour the landscape, archiving their past extents, and the contemporary retreat of nearly all the world's glaciers is iconic of anthropogenic climate change (Balco (2009); Vaughan et al. (2013)). The working paradigm has been that records of past or observations of present glacier fluctuations reflect long-term changes in the mass balance, resulting from changes in local meteorology, i.e. climate change (Oerlemans (2001)); Vaughan et al. (2013)). Recent work, however, challenges this paradigm by illustrating that glacier fluctuations can also occur from short-term mass balance changes driven by variability in the meteorology, which we associate with weather (Oerlemans (2000), Roe and O'Neal (2009); Huybers and Roe (2009); Roe (2011); Anderson et al. (2014); Roe and Baker (2014)). Ultimately, however, climate change and variability drive glacier change through the mechanisms by which mass is lost and gained on glaciers. By understanding these mass loss and gain mechanisms, glaciers can function as powerful archives of past climate change

and barometers of current change.

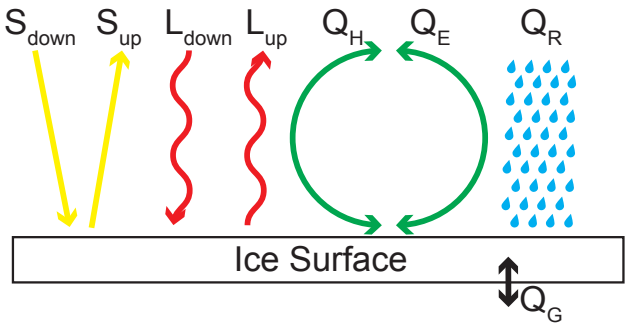

Figure 1.2: Primary energy fluxes into and out of the surface of a glacier. S is the shortwave radiation and is directed into the glacier surface (down) or directed from the surface into the atmosphere (up). L is the longwave radiation and is directed both up and down. Q_H is the sensible heat flux and Q_E is the latent heat flux; each can be directed either into or out of the surface, depending on the thermodynamic conditions of the glacier surface and overlying atmosphere. Q_R is the flux of heat into the ice from liquid water falling on the surface. Q_G is the flux of heat between the glacier surface and the interior ice; its direction depends on the thermodynamic conditions of the surface and the interior ice.

Mass is gained on a glacier primarily through solid precipitation (i.e. snow) and through secondary processes such as deposition of ice directly on the glacier from the atmosphere or transport by wind or avalanches (Cogley et al. (2011)). The amount of precipitation and its phase (i.e. snow versus rain) are directly related to the local meteorology. The two dominant mass loss processes for mountain glaciers are melt and sublimation (Cogley et al. (2011)). Mass loss on mountain glaciers relates to local meteorology through the energy fluxes at the glacier surface (Figure 1.2). Melting on the glacier surface occurs as a closure of the surface energy balance. If there is a net energy flux into the surface, then the surface will warm to return the surface to equilibrium. The glacier surface, however, cannot exceed the melting point (0° for typical conditions), and once this point is reached, any surplus energy at the surface must be consumed by a phase transition of ice (or snow) into water (i.e melting). This qualitative relationship can be quantified as the rate of surface lowering in meters water

equivalent per second (m w.e. s^{-1}) by the following:

$$Melt = \begin{cases} \frac{Q_M}{L_f \ \rho_{water}}, & \text{if } T_s = 0 \text{ °C } \& \ Q_M > 0 \\ 0, & \text{else} \end{cases} \tag{1.1}$$

where Q_M is the energy available for melting, T_s is the temperature of the ice surface, L_f is the latent heat of fusion, and ρ_{water} is the density of water. The second mass loss process, sublimation, occurs when the latent heat flux is directed from the ice surface to the atmosphere and can be quantified as a rate of surface lowering in m w.e. s^{-1} as follows:

$$Sublimation = \frac{Q_E}{L_s \ \rho_{water}} \tag{1.2}$$

where Q_E is the latent heat flux and L_s is the latent heat of sublimation. The forms of the two mass loss equations (eq. 1.1 & eq. 1.2) are similar, but the values of the latent heat terms differ vastly, with the latent heat of sublimation being ~8.5x greater than that of melting. As such, watt-for-watt, melting is ~8.5x more effective at removing mass from the glacier surface.

The energy available for melting (Q_M) (illustrated in Figure 1.2) is:

$$Q_M = S + L + Q_H + Q_E + Q_R \tag{1.3}$$

where S is the net shortwave radiation flux, L is the net longwave radiation flux, Q_H is the sensible heat flux, and Q_R is the heat provided by rain falling on the glacier surface. The amount of available melt energy and the magnitude (and direction) of the sensible heat flux ultimately depend on meteorological variables. How changes in the meteorological variables effect the amount of mass loss and gain (i.e. the mass balance) and how the associated mass balance changes result in changes in glacier extent are defined as the *glacier-climate interactions*. The pathway from a change in a climate variable to an associated glacier change

(or the inverse: glacier change $\rightarrow$ to climate change) is far from direct. Elucidating these interactions in a quantitive way has been a large focus of the glaciological community for decades.

In the mid and high latitudes, substantial progress has been made on this front. Through extensive field measurements of the mass loss and gain on a glacier and the local meteorology, correlations between mass balance and climate variables have been made. Mid and high latitude glaciers can be viewed as having two distinct mass balance seasons: 1) an accumulation season (winter) and 2) and ablation season (summer), and to successfully model their mass balance, climate data about the winter-time precipitation rates (i.e. accumulation season) and summer-time temperatures (i.e. ablation season) are needed (Cuffey and Paterson (2010)). Temperature acts as a proxy for summertime mass loss through empirical melt models such as a positive degree day (PDD) model (Braithwaite and Olesen (1989)). The physical bases for why increased temperature causes greater melt has been attributed to a combination of a greater longwave radiation flux (Ohmura (2001)) and greater sensible heat flux (Braithwaite (1981)) from the atmosphere into the glacier surface. Using these mass balance models and paradigms, it has been shown that changes in mid and high latitude glaciers lengths primarily reflect temperature changes (Oerlemans (2005); Anderson and Mackintosh (2006); Leclercq and Oerlemans (2012)), making these glaciers useful paleothermometers and providing a basis for forecasting their evolution in a warming world.

For tropical glaciers, the story is more complicated due to three primary reasons. First, field campaigns on tropical glaciers to measure the mass balance and local meteorology are limited both spatially and temporarily. Second, the paradigms developed for mid and high latitude glaciers about two distinct mass balance seasons do not apply in the tropics, with ablation on tropical glaciers occurring year round and maximum accumulation often happening concurrent with maximum ablation (Figure 1.3). Third, where data from available field studies are available, day-to-day variations in melt tend to correlate poorly with temperature (Sicart et al. (2008)). The dominant source for melt energy at tropical glaciers is

usually associated with absorbed shortwave radiation (Wagnon et al. (1999); Francou et al. (2003); Mölg and Hardy (2004); Francou et al. (2004); Sicart et al. (2008)), with supporting roles played by humidity (Kaser and Osmaston (2002); Vuille et al. (2008b)) or cloud cover (Francou et al. (2003); Francou et al. (2004); Sicart et al. (2005); Sicart et al. (2010)). Without a strong linkage between short term melt and temperature, empirical melt models, such as a PDD model, have been largely rejected for tropical glaciers (Francou et al. (2005); Sicart et al. (2008)). Interestingly at longer timescales, correlations between mass balance variability and temperature emerge. At Zongo Glacier in Bolivia, significant correlations between annual variability in the glacier-wide melt and temperature have been observed (Sicart et al. (2008)). Furthermore, the nearly synchronous retreat of tropical glaciers from their late-Holocene maximum extents (and their continued contemporary retreat) can be best explained by gradual warming over the last century (Rabatel et al. (2008); Rabatel et al. (2013) López-Moreno et al. (2014)). This contrast in the important climatological drivers of tropical glacier change between short and long timescales highlights the importance of continued study of glacier-climate interactions in the tropics. Also, without empirical relationships and physical bases linking tropical glacier change to one or a few climate variables, their application as a paleoclimate proxy and forecasts of their evolution in a warming world remain elusive.

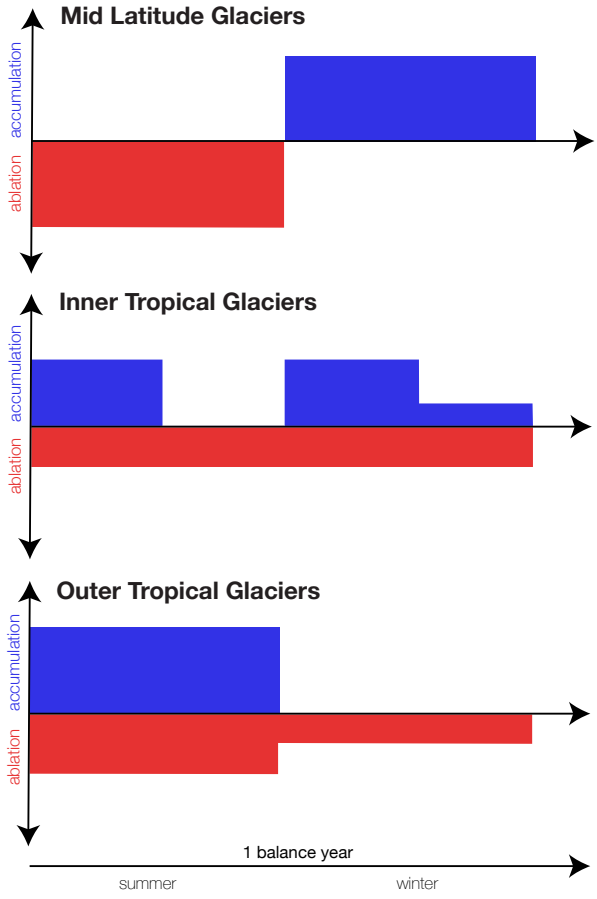

Figure 1.3: Amount and timing of accumulation (blue) and ablation (red) over the course of a year for glaciers in different climate regimes. Adapted: Kaser et al. (1996).

1.2 Setting of Low Latitude Glaciers

A study of tropical glaciers is not complete without extensive consideration of the South American Andes. Although tropical glaciers are found on four continents, the vast majority are in South America (see Figure 1.1). From the most recent Randolph Glacier Inventory (version 5.0, released July 20, 2015) (Pfeffer et al. (2014)), >99.6% are found in the Andes by area (>98% by basin count). Determining which Andean glaciers are deemed tropical could vary slightly, depending on specific criteria chosen for whether a glacier is tropical or not. Some criteria focus on the relative amplitudes of the diurnal and seasonal temperature cycles while others focus on the regions swept out by the seasonal progression of the intertropical

convergence zone (ITCZ) (Kaser et al. (1996); Kaser (1999); Kaser (2001)). In this dissertation, however, a simple criterion is employed: a glacier is deemed tropical if it falls between roughly the Tropics of Cancer and Capricorn, which is the distinction used in the Randolph Glacier Inventory. In the Randolph Glacier Inventory, tropical Andean glaciers range from ∼10.8°N to ∼24.7°S.

The Randolph Glacier Inventory (Pfeffer et al. (2014)) provides vital geographic data about tropical glaciers including their latitude, longitude, and hypsometric profiles. From the hypsometric profiles, the mean elevation and range of each glacier can be quantified. In Figure 1.4, the geographic location of each distinct glacier is indicated as well as the elevational distribution of all tropical Andean glaciers. The total areal coverage of tropical Andean glaciers is 2,338 km^2, with a mean elevation ($Z_{50\%}$) of 5,172 meters above sea level (m a.s.l.) (data source: Randolph Glacier Inventory (Pfeffer et al. (2014))). A useful metric for the fate of a glacier in a changing climate is the elevation span of the glacier. This span is quantified by calculating the range over which the middle 50% of the glacier (by area) is found (Z_{range}) (Figure 1.4b). For tropical Andean glaciers, the middle 50% of area is found between 4,992 and 5,368 m a.s.l., spanning a range of <400 m (data source: Randolph Glacier Inventory (Pfeffer et al. (2014))). Glaciers that span a larger elevation range will fare better in a warming world than glaciers that only span a narrow elevation range, all other things being equal. As noted by previous authors (e.g. Kaser (1995)), tropical glaciers are not evenly distributed above and below their mean elevation as is more often the case for mid latitude alpine glaciers, such as those in the Alps. Comparing the observed elevation distribution to that of a normal distribution highlights the truncation of tropical glaciers at lower elevations and the long tail to higher elevations (Figure 1.4).

The elevational distribution of tropical glaciers is not uniform but instead displays an overall regional structure. The glaciers with the lowest mean elevation are those at the lowest latitudes, with an increasing mean elevation moving poleward. There is also an east-west elevation gradient, with the highest mean elevations in the western Andes, such as in

western Peru and Bolivia and northern Chile. The distribution of elevation ranges is less geographically structured, reflecting the specific geography of the mountains in the Andes. The structure in the mean evolution likely reflects the different climate settings of tropical glaciers.

The mean elevation distribution of tropical Andean glaciers can be partially explained by variations in precipitation (Figure 1.5). Tropical Andean precipitation primarily occurs due to deep convection storms, and the moisture is advected from the east by the mid-level easterlies (i.e. trade winds), creating a strong east-west precipitation gradient (Garreaud (2009)). In much the same way, there is a strong east-west gradient in the mean glacier elevation, with lower elevation glaciers along the eastern edge of the Andes and considerably higher elevation glaciers in the western Andes (Figure 1.4). The lowest mean elevation glaciers are found at the lowest latitudes, which correspond with some of the wettest regions in the tropical Andes. The east-west precipitation gradient is maximum in southern Peru, Bolivia, and northern Chile (Garreaud (2009)), and some of the highest mean elevation tropical glaciers are found on the western edge of the Andes in this region. Some of the extreme dryness along the west coast from southern Peru to northern Chile also results from upwelling of cold water along the coast, which enhances subsidence, further drying the region (Garreaud (2009)). The net annual precipitation amount provides a first-order predictor for the elevation at which tropical Andean glaciers are found.

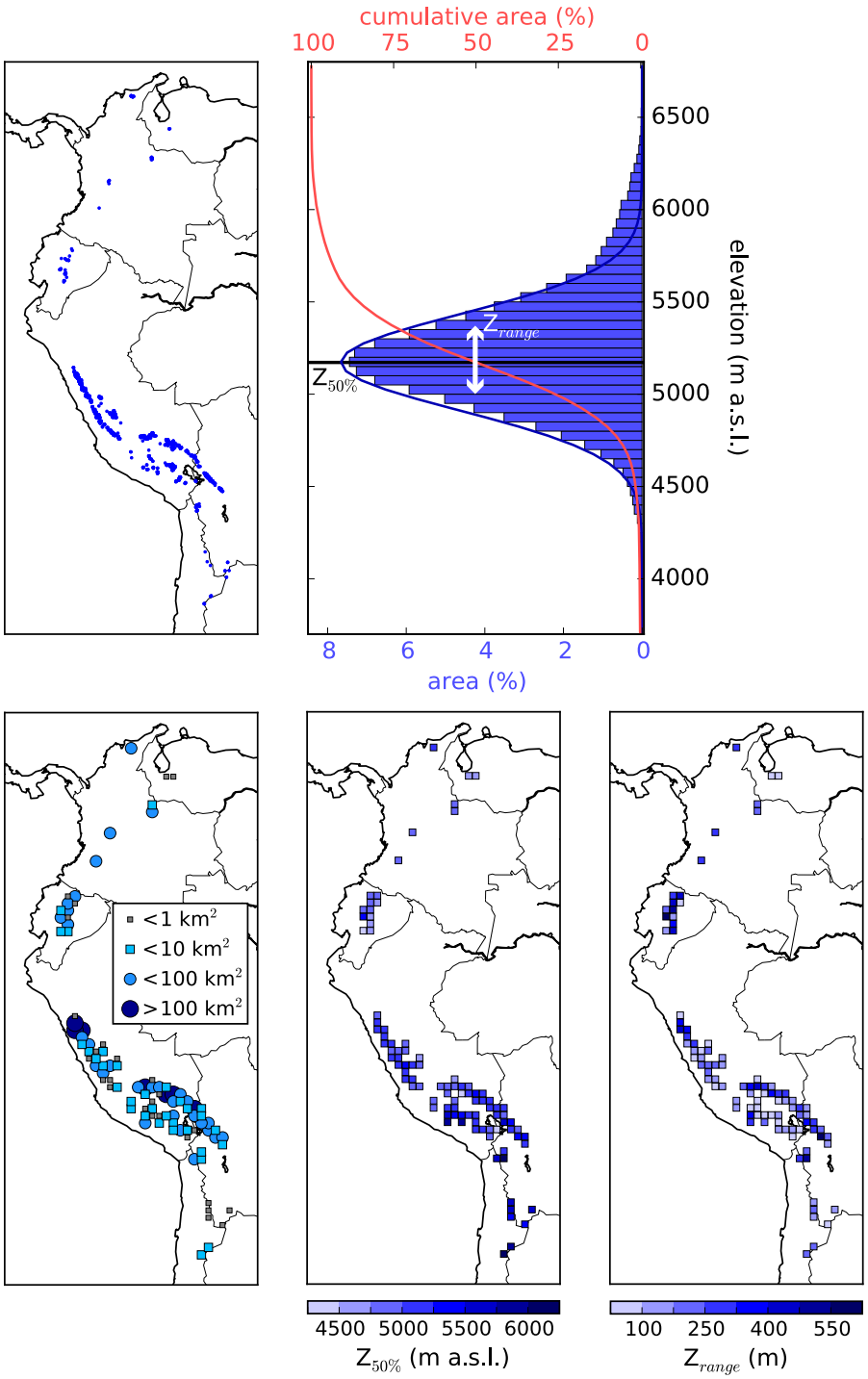

Figure 1.4: Geographic data on tropical Andean glaciers, including: latitude, longitude, and elevation (top row). Area and elevational information about tropical Andean glaciers after mapping them onto a 0.75° × 0.75° grid (bottom row). Z_{mean} is the elevation at which 50% of the glacier area lies above and 50% lies below. Z_{range} is the elevation range over which the middle 50% of the glacier resides, i.e. the elevation difference between $Z_{25\%}$ and $Z_{75\%}$. Data: Randolph Glacier Inventory (Pfeffer et al. (2014)).

Variations in tropical Andean temperatures, in contrast, are a poor indicator for the mean elevation of tropical Andean glaciers (Figure 1.5). Free atmosphere temperature reanalysis output is used as a surrogate for temperature data at the high elevations in the Andes because data from stations are scarce and existing records span only a few years (Vuille et al. (2003); Bradley et al. (2009)). In the tropics, however, free atmosphere temperatures differ only slightly from high elevation surface temperatures (Seidel and Free (2003)), making free atmosphere temperatures a viable surrogate for temperatures on tropical Andean glaciers. Looking at the 500 hPa free atmosphere temperatures, spatial variability is minimal, with annual average free atmosphere temperatures varying by less than 0.25°C at the latitude-longitude locations of glaciers in Peru, Ecuador, Columbia, and Venezuela (see Figure 1.5). South of Peru, there is a north-south temperature gradient, with higher latitudes having a cold annual mean temperature, but within a latitudinal band there is still minimal temperature variability. The homogeneity of the tropical free atmosphere is consistent with the Weak Temperature Gradient Approximation (Pierrehumbert (1995)) but highly inconsistent with the spatial pattern of mean elevations of tropical glaciers (Figure 1.4). Looking only at temperature, one might predict that the lowest elevation glaciers would correspond to the coldest 500 hPa temperatures, which are found in northern Chile. The glaciers in northern Chile, however, have the highest mean elevations. The glaciers with the lowest mean elevations are the ones with with the warmest 500 hPa temperatures. The geographic setting of tropical Andean glaciers seems to reflect the mean climate setting of the glacier and in particular the net annual precipitation. In addition to defining the geographic setting, the climate setting also determines the specifics of how glaciers respond to climate change (Kaser (2001); Favier et al. (2004b); Fujita (2008b); Fujita (2008a); Rupper and Roe (2008); Sagredo et al. (2014)). As such, an understanding of a tropical Andean glacier's climate setting is vital for interpreting and generalizing results more broadly.

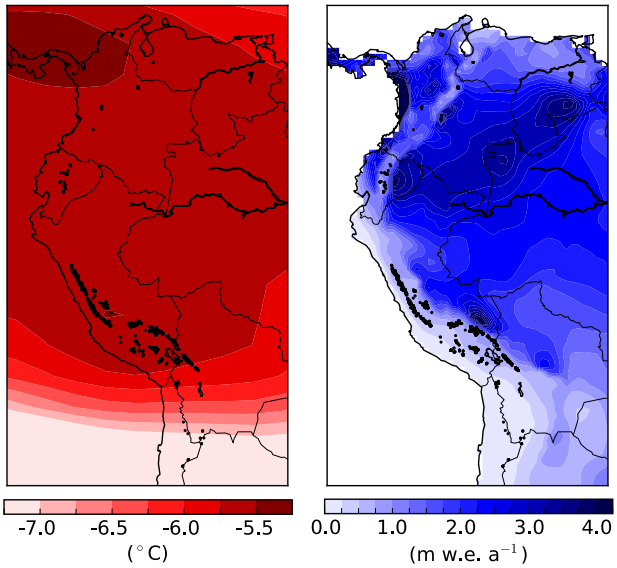

Figure 1.5: Climate setting for Andean tropical 1980 - 2009 CE. Annual average 500 hPa temperature (left column), and net annual surface precipitation (right column). The locations of Andean glaciers are indicated by black dots. Data: temperature: NCEP-DOE Reanalysis II (Kanamitsu et al. (2002)); precipitation: CRU-Ts v3.23 (Harris et al. (2014)); glacier geography: Randolph Glacier Inventory (Pfeffer et al. (2014)).

1.3 Dissertation Objectives

The objective of this dissertation is to develop a framework to quantitatively interpret the climatological signal embedded in geologic records and present observations of tropical glacier change. The dissertation presents a three pronged approach: 1) enriching the understanding of glacier-climate interactions at low latitudes, 2) illustrating the value of tropical paleoclimate reconstructions from geologic records of glacier change, and 3) deciphering the climate signal associated with tropical glacier length changes.

In Chapter 2, a regional-scale surface energy and mass balance model is developed and implemented to study glacier-climate interactions for three climatologically distinct tropical glaciers. The model is a continuation of past studies using regional-scale surface energy and mass balance models but features significant changes to the design and implementation. It is solved on a vertical grid, allowing for mass loss and gain processes to be simulated at

all elevations on the glacier. Also, it adds additional physical processes, such as a dynamic albedo model and a parameterization for the longwave atmospheric opacity that includes cloud cover. Finally, the model utilizes recent data from the Randolph Glacier Inventory, which allow for the simulation of not only the equilibrium line altitude response to climate change and variability but also the glacier-wide mass balance. The results provide a geographically varied and temporally rich picture of how glaciers respond to climate change that allows for comparisons of glacier-climate interactions at different tropical glacier climate settings as well as at different elevations for a given geographic location.

In Chapter 3, a coupled mass balance and flow model is implemented to constrain Little Ice Age (1330 - 1850 CE) and Younger Dryas (12.8 - 11.5 thousand years ago) climate changes at the world's largest tropical ice mass, the Quelccaya Ice Cap, Peru. Previous methods that have been applied at higher latitude glaciers (e.g. Anderson and Mackintosh (2006)) are modified to produce one of the first quantitative Tropical Andean paleoclimate reconstructions from records of glacier change. These reconstructions are compared to output from global climate model simulations to evaluate mechanisms for regional and global climate change during these time periods.

In Chapter 4, a coupled mass balance and flow model is implemented for idealized glaciers to quantify the impact of interannual climate variability on the mean state of a glacier. Results from Chapter 2 and Chapter 3 hint that interannual climate variability not only causes mass balance and glacier length fluctuations around the equilibrium location but also, in part, defines the mean state of the glacier. Since the interannual climate variability causes not just fluctuations but also a change in the mean state, it should be viewed as introducing a nonlinearity into the system. The idealized modeling approach allows for both the mechanisms for this nonlinearity and its impact on interpreting changes in glacier length to be presented.

These research topics were born out of a general desire to understand the physical processes responsible for global and regional climate change and variability since the Last Glacial

Maximum. At first, tropical glaciers were viewed solely as a tool through which to constrain past low latitude climate changes. Through this dissertation, however, tropical glaciers as a research focus came into their own right. This dissertation occurred concurrent with exciting developments in the discipline, with significant progress having been made in the last 40 years of study but many questions still outstanding. By applying an idealized modeling perspective and integrating a wealth of new data, this dissertation seeks to rephrase existing problems into more tractable questions and supply new insights.

Chapter 3 has been published in the *Quaternary Science Reviews* (Malone et al. (2015)). The model and the key results and discussions of Chapter 2 have been presented at the 2015 Geological Society of America Annual Meeting and the 2015 American Geophysical Sciences Fall Meeting. The model and key results and discussions of Chapter 4 have been presented at the 2016 American Geophysical Union Annual Meeting. Manuscripts are in preparation for Chapter 2 and Chapter 4.

CHAPTER 2

CLIMATE DRIVERS OF TROPICAL ANDEAN GLACIER CHANGE

The objective of this chapter is to identify the key components of the climate system responsible for tropical glacier change by developing and implementing a regional-scale numerical model of how glaciers relate to climate. Understanding the key components of the climate system responsible for tropical glacier change allows for these glaciers to be better used as a proxy for past climate changes and their future evolution to be more accurately forecasted. This understanding has been well established for the mid and high latitude glaciers, with mass balance changes primarily reflecting changes in wintertime snowfall and summertime temperatures (Cuffey and Paterson (2010)) and length changes primarily reflecting summertime temperature changes (Anderson and Mackintosh (2006)). Through integration of countless field measurement and modeling studies for mid and high latitude glaciers, the community now has models that can perform basic predictions of glacier extent (Oerlemans (2005); Leclercq and Oerlemans (2012)). Such an understanding and similar models for tropical glaciers, however, do not yet exist, in part due to the three obstacles outlined in Chapter 1.1: 1) limited field measurements (both temporarily and spatially), 2) inapplicability of mass balance paradigms developed for mid and high latitude glaciers to tropical glaciers, and 3) the lack of a physical mechanism linking daily temperature to mass loss rates in the limited field studies that do exist.

Field campaigns in the tropical Andes through the Great Ice Program (a coordinated effort between Andean and European scientists) began in the 1990s with continuous year-to-year mass balance measurements at two Bolivian glaciers and has expanded through the mid 1990s to mid 2000s to also monitor glaciers in Ecuador, Peru, and Columbia (Rabatel et al. (2013)). As part of this program, some of the monitored glaciers have also had meteorological station measurement studies conducted to link mass balance variability at the site of the

meteorological station to energy fluxes and ultimately the climate system (Rabatel et al. (2013)). Results from these point-scale studies indicate that variability in the available melt energy primarily reflects variability in the net shortwave radiation (Wagnon et al. (1999); Francou et al. (2003); Favier et al. (2004a); Favier et al. (2004b); Francou et al. (2004); Sicart et al. (2008)). Net longwave radiation (Francou et al. (2003);Francou et al. (2004); Sicart et al. (2005); Sicart et al. (2010)) and the latent heat flux (Kaser and Osmaston (2002); Vuille et al. (2008b)) have also been suggested as playing a secondary role. The primary climatological variable attributed to variations in tropical glacier melt is precipitation and in particular its amount, frequency, and phase (i.e. rain versus snow) (Wagnon et al. (1999); Favier et al. (2004a); Favier et al. (2004b); Sicart et al. (2005)). Cloud cover (Sicart et al. (2005); Sicart et al. (2010)), windspeed (Kaser and Osmaston (2002)), and relative humidity (Kaser and Osmaston (2002); Vuille et al. (2008b)) have also been suggested as playing a lesser secondary role. Results from similar point-scale studies on Mount Kilimanjaro, in East Africa, suggest that variability in the absorbed shortwave radiation flux is the primary driver of melt variability and that the precipitation drives mass balance variability, going as far as to illustrate that a 20% change in precipitation produces a 2-4x larger change in the mass balance as a 1°C temperature change (Mölg and Hardy (2004); Mölg et al. (2008)). These results could suggest that temperature does not play a dominant role in driving tropical glacier change. Tropical glacier change at timescales ranging from millennial (Jomelli et al. (2011)) to decadal (Favier et al. (2004a); Rabatel et al. (2008); Rabatel et al. (2013); López-Moreno et al. (2014)), however, are often associated with regional warming, suggesting that temperature plays a significant role in dictating tropical glacier change.

A physical link between daily melting and air temperature has not been found at the longest monitored glacier in the tropical Andes, Zongo Glacier, Bolivia (Sicart et al. (2008)), but at interannual and longer timescales, temperature has been suggested to dictate mass balance variability through co-variation with other climate variables (Francou et al. (2003)) or its role in determining the phase of precipitation (Favier et al. (2004b); Rabatel et al.

(2013)). Two recent studies using spatially distributed surface energy and mass balance models, which simulate the energy flow and mass balance balance at multiple points on the glacier, suggest that generalizing the results from a point-scale study to glacier-wide mass balance could result in incorrect conclusions (Sicart et al. (2011); Gurgiser et al. (2013)). Gurgiser et al. (2013) argue that the glacier-wide mass balance during the 2-year study period of the study is determined by the processes occurring at the lowest elevations of the glacier, which are highly dependent on temperature. The Sicart et al. (2011) and Gurgiser et al. (2013) studies, however, are limited to only a few years of analyses, due to limited meteorological data for the glaciers, and these studies highlight the need for additional and longer-duration studies of glacier-climate interactions at multiple points on tropical glaciers.

Glacier-climate interactions in the tropics may also reflect the specifics of a glacier's climatological setting. Previous research suggests that glaciers in different climate settings could respond differently to similar climate changes (Kaser (2001); Favier et al. (2004b); Fujita (2008b); Fujita (2008a); Rupper and Roe (2008); Sagredo et al. (2014)). Tropical glaciers have been broadly divided into two climate settings: 1) *Inner Tropical Glaciers* and 2) *Outer Tropical Glaciers*, which primarily reflect a latitudinal difference in the seasonality of precipitation (Kaser et al. (1996); Kaser (1999); Kaser (2001)). Previous research on tropical glaciers has focused on determining similarities and differences in glacier-climate interactions between these two classes of tropical glaciers (e.g. Wagnon et al. (1999); Francou et al. (2003); Favier et al. (2004a); Favier et al. (2004b); Francou et al. (2004); Sicart et al. (2005)). Superimposed over this broad division, however, is a sharp east-west precipitation gradient, with the eastern tropical Andes being significantly wetter than the western tropical Andes (see Figure 1.5). The amount of precipitation has long been known to affect the specifics of glacier-climate interactions (e.g. Meier (1984); Oerlemans and Fortuin (1992)). As such, to gain an understanding of the breadth of glacier-climate interactions, tropical Andean glaciers are defined as falling into three climate regions: 1) wet inner tropics; 2) wet outer tropics; and 3) dry outer tropics.

The objective of this chapter is to elucidate glacier-climate interactions in the tropics, accounting for both differences stemming from climate setting and elevation. A regional-scale surface energy and mass balance model is developed and implemented at the geographic location of three tropical glaciers that represent the three distinct climate settings identified above. Regional-scale surface energy and mass balance models have been implemented successfully in elucidating the sensitivity of a glacier's equilibrium line altitude (ELA) to different types of climate change in data-scare regions such as the Himalayas (Rupper and Roe (2008); Rupper et al. (2009)) and the Andes (Sagredo et al. (2014)). The ELA is the elevation at which net annual ablation balances net annual accumulation, and its sensitivity to different types of climate change is one metric for glacier-climate interactions.

In this chapter, the framework for past regional-scale surface energy and mass balance modeling studies is modified to allow for calculations of the mass loss and gain at the daily time-scale and at all elevations of the glacier. Modifications include a longwave radiation scheme that incorporates the impact of cloud cover on the opacity of the atmosphere, which is a process important for modulating the available melt energy for both inner (Francou et al. (2004); Sicart et al. (2010)) and outer (Francou et al. (2003); Sicart et al. (2005); Sicart et al. (2010)) tropical glaciers. Additionally, a dynamic albedo model is included, which is a component that has been identified as imperative for future regional-scale modeling in the tropics (Fernández and Mark (2016)). Variation in the glacier surface albedo with respect to elevation has been identified as a dominant feature for tropical glacier-climate interactions (Kaser (1995); Kaser (2001)), and day-to-day variation in surface albedo has been identified as the primary cause of short-term variability in the absorbed shortwave radiation (e.g.Wagnon et al. (1999); Favier et al. (2004b); Mölg and Hardy (2004); Sicart et al. (2008)). The model output is also used in concert with the hypsometric profiles for the representative glaciers at the three geographic locations in order to calculate the net mass balance (NMB). The NMB is the integral of the net annual mass loss and gain over the entire glacier area, which is then divided by the glacier area. Its sensitivity to climate

change is another metric for glacier-climate interactions. NMB changes are what ultimately drive glacier length advances, retreats, and fluctuations, with negative NMB values driving glacier upslope retreats, and vice versa.

This chapter presents the climate variables responsible for year-to-year variations in the NMB and ELA and the day-to-day variations in the accumulation, ablation, and melt at different elevations. The model is implemented at three different geographic locations that contain tropical Andean glaciers, and these three locations span the range of climate settings for tropical Andean glaciers. The chapter also attempts to resolve the apparent discrepancy for tropical glaciers between the climate variables responsible for short-term (daily to monthly) mass balance variability and those responsible for longer-term (annual to interannual) change (Sicart et al. (2008)).

2.1 Three Representative Tropical Glaciers

The model is implemented at the geographic location of three well-known tropical Andean glacier complexes that represent the distinct climate settings in the tropical Andes. The NMB is calculated using the hypsometric profile for the glacier at each of the three locations. The three regions have been shown to have distinct climatologies (Sagredo and Lowell (2012)), and the study in this chapter will explore how these differences affect the ways in which the glacier interacts with climate. The three glaciers are: 1) Volcán Antisana, Ecuador (78.15°W, 0.49°S) (wet inner tropics); 2) the Quelccaya Ice Cap, Peru (70.83°W, 13.93°S) (wet outer tropics); and 3) Nevado Sajama, Bolivia (68.88°W, 18.11°S) (dry outer tropics) (Figure 2.1). Each representative location has had at least limited meteorological measurements, e.g. air temperature, wind speed, and longwave and shortwave radiation, over the past two decades.

The northern-most and lowest mean elevation glacier, Volcán Antisana, is located in the eastern cordillera of the Andes in Ecuador. Multiple glaciers descend from its peak, and on its northwest slope, glaciers 15α and 15β are some of longest-monitored tropical glaciers. Multiple papers have been published on the surface energy balance from meteorological

stations location on and around two glaciers on the northwest slope (e.g. Favier et al. (2004a); Favier et al. (2004b)). Melting at this site is primarily associated with the all-wave (i.e. sum of the net shortwave and net longwave) radiation, whose variability primarily reflects net shortwave radiation through fluctuations in the albedo of the glacier surface (Favier et al. (2004a)). At this site, albedo changes reflect the frequency and phase of precipitation (i.e. rain versus snow), and variations in albedo have been linked to changes in the elevation of the zero degree isotherm at the time of the precipitation event (Favier et al. (2004a)); Favier et al. (2004b)). As such, the year-to-year mass balance variability has been associated with temperature variability (Favier et al. (2004b)), and, in fact, an empirical melt model dependent only on the air temperature has been proposed (Manciati et al. (2014)). The climate setting is a wet inner tropical glacier with rainfall throughout the year, though maxima occur in the spring and fall. The average annual precipitation for the 30-year period of this study is 1.980 m w.e. a^{-1}, and the mean temperature at the 50% elevation (i.e. median elevation from the Randolph Glacier Inventory hypsometric profile) is 0.23°C. The aggregate of the glaciers around the volcano (from the Randolph Glacier Inventory) has a mean elevation of 4944 meters above sea level (m a.s.l.), spanning a range of ∼1,400 m between ∼4,300 m a.s.l. to ∼5,700 m a.s.l. The ELA is estimated at 5,030 m a.s.l. (Favier et al. (2004a)), without specification as to the time period over which it is calculated.

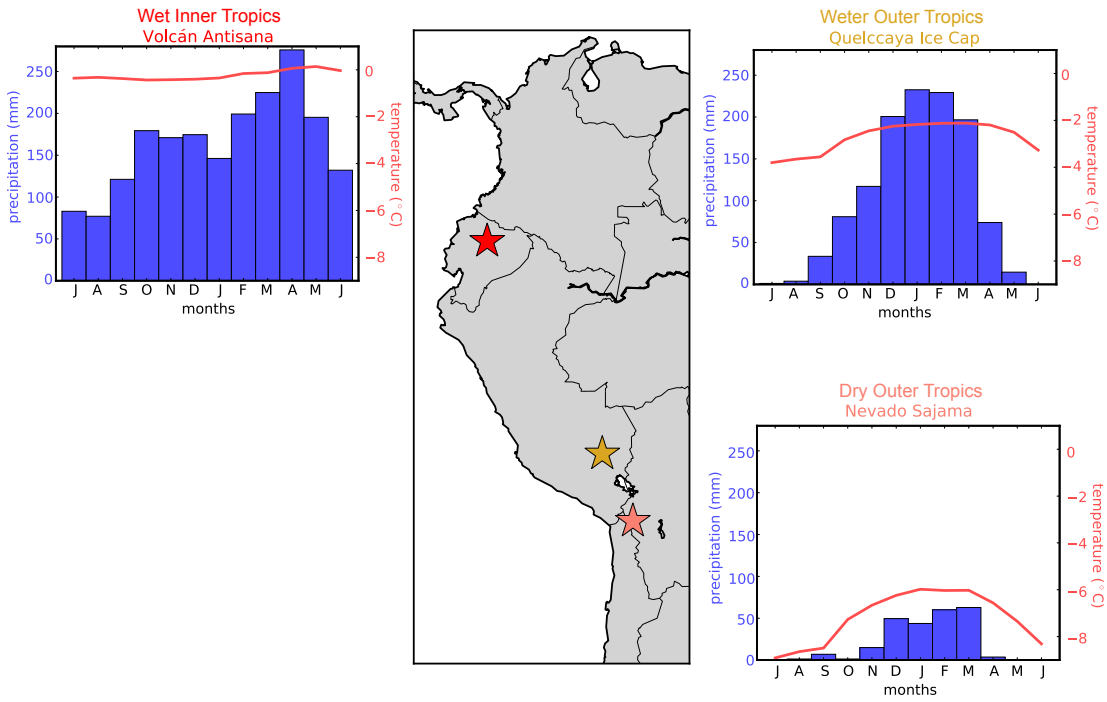

Figure 2.1: Three case study tropical glaciers: Volcán Antisana, Ecuador (red); the Quelccaya Ice Cap, Peru (yellow), and Nevado Sajama, Bolivia (pink). For each, the typical monthly mean temperature and net monthly precipitation from thermal year 1980 - 2009 CE are included. Data: temperature: NCEP-DOE Reanalysis II (Kanamitsu et al. (2002)); precipitation: CRU-Ts v3.23 (Harris et al. (2014)).

The Quelccaya Ice Cap, located in the eastern cordillera of the Andes in southern Peru, is the world's largest tropical ice mass (Thompson et al. (2006)). Multiple ice cores have been drilled from its summit (Thompson et al. (1986); Thompson et al. (2013)) and the geomorphic record of past ice cap extents has been well documented (Mercer et al. (1975); Mercer and Palacios (1977); Goodman et al. (2001); Mark et al. (2002); Kelly et al. (2012); Stroup et al. (2014); Kelly et al. (2015)). The geomorphic record has also been used as a tropical paleoclimate proxy (Malone et al. (2015)). Meteorological stations have been monitored on and off since the mid 1970's (Hastenrath (1978)). Since the mid 2000's, the University of Massachusetts at Amherst has been managing a station at the summit (correspondence with Dr. Douglas Hardy). The climate setting is a wet outer tropical glacier with a majority of the precipitation (>70%) falling during the summer months (Thompson et al. (2013)).

The average annual precipitation for the 30-year period of this study is 1.184 m w.e. a^{-1}, and the mean temperature at the 50% elevation is -2.74°C. The aggregate of the glaciers making up the ice cap have a mean elevation of ∼5,384 m a.s.l., spanning a range of ∼ 800 m between ∼4,900 m a.s.l. to ∼5,700 m a.s.l. The end-of-dry-season snowline altitudes, used as surrogate for outer tropical glacier ELAs (Rabatel et al. (2012)), indicate that the ELA is variable with time, but places it around 5,300 m a.s.l (Mercer and Palacios (1977)) and 5,250 m a.s.l. (Thompson (1980)) for the early part of the study time period and between 5,344 and 5,526 m a.s.l. more recently (Hanshaw and Bookhagen (2014)).

The southern-most and highest elevation tropical glacier, Nevado Sajama, is located in the western cordillera of the Andes near the boarder between Bolivia and Chile. Multiple glaciers extend down valleys on this isolated volcano, which stands ∼2,500 m above the surrounding Altiplano. Moraines marking past glacial extents within these valleys have been catalogued and dated as well as interpretations of ELA changes responsible for the associated glacier advances (Smith et al. (2009)), but no rigorous quantification of the glacier-climate interactions at Nevado Sajama has been made. An ice core has been extracted from the summit, spanning the past 25,000 years (Thompson et al. (1998)). A meteorological station operated on the summit from the mid 1990s until the early 2000s (Hardy et al. (1998); Hardy et al. (2003)). The climate setting is a dry outer tropical glacier with a majority of the rainfall in the austral summer months (Vuille et al. (1998); Hardy et al. (1998)). The average annual precipitation for the 30-year period of this study is 0.245 m w.e. a^{-1}, and the mean temperature at the 50% elevation is -7.20°C. The aggregate of the glaciers on this extinct volcano has a mean elevation of ∼6,060 m a.s.l., spanning a range of ∼1200 m between ∼5,350 m a.s.l. to ∼6,550 m a.s.l. The snowline at Nevadjo Sajama is quite variable year-to-year, but has been showing an increasing trend from the 1980s through the 1990s based on 14 reconstructions during this period using remote sensing data, with a snowline altitude of 5,300 m a.s.l. in 1980 and 5,800 m a.s.l. in 1998 (Arnaud et al. (2001)).

2.2 Methods

2.2.1 Regional-Scale Surface Energy and Mass Balance Modeling

The mass balance at a point on a glacier is the difference between mass gain (accumulation) and mass loss (ablation) over a period of time (usually 1-year). The net mass balance (NMB) for that given time is simply the integral of the mass balance over the entire glacier area and divided by the glacier area. As highlighted in Section 1.1, ablation occurs through energy transfer between the ice and atmosphere. Thus to model the mass loss, a surface energy balance model is employed. Consistent with other regional-scale surface energy and mass balance modeling studies (e.g. Rupper and Roe (2008)), the ground heat flux is ignored from Equation 1.3. By convention, fluxes are positive when directed into the ice surface and negative when directed from the ice surface into the atmosphere. Energy flows into and out of the ice surface are tracked, and mass is lost through sublimation and closure of the surface energy balance. Mass is gained through deposition and solid accumulation. The combined tracking of the energy flows and mass loss/gain processes makes this model a surface energy and mass balance (SEMB) model.

The two radiative fluxes are from shortwave radiation (S) and longwave radiation (L). The net shortwave radiation (S) at the glacier surface is:

$$S = S_{\downarrow} \, (1 - \alpha) \tag{2.1}$$

where $S_{\downarrow}$ is the incident shortwave radiation and α is the albedo of the surface. The albedo (α) on glaciers varies wildly both spatially and temporally. A commonly used albedo parametrization depends on the age and depth of the snowfall (Hock (2005)). The surface albedo varies between a constant ice albedo (α_{ice}) and a time-dependent snow albedo ($\alpha_{snow}(t)$), depending on the thickness of the snow cover. Simultaneously, the time-dependent snow albedo varies between a constant fresh snow albedo ($\alpha_{fresh\ snow}$) and a

constant firn albedo (α_{firn}), depending on the duration of time since the last snow fall event. The albedo is described using the form from Oerlemans and Knap (1998):

$$\alpha = \alpha_{snow}(t) + (\ \alpha_{ice} - \alpha_{snow}(t)\ ) \exp(\frac{-d}{d^*}) \tag{2.2}$$

where d is the depth of snow cover at time t and d^* is a characteristic depth. The time-dependent snow albedo is described by:

$$\alpha_{snow}(t) = \alpha_{firn} + (\ \alpha_{fresh\ snow} - \alpha_{firn}\ ) \exp(\frac{-s}{t^*}) \tag{2.3}$$

where s is the number of days since the last snow fall and t^* is a characteristic time-scale. The net longwave radiation at the glacier surface (L) is:

$$L = L_{\downarrow} - L_{\uparrow} \tag{2.4}$$

where $L_{\downarrow}$ is the longwave radiation incident to the surface and $L_{\uparrow}$ is the longwave radiation from the surface to the overlaying atmosphere. Both terms are described by the Stefan-Boltzmann equation with the assumption that the ice surface behaves like a blackbody to longwave radiation and that the incident longwave radiation can be described by the near-surface air temperature and an effective atmospheric emissivity (ϵ_{eff}):

$$L_{\downarrow} = \epsilon_{eff}\ \sigma\ T_a^4 \tag{2.5}$$

$$L_{\uparrow} = \sigma\ T_s^4 \tag{2.6}$$

where σ is the Stefan-Boltzmann constant, T_a is the temperature of the near-surface air, usually at 2 m above the glacier surface, and T_s is the temperature of the glacier surface. The opacity of the overlying atmosphere to infrared radiation depends on a variety of factors, including the concentration of greenhouse gases, of which water vapor is the most variable

in time for a given location, and the amount and type of cloud cover. A variety of parameterizations are used in the literature for site-specific and regional-scale surface energy and mass balance modeling studies. In this study, a parameterization presented by Konzelmann et al. (1994) and utilized often in the literature (see Hock (2005)), is implemented:

$$\epsilon_{eff} = \epsilon_{cs}\ (1 - n^b) + \epsilon_{oc}\ n^b \tag{2.7}$$

where ϵ_{cs} is the clear-sky emissivity, ϵ_{oc} is the emissivity with complete cloud cover, n is the cloud fraction, and b is an empirical parameter. The clear-sky emissivity is itself variable, depending on the water vapor concentration as follows:

$$\epsilon_{cs} = \epsilon_{cs0} + C_{vap}\ (\frac{RH_a\ p_{sat}(T_a)}{T_a})^{\frac{1}{8}} \tag{2.8}$$

where ϵ_{cs0} is the clear-sky emissivity coming from greenhouse gases other than water vapor, C_{vap} is a parameter to describe how the clear-sky emissivity increases with increased water vapor concentration, RH_a is the relative humidity of the air overlying the glacier surface (2 m above the surface), and p_{sat} is the saturation vapor pressure of the air overlaying the glacier surface.

The remaining fluxes are those relating to heat and include two turbulent fluxes (sensible (Q_H) and latent (Q_E) heat) and heat added to the glacier when liquid precipitation falls onto the frozen surface (Q_R). The two turbulent fluxes use the commonly applied bulk aerodynamic expressions (e.g. Hock (2005), Cuffey and Paterson (2010)):

$$Q_H = C_H\ \rho_0\ \frac{p(z)}{p_0}\ c_p\ U\ (T_a - T_s) \tag{2.9}$$

$$Q_E = C_E\ \frac{\rho_0}{p_0}\ \frac{R_{air}}{R_{vap}}\ L_{s,v}\ U\ (RH_a\ p_{sat}(T_a) - RH_i\ p_{sat}(T_s)) \tag{2.10}$$

where C_H and C_E are the exchange coefficients of heat and water vapor, ρ_0 is the density of (dry) air at standard temperature and pressure, p_0 is sea-level atmospheric pressure, c_p is

the specific heat of (dry) air (at constant pressure), U is the windspeed of the atmosphere over the ice (at 2 m above the surface), R_{air} is the gas constant for (dry) air, R_{vap} is the gas constant for water vapor, $L_{s,v}$ is the latent heat of sublimation and vaporization, respectively, depending on whether the surface is below or at the freezing point, and RH_i is the relative humidity of the air directly in contact with the glacier surface. The form of the exchange coefficients varies depending on the stability of the overlying air, as described by the Richardson number:

$$Ri = \frac{g}{T_a} \frac{(T_a - T_s)\ (z - z_0)}{U^2} \tag{2.11}$$

where g is the acceleration due to gravity and z is the height above the ice surface of the temperature and vapor pressure measurements (2 m). When air is stably stratified ($Ri > 0$), the amount of heat or vapor exchanged between the glacier surface and overlying air is reduced until a critical value (Ri_c) is reached, above which turbulent exchanges are assumed to cease. The exchange coefficient for a property X is described by:

$$C_X = \begin{cases} \frac{\kappa^2}{ln(\frac{z}{z_0})\ ln(\frac{z}{z_{0,X}})}, & \text{if } Ri < 0 \\ \frac{\kappa^2}{ln(\frac{z}{z_0})\ ln(\frac{z}{z_{0,X}})}\ (1 - \frac{Ri}{Ri_c})^2, & \text{if } 0 \leq Ri \leq Ri_c \\ 0, & \text{if } Ri > Ri_c \end{cases} \tag{2.12}$$

where κ is the von Kármán constant, z_0 is the roughness length for momentum, and $z_{0,X}$ is the roughness length for either heat or water vapor. The rain heat flux (Q_R) is modeled using:

$$Q_R = \rho_w\ c_w\ P\ (T_a - T_s) \tag{2.13}$$

where ρ_w is the density of water, c_w is the heat capacity of water, and P is the precipitation rate.

To calculate the saturation vapor pressure for a given temperature, the empirical rela-

tionship from Bolton (1980) is used:

$$p_{sat}(T) = p_{sat_0} \exp(\frac{A\,T}{T+B}) \tag{2.14}$$

where T is the temperature in degrees Celsius, p_{sat_0} is the saturation vapor pressure at the triple point, and A and B are empirical constants. An empirical model for vapor pressure is used instead of an analytic solution to the Clausius-Clapeyron relationship since the former can be fit to data within 0.1% over a temperature range from -30°C $\leq$ T $\leq$ 35°C (Bolton (1980)) while the latter requires an approximation of a constant latent heat value, which over the temperature range of this study in fact varies.

At a given latitude and longitude, the model assumes that the 2-meter air temperature follows a linear lapse rate over the elevation range:

$$T_a = T_0 - \Gamma\,(Z - Z_0) \tag{2.15}$$

where T_a is the air temperature at a given elevation, Z, T_0 is the temperature at a reference elevation, Z_0, and Γ is the lapse rate. All other model variables vary only with respect to longitude and latitude and not also with respect to elevation.

Surface accumulation is the sum of solid precipitation (P_{solid}) and deposition ($Deposition$), where the phase of precipitation is solely a function of temperature and is described by:

$$P_{solid} = \begin{cases} P, & \text{if } T_a \leq 0°C \\ 0, & \text{else} \end{cases} \tag{2.16}$$

where P is the precipitation rate at the elevation of T_a. Deposition has the same mathematical form as sublimation (Eq. 1.2) and occurs when the latent heat flux is positive (into the ice). Values for the SEMB model climate variables and parameters and physical constants are found in Appendix A. The above SEMB model formulations are for a horizontal surface

without the influences of valley wall shading, reflectance, or terrain longwave components.

2.2.2 Model Inputs, Outputs, and Validation Methods

The model described above can be implemented to elucidate the dominant climate variables responsible for glacier mass loss and gain at timescales ranging from daily to the duration of the simulation and at different elevations along the glacier. The parameterizations for the longwave radiation flux (Konzelmann et al. (1994)) and surface albedo (Oerlemans and Knap (1998)) have been developed and the specific parameter values have been optimized at daily timescales (Oerlemans and Knap (1998); Konzelmann et al. (1994); Sicart et al. (2011); Gurgiser et al. (2013)), providing a shortest timescale for the model.

Model inputs at a daily timescale are necessary for the following climate variables: 2-meter air temperature (T_a), precipitation rate (P), atmospheric pressure (p), incident shortwave radiation (S_{down}), windspeed (U), cloud cover (n), and relative humidity of the atmosphere (RH_a). Meteorological data pertaining to the model inputs are scarce at the location of tropical glaciers (Vuille et al. (2003); Bradley et al. (2009)). When available, such data are limited to only specific glaciers and short time periods that are often not continuous and/or do not overlap with studies at other locations. Therefore, reanalysis output is used as a surrogate for climate data for exploring the glacier-climate interactions across various timescales and geographic locations. Consistent with previous regional-scale glacier-climate interaction modeling studies, it is assumed that reanalysis output is able to capture the spatial pattern of climate within the study region (Rupper and Roe (2008); Sagredo et al. (2014)). It is also assumed that reanalysis output is able to validly represent daily and longer time-scale variability in the climate inputs.

The SEMB model climate inputs are extracted from the daily mean output of the NCEP-DOE Reanalysis II (NCEP-DOE R2) (Kanamitsu et al. (2002)) product. NCEP-DOE R2 products are distributed at a $2.5^\circ \times 2.5^\circ$ resolution, and to extract the signal at the location of the study glacier, the reanalysis output are linearly interpolated along great circles to the

latitude and longitude location of the glacier of study. Surface output from the NCEP-DOE R2 product is used for the precipitation rate (P), incident shortwave radiation (S_{down}), windspeed (U), cloud cover (n), and relative humidity of the atmosphere (RH_a), and these values are assumed to not change with elevation in the model. Free atmosphere output from the NCEP-DOE R2 product is used for the 2-meter air temperature (T_a) and surface pressure (p) at the glacier. The 2-meter air temperature at the glacier is extracted at the 50% elevation of the glacier, as determined by the Randolph Glacier Inventory (Pfeffer et al. (2014)), by linear interpolation using the daily mean geopotential height. The free atmosphere temperature is assumed to follow a linear lapse rate (Γ), which is also determined at the 50% glacier elevation by linear interpolation using the daily mean geopotential height, consistent with methods from Bradley et al. (2009).

The NCEP-DOE R2 product, which provides output at a daily timescale but at a coarse spatial resolution, is unable to capture the regional precipitation gradients found in the Andes. The Climate Research Unit time-series version 3.23 (CRU-Ts v3.23) Harris et al. (2014)) gridded data product, which provides a higher spatial resolution ($0.50^\circ \times 0.50^\circ$) but coarser temporal resolution (monthly) picture of precipitation, is able to capture the spatial distribution of Andean precipitation (see Figure 1.5). As such, the daily precipitation inputs to the SEMB model are adjusted so that the net monthly precipitation in the SEMB model input agrees with the net monthly precipitation at the location of the glacier from the CRU-Ts v3.23 gridded data product. Previous regional-scale SEMB modeling in the Andes have also used a hybrid of reanalysis and gridded data products (e.g. Sagredo et al. (2014)).

The output of the SEMB model is the daily mass loss (melt and sublimation) and mass gain (solid accumulation and deposition) for each model grid cell. In addition, the energy fluxes for each grid cell and the glacier surface temperature are output. The model is implemented on a vertical grid, which spans a range of 5,000 m – 2,500 m above the 50% elevation and 2,500 m below – with a 5 m vertical resolution. Three main components of the mass balance output are utilized: 1) year-to-year variations in the net mass balance

(NMB), 2) year-to-year variations in the equilibrium line altitude (ELA), and 3) day-to-day variations in the mass loss and gain at an elevation in the ablation zone, at the ELA, and at an elevation in the accumulation zone. These three components of the mass balance output are compared to the model energy fluxes and ultimately the input climate variables. These comparisons help to elucidate the dominant climate variables and mechanisms driving mass balance changes across different timescales and elevations for tropical glaciers in varying climate settings.

Model performance is evaluated along three avenues: 1) how well does the model output compare to what is observed at the three study sites, 2) how well does the model output capture the year-to-year variability in the NMB, and 3) how well does the model output capture the relationship between climate variables and energy fluxes at the daily timescale in comparison to the literature. Along the first avenue, the model output can be compared to measurements and observations at the study glaciers. First, the modeled ELA can be compared with observations of the ELA. Second, for glaciers that has measurements of NMB data, the modeled NMB can be compared with the data. Third, observations about the trend of glacier change can be used to evaluate the model. If glaciers have been observed to be retreating and/or have increasing ELAs, then the model should predict a negative mass balance trend or long-term average NMB. Along the second avenue, year-to-year changes in the modeled NMB can be compared with the limited data that exist for tropical glaciers. Along the third avenue, model output at various elevations can be used to perform 'virtual' point-scale studies to relate daily mass balance at that elevation to the energy fluxes and climate variables.

The model described in this chapter is a regional-scale model, solved for a horizontal glacier surface, and driven with input from reanalysis, and the model output and input should not be expected to match one-to-one with meteorological data and glacier observations. In particular, model output, such as the ELA, may be expected to be higher or lower than the observed ELA on the order of a few hundred meters, as observed in past regional-scale

SEMB modeling studies (e.g. Sagredo et al. (2014)). Offsets in the elevation at which mass is lost and gained would also affect the magnitude and sign of the NMB, and discrepancies between measured and modeled NMB may be expected. Year-to-year variability in the NMB, however, should agree more closely with observations, if the model is capturing the key physical processes. The model output that should be expected to most accurately represent observations is the correlation between model input and output as part of the 'virtual' point-scale studies. If the model is faithfully representing the key physical processes, then these 'virtual' point-scale studies should produce similar results and conclusions as in the literature. The first validation avenue, and to a lesser degree the second, requires that the model input faithfully represent the meteorology and hypsometry at the site, and slight discrepancies in these factors could result in large discrepancies in the output. The third validation avenue, however, focuses primarily on the whether the model is able to capture the key physical processes that are occurring at tropical glaciers, and this avenue is also the one that most aligns with the objectives of this chapter.

2.2.3 Experiment 1: Mass Balance Response To Contemporary Climate Signal

To determine the dominant climate drivers of recent glacier change, the SEMB model is run for 32 model years with daily mean climate inputs from 1979 to 2010 CE. This study differs from previous regional scale studies of glacier-climate interactions (e.g. Rupper and Roe (2008); Sagredo et al. (2014)) in that the model is run in a time-evolving fashion. Both Rupper and Roe (2008) and Sagredo et al. (2014) explore glacier-climate interactions by running their models for one model year, using a climatology as the input, and climate change and variability is simulated by varying the means and amplitudes of the climatology. In contrast, this study uses a climate input signal that is time-evolving, and the glacier-climate interactions are elucidated by relating the variability in the output to the variability in the input. The model output is analyzed for the 30-year period: thermal year (TY) (July

1 - June 30) 1980 - 2009 CE.

2.2.4 Experiment 2: Mass Balance Response To Certain Climate Signals

In addition to determining the key climate drivers of tropical glacier change, a direct linkage between climate input and the glacier output metrics is desired. In Experiment 1, the model is forced with multiple time-evolving inputs, which is a novelty of the modeling approach implemented in this chapter. Such a method, however, shrouds direct cause-and-effect relationships. To better quantify the cause-and-effect relationship, a second series of simulations is run. Different combinations of inputs are taken directly from the reanalysis while others are the 30-year mean annual cycle as determined by the reanalysis. Four combinations are taken: 1) only the temperature comes directly from the reanalysis output while all other variables are the 30-year mean annual cycle, 2) only the precipitation comes directly from reanalysis, 3) both temperature and precipitation come from reanalysis, and 4) temperature and precipitation inputs are the 30-year mean climatologies, while all others variables come directly from the reanalysis. Simulations 1 - 3 address the role of temperature and precipitation on tropical glacier-climate interactions, both of which have long been cited as the two dominant climate variables affecting glacier variability (Oerlemans and Fortuin (1992)), albeit mainly pertaining to mid and high latitude glaciers. Simulation 4 addresses the role of some of the additional climate variables often cited as drivers of tropical glacier change.

2.3 Results

2.3.1 Model Output And Validation

Figure 2.2, (left column) provides one method to concisely visualize the output for the 30-year period (TY 1980 - 2009). The curve, which is the aggregate vertical mass balance profile, represents the net mass loss and gain at each model elevation over the entire 30-year period divided by the time period length. Aggregate vertical mass balance profiles allow for

the calculation of the net equilibrium line altitude (ELA), i.e. the elevation at which there is zero net mass loss or gain over the 30-year period. The lowest elevation (and latitude) glacier, Volcán Antisana, is also the glacier with the lowest modeled net ELA (4,895 m a.s.l.). The Quelccaya Ice Cap has the second lowest modeled net ELA, at 5,090 m a.s.l. The high, cold, and dry outer tropical glacier, Nevado Sajama, has a significantly higher modeled net ELA, at 6,240 m a.s.l.

In regards to the first validation avenue, the modeled net ELA for the 30-year period is lower than the observed ELA at Volcán Antisana (4,895 m a.s.l. versus ∼5,000 m a.s.l.) and the Quelccaya Ice Cap (5,090 m a.s.l. versus between ∼5,250 m a.s.l. and ∼5,500 m a.s.l.). Nevado Sajama has a significantly higher modeled net ELA than observed ELA (6,240 m a.s.l. versus between ∼5,300 m a.s.l. and ∼5,800 m a.s.l.). The modeled net ELAs, however, are able to capture the spatial trend of ELAs in the tropical Andes – the lowest latitude glaciers have the lowest ELAs and the dry, higher latitude tropical glaciers have significantly higher ELAs (Sagredo et al. (2014)). A previous study in the Andes using a regional-scale SEMB model to calculate ELAs and ELA sensitivity to climate change has also been able to capture the regional distribution of ELAs, while also producing modeled ELAs that differed from inferred ELAs on the order of a few hundred meters (Sagredo et al. (2014)). Past research using regional-scale SEMB models illustrates that this approach provides useful insights about glacier sensitivity to climate change and regional variability, by capturing the physical mass loss and gain processes and the key spatial patterns of the climate inputs, even if the model is unable to fully represent observations (Rupper and Roe (2008); Sagredo et al. (2014)).

Using the aggregate vertical mass balance profile in concert with the elevation distributions from the Randolph Glacier Inventory (Pfeffer et al. (2014)) allows for the calculations of the average net mass balance (NMB), i.e. the net mass loss and gain integrated over the entire glacier area for the 30-year period, divided by the total glacier area and time period length. Applying this method, Volcán Antisana and Nevado Sajama both have modeled neg-

ative average NBMs at -1.31 m w.e. a^{-1} and -0.55 m w.e. a^{-1}, respectively. The modeled average NMB for the Quelccaya Ice Cap, in contrast, is positive at 0.89 m w.e. a^{-1}.

Measured interannual NMB at Volcán Antisana suggest that from 1995 to 2010, Volcán Antisana had an average NMB of -0.59 m w.e. a^{-1} (data from the World Glacier Monitoring Service). Measured interannual NMB data at Nevado Sajama are not available, but ELAs have been primarily increasing in the recent past (Arnaud et al. (2001)), suggesting that Nevado Sajama is in a retreat and negative mass balance phase. The modeled positive average net mass balance at the Quelccaya Ice Cap, however, is inconsistent with observations of continued and perhaps even accelerating ice cap retreat over the past 30+ years (Thompson (2000); Thompson et al. (2011); Thompson et al. (2013); Hanshaw and Bookhagen (2014)). This discrepancy between the modeled average NMBs and observations of retreat at the Quelccaya Ice Cap reflects the modeled net ELA being significantly lower (>150 m) than the observed ELAs at the ice cap. At Volcán Antisana, the modeled net ELA is also lower (∼100 m), but the net modeled average mass balance is negative, in part because the hypsometric profile from the Randolph Glacier Inventory extends to notably lower elevations than the well-studied glacier at the volcano, glacier 15-α (see discussion below for more details). The negative modeled average NMB at Nevado Sajama can be accounted for by the significantly higher (>400 m) modeled net ELA than observed ELAs at the mountain. The model input precipitation for Nevado Sajama is significantly (30% - 80%) less than the precipitation rate observed at the nearby village or measured in the upper part of the ice core (Thompson et al. (1998)). Dry Andean glaciers have been shown to have highly sensitive ELAs to precipitation (Sagredo et al. (2014)). This high sensitivity of the ELA to precipitation can account for some of the significant difference between modeled net ELA and observations. This discrepancy would account for some of the modeled negative average NMB.

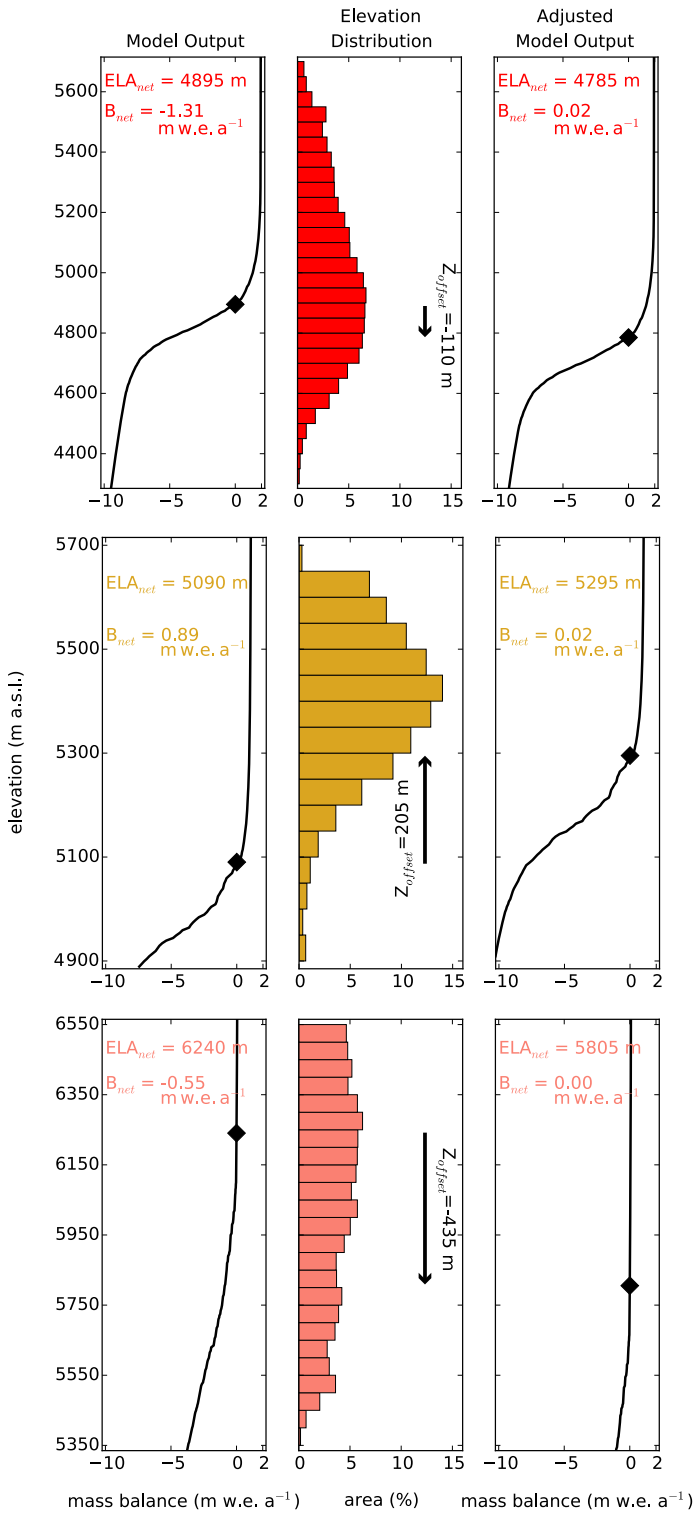

Figure 2.2: 30-year simulated vertical mass balance profiles (left), RGI hypsometric profiles (middle), and adjusted vertical mass balance profiles (right) that bring the glacier into equilibrium given the vertical mass balance and hypsometric profiles.

The vertical discrepancies between the modeled mass balance profiles and the observed glacial hypsometries present a challenge for calculating the interannual NMB at the three study glaciers. The magnitude and sign of the NMB depends on the how the hypsometry relates to the elevational distribution of mass loss and gain (Oerlemans (2001)). To account for the vertical discrepancies in the SEMB model output and the Randolph Glacier Inventory hypsometries (Pfeffer et al. (2014)), the model outputs are interpolated to the glacier hypsometry by means of a vertical transpose (see Figure 2.2, middle column). The vertical transpose in the interpolation scheme is the vertical offset of the aggregate vertical mass balance profile needed so that the average NMB over the 30-year period is zero.

The interpolation from model output to the glacier geometry is only implemented when calculating the NMB. After the interpolation, the modeled net ELAs are: 1) Volcán Antisana, 4785 m a.s.l., 2) Quelccaya Ice Cap, 5,292 m a.s.l., and 3) Nevado Sajama, 5,805 m a.s.l. For the Quelccaya Ice Cap and the Nevado Sajama, these interpolated modeled net ELAs are more consistent with the observed ELAs. For Volcán Antisana, the interpolated modeled net ELA is further from the observed ELA than before the interpolation. Once the interpolations are applied to the vertical mass balance profiles, however, the accumulation area ratios (AARs) for the three study glaciers agree very well with the expected AARs values for tropical glaciers. Using the adjusted ELAs and the hypsometric profiles, all three glaciers have AARs of between 70% and 74%. Typical AAR-values for tropical glaciers range between 70% and 80% tropical glaciers (Kaser and Osmaston (2002)). The agreement between the modeled and expected AARs provides another piece of evidence to suggest that the model output and the interpolation between the output vertical grid and the glacier hypsometry are able to capture the major mass balance features of tropical glaciers.

The second avenue of model validation evaluates the model's ability to capture the year-to-year changes in the NMB (see Chapter 2.3.2). Measurements of NMB on tropical glaciers are limited in their spatial and temporal scope. Of the three study sites in this chapter, only the Volcán Antisana has a NMB observation record, being recorded for glacier 15-α,

on the northwest side of the volcano. The modeled NMBs are calculated for the aggregate hypsometry of all the glaciers on Volcán Antisana and is compared to the measured NMB time series on the glacier 15-α (Figure 2.3). For the full 16-year period (1995 through 2010), the correlation between the two time series is statistically significant ($p<0.01$), albeit not overwhelming ($r^2 = 0.45$). Excluding the first year in the regression, 1995, the correlation is much stronger ($r^2 = 0.65$). Also, the direction of year-to-year changes in the NMB between the model agree for all years except for 2002 to 2003 and 2003 to 2004. Direct comparison between these two time series, however, does require some caution. The hypsometry used to quantify the modeled NMB differs from the hypsometry of the glacier 15-α. Glacier 15-α is long and narrow, snaking down the northwest side of the volcano to a lowest elevation of $\sim$4800 m a.s.l. (Favier et al. (2004a)). The hypsometric profile used in the regional-scale model is the aggregate of all glaciers on the volcano and extends down to a lowest elevation of $\sim$4300 m a.s.l. Oerlemans (2001) illustrate how adjacent glaciers subjected to a similar climate forcing can respond with different magnitudes and at times even signs in their NMB due to differences in their hypsometry. While the modeled NMB anomalies at Volcán Antisana do not agree one-to-one with the observations at glacier 15-α, there is a statistically significant correlation between the two time series and the year-to-year changes agree to first order.

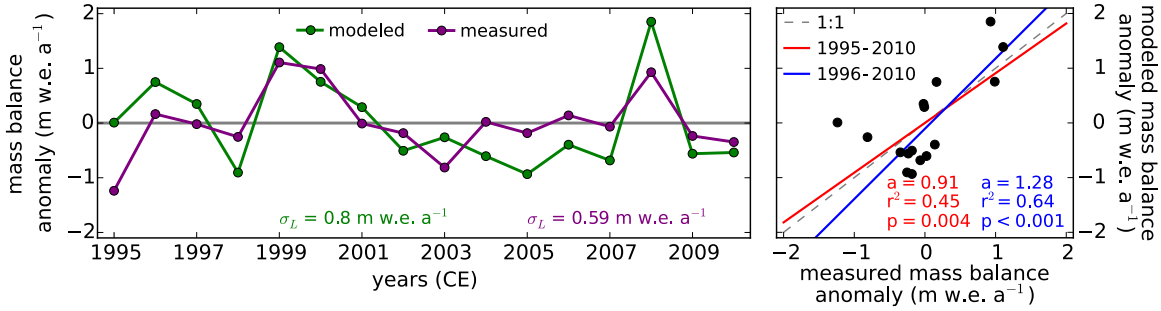

Figure 2.3: Comparison between measured and modeled net mass balance on Volcán Antisana from calendar year 1995 to 2010 as a time series (left) and comparison plot (right). In the comparison plot, the two regression lines are provided: 1995 - 2010 (red) and 1996 - 2010 (blue). The coefficient of determination (r^2) and regression coefficient (a) are indicated for both regression lines. Both time series represent anomalies. The average modeled NMB from 1995 to 2010, after the interpolation from model elevation to glacier elevation is applied is 0.05 m w.e. a^{-1}. The average measured NMB for the same period is -0.59 m w.e. a^{-1}. Data: World Glacier Monitoring Service.

For the Quelccaya Ice Cap, the magnitude of modeled NBM variability, as quantified by the standard deviation of NMB time series (σ_{NMB}), can be compared to the magnitude of observed variability at two other wet tropical glaciers: 1) Zongo Glacier, Bolivia and 2) Chacaltaya Glacier, Bolivia. The modeled σ_{NMB} at the Quelccaya Ice Cap from TY 1980 - 2009 is 0.78 m w.e. a^{-1} (see Chapter 2.3.2). The measured σ_{NMB} at Zongo Glacier from 1992 to 2013 is 0.64 m w.e. a^{-1} (data retrieved from the WGMS database). For Chacaltaya glacier, the measured σ_{NMB} from 1992 to 2008 is 0.84 m w.e. a^{-1} (data retrieved from the WGMS database). The modeled σ_{NMB} for the Quelccaya Ice Cap falls between the observed σ_{NMB}'s for the two wet outer tropical glaciers with the longest NMB data record, suggesting that the model is able to produce a comparable magnitude of year-to-year NMB variability. NMB measurements for dry tropical glaciers are not available, and the model NMB output for Nevado Sajama cannot be evaluated against data.

The third avenue of model validation evaluates the ability of the model to capture the input-output relationships at a single elevation of the glacier (see Chapter 2.3.5). Studies using a meteorological station in the ablation zone of both inner (Favier et al. (2004a);

Favier et al. (2004b); Sicart et al. (2008)) and outer (Sicart et al. (2005); Sicart et al. (2008); Sicart et al. (2010)) wet tropical glaciers find that day-to-day melt primarily reflects all-wave radiation variation and that temperature correlates only weakly with surface melt. Using data for Volcán Antisana's glacier 15-α (wet inner tropical glacier) and Zongo Glacier Bolivia (wet outer tropical glacier), Sicart et al. (2008) illustrate that net all-wave radiation accounts for >90% of the day-to-day variations in available melt energy, whereas air temperature correlates only poorly with daily melt ($r^2 < 0.3$). Looking at the correlations between modeled daily melt and different energy fluxes and SEMB climate inputs, at 100 m below the ELA all-wave radiation is the dominant driver of day-to-day variations in melt ($r^2 \sim$ 97%) at both wet tropical glaciers, while temperature only weakly correlates with day-to-day melt variability ($r^2 \sim 0.3$). The ability of the model to capture similar results to those observed at point-scale studies on tropical glaciers suggests that the model is able to capture the dominant processes occurring on wet tropical glaciers.

Similar point-scale field studies on dry tropical Andean glaciers are unknown to the author, but the net annual precipitation at Mt. Kilimanjaro is similar to that at Nevado Sajama, providing a possible comparison site with published point-scale studies. From point-scale studies on meteorological stations on Mt. Kilimanjaro, well above the zero degree isotherm, Mölg and Hardy (2004) and Mölg et al. (2008) find that daily melt primarily reflects variations in absorbed shortwave radiation and that temperature has virtually no short-term impact on melt variability, while the frequency of snowfall primarily dictates melt variability. Looking at the correlation between daily melt and all-wave radiation, Nevado Sajama has a significant correlation between daily melt all-wave radiation and that precipitation helps to modulate variability in the radiation; temperature has essentially no impact on the mass balance in the accumulation zone. These results agree with the observations at Mt Kilimanjaro and suggest that the model is able to capture the key physical processes for dry tropical glaciers as well.

The three avenues above for model validation suggests that the model is able to produce

output that can be used to meet the objective of this chapter: to elucidate the key climate variables responsible for glacier mass loss and change at different tropical glaciers climate settings across multiple timescales and elevations. While the model seems to have vertical offsets in the rate of mass loss and gain at different elevations relative to observations, it does seem to be able to capture the dominant processes for mass loss and gain in the different zones of a glacier. By applying the vertical interpolation between the model grid and the Randolph Glacier Inventory hypsometric profiles, the modeled aggregate mass balance profiles, as described above, seem to be able to capture the relative timing and magnitude of NMB variability at tropical Andean glaciers.

In the following subsections, the interannual variability in the NMB and ELA will be discussed along with their relationships to the climate inputs. Also, the processes for mass loss and gain at different glacier elevations will be discussed, providing insights into how the results and conclusion of past point-scale studies reflect the choices about where on the glacier the meteorological station is located. These dynamic (i.e. time evolving) metrics for glacier-climate interactions provide useful information for elucidating the key climate variables responsible for past and present tropical glacier change and can aid in future forecasts of tropical glacier evolution.

2.3.2 Modeled Year-To-Year Variability

The NMB time series and statistics are found in Figure 2.4. The two wet tropical glaciers have a similar magnitude of NMB anomalies (quantified as the 1-σ value of the mass balance time series). Nevado Sajama, in contrast, has a significantly lower magnitude of NMB anomalies. A lower NMB variability for Nevado Sajama is not surprising since the amount of annual precipitation at the glacier is significantly less than for wet tropical glaciers ($\sim$8x less than Volcán Antisana and $\sim$5x less than the Quelccaya Ice Cap). In terms of significant ($p < 0.05$) NMB trends over this 30-year period, both the Quelccaya Ice Cap ($p = 0.001$) and Nevado Sajama ($p < 0.001$) have negative NMB trends. The Volcán Antisana, although

having a variable NMB time series, does not have have a significant trend (p = 0.937).

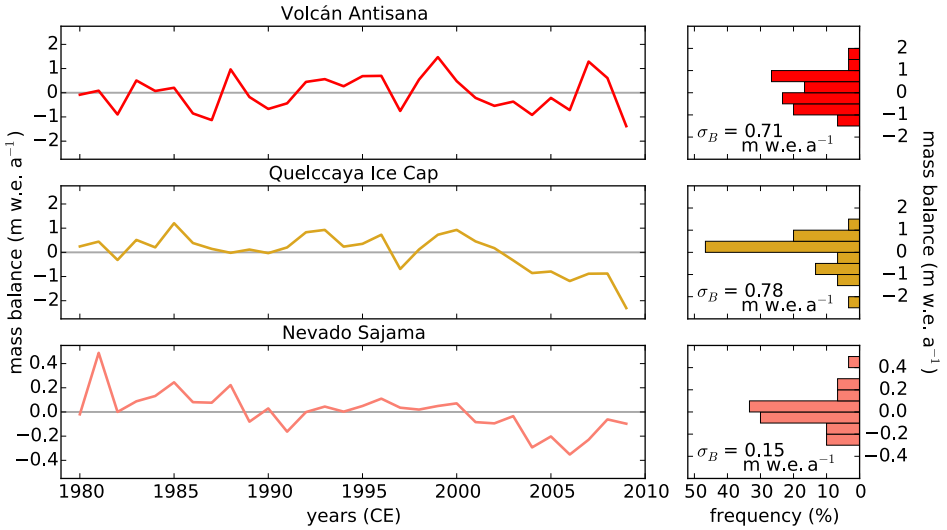

Figure 2.4: 30-year simulated net mass balance anomalies (left) and histogram of the time series (right) for Volcán Antisana (top), the Quelccaya Ice Cap (middle), and Nevado Sajama (bottom). The magnitude of the net mass balance variability (σ_B) is indicated.

The simulated ELA time series and statistics for the three case-study glaciers are found in Figure 2.5. ELAs are presented as anomalies from the net ELA (i.e. the elevation at which there is zero net mass loss or gain over the 30-year simulation). Just as with the NMB, the two wet tropical glaciers have similar magnitude ELA anomalies. Nevado Sajama, by contrast, has a substantially more variable ELA time series. The missing year in the simulated ELA time series for Nevado Sajama represents a year when there was no elevation on the modeled grid at which accumulation balances ablation. This year (TY 1991 CE) is particularly dry, and even at the highest elevation in the model, net sublimation exceeds net accumulation. For all three glaciers, the largest ELA excursions from the net ELA (i.e. the elevation at which there is no net loss or gain over the 30-year period) are to higher elevations. There is also an asymmetry in the ELA time series with regards to the net ELA. The two wet tropical glaciers both have a higher net ELA (i.e. the elevation over the 30-year simulation with zero net mass loss or gain) than mean ELA (i.e. the arithmetic mean of the ELA time series). The dry tropical glacier, Nevado Sajama, has a lower net ELA than mean ELA.

Just as with the NMB time series, only the Quelccaya Ice Cap and Nevada Sajama have significant trends in ELA anomalies; both are increasing over the 30-year simulation (p = 0.014 and p = 0.039).

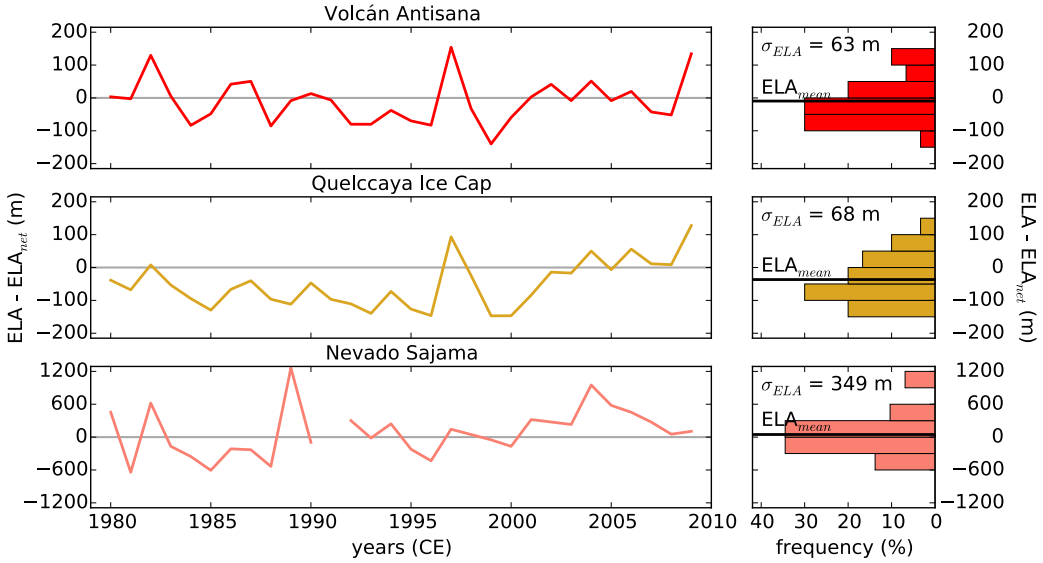

Figure 2.5: 30-year simulated ELA anomalies (left) and histogram of the time series (right) for Volcán Antisana (top), the Quelccaya Ice Cap (middle), and Nevado Sajama (bottom). The magnitude of the ELA variability (σ_{ELA}) is indicated. Also, the mean of 30-year time series of ELAs is presented (ELA$_{mean}$) that for all three glaciers differs from the net ELA (ELA$_{net}$).

2.3.3 Modeled Year-To-Year Variability and Variability in the Climate Inputs

A first approach at elucidating the dominant climate drivers for changes at the three simulated glaciers is to look for correlations between the two metrics for glacier-climate interactions (year-to-year net mass balance (NMB) variability and equilibrium line altitude (ELA) anomalies) and anomalies in the input model variables: temperature, lapse rate, shortwave radiation, windspeed, precipitation, relative humidity, and cloud cover. Since both the NMB and ELA are annual quantities, averaging of the climate variables is necessary. Correlations are found between these two glacier metrics and the annual average and the austral winter

(JJA), austral fall (SON), austral winter (DJF), and austral spring (MAM) averages. A data table with the regression coefficients and coefficients of determination between each metric for glacier-climate interactions and the climate inputs is found in Appendix B.

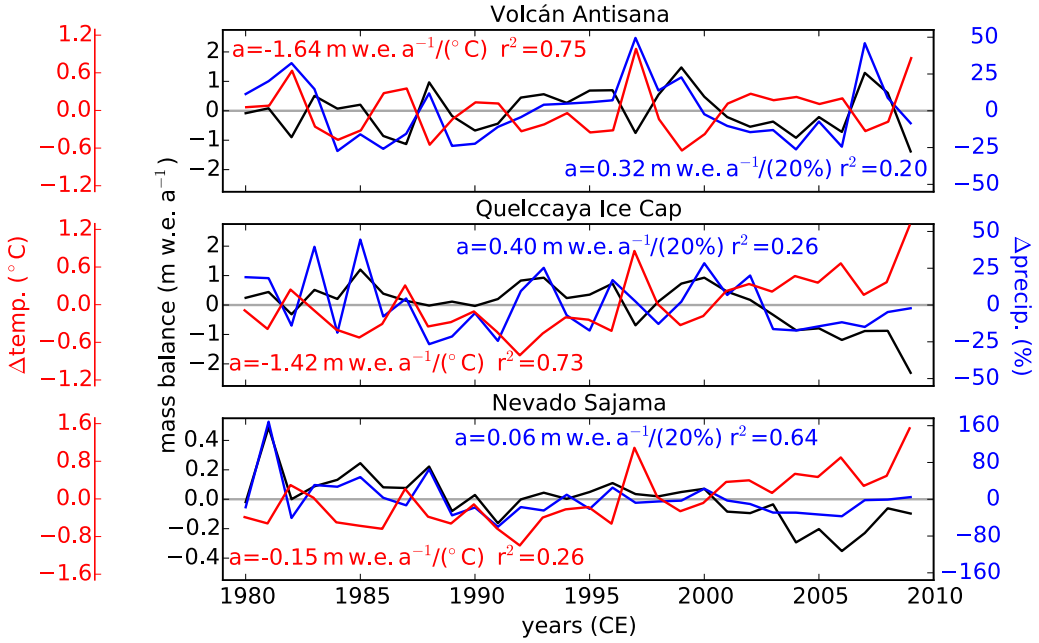

Figure 2.6: 30-year simulated net mass balance variability (black), annual average temperature anomalies (red), and annual net precipitation anomalies (blue) for Volcán Antisana (top), the Quelccaya Ice Cap (middle), and Nevado Sajama (bottom). Regression coefficients (a) and coefficients of determination (r^2) are included.

As with the magnitude of variability, the two wet tropical glaciers have similar statistically significant correlations between year-to-year variations in the NMB and model inputs while Nevado Sajama, the dry tropical glacier, tells a slightly different story. The two wet tropical glaciers, Volcán Antisana and the Quelccaya Ice Cap, have very strong statistical correlations ($p<0.001$) between NMB variability and anomalies in temperature inputs at all timescales. For both glaciers, the 'best' agreement between NMB variability and temperature anomalies comes at the annual average timescale as determined by the coefficient of determination (r^2-value) in the least square linear regression between the two time series. Nevado Sajama has a statistically significant ($p< 0.05$) correlation between NMB variability and temperature anomalies at all times except for austral summer (DJF), with the best fits at the austral fall

(SON) and austral (DJF) timescales. In both cases, however, the coefficient of determination (r^2-value) is $\leq$0.3, indicating a less dominant relationship between NMB variability and temperature anomalies for the dry tropical glacier than with the two wet tropical glaciers. The strongest correlation between Nevado Sajama's NMB variability and anomalies in a climate input is with precipitation. The 'best' fit is on the net annual timescale, and at this timescale there is a very strong statistical correlation ($p<0.001$). The correlation of determination, however, is smaller than for the best fits for the two wet tropical glaciers. Additional statistically significant correlations between NMB variability and anomalies in the climate inputs occur (see Appendix B), but they are secondary. The time series of the NMB variability and anomalies in the annual average temperature and net annual precipitation for all three glaciers are found in Figure 2.6.

Looking at year-to-year variations in the ELA, once again, the two wet tropical glaciers tell a similar story while Nevado Sajama tells a different story. Both Volcán Antisana and the Quelccaya Ice Cap have very strong statistical correlations ($p < 0.001$) between ELA anomalies and temperature anomalies at all timescales. The Volcán Antisana has slightly better agreement than the Quelccaya Ice Cap as indicated by the coefficient of determination. The correlation with temperature for the two wet tropical glaciers can also be viewed in terms of changes in the freezing level height (i.e. zero degree isotherm), which have very strongly significant correlation ($p < 0.001$) at all timescales. For both glaciers, the regression coefficient between ELA anomalies and freezing level height anomalies is slightly less than one, suggesting that a 1-m change in the freezing level height yields a slightly less than 1-m change in the ELA. Unlike with NMB variability, Nevada Sajama does not have a statistically significant correlation between ELA anomalies and temperature anomalies, except in the austral fall (MAM). Even then, however, the coefficient of determination is small. As was the case with the net mass balance anomalies, the strongest correlation at Nevado Sajama is between ELA anomalies and precipitation anomalies. At the net annual timescale, the correlation is very strong ($p < 0.001$) and the coefficient of determination is the largest,

albeit much smaller than the coefficients of determinations between ELA anomalies and temperature for both wet tropical glaciers. Additional statistically significant correlations between ELA anomalies and anomalies in the climate inputs occur (see Appendix B), but they are secondary. The time series of ELA anomalies and anomalies in the annual average temperature and net annual precipitation are found in Figure 2.7.

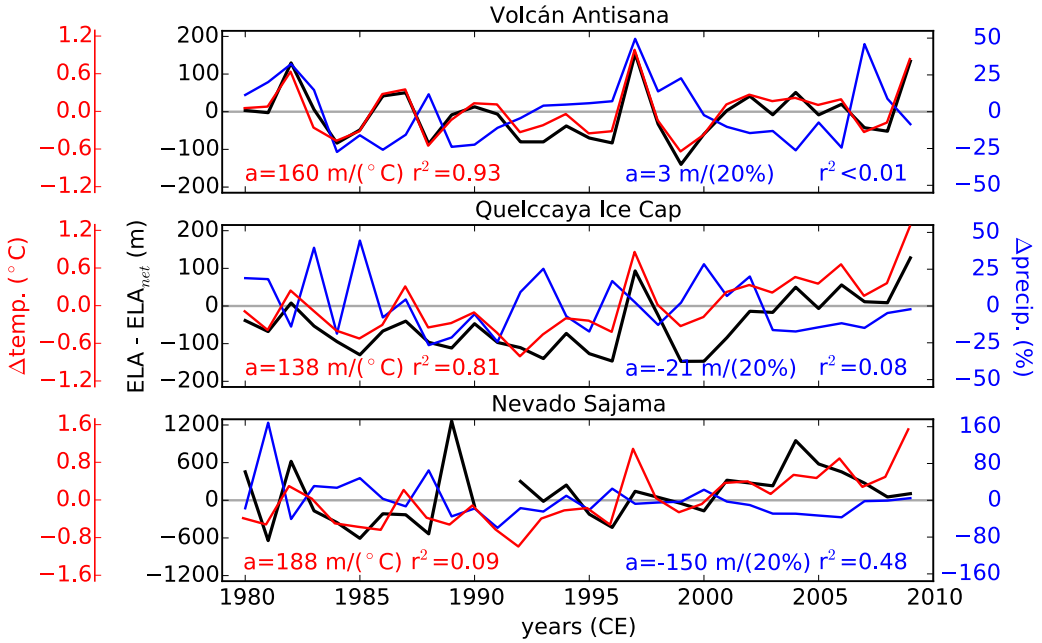

Figure 2.7: 30-year simulated ELA anomalies (black), annual average temperature anomalies (red), and annual net precipitation anomalies (blue) for Volcán Antisana (top), the Quelccaya Ice Cap (middle), and Nevado Sajama (bottom). Regression coefficients (a) and coefficients of determination (r^2) are included.

2.3.4 Modeled Year-To-Year Variability and Variability in the Specific Climate Inputs

A more direct experiment as to the sensitivity of these two glacier-climate interaction metrics to different climate inputs is to drive the SEMB model with one or a few of the climate inputs while holding the others fixed at an annual cycle for the 30-year climatology. Experiments are conducted where a) only the temperature input is allowed to evolve from year-to-year, b)

only the precipitation input is allowed to evolve from year to year, c) both temperature and precipitation inputs are allowed to evolve from year-to-year, and d) all climate inputs other than temperature and precipitation are allowed to evolve from year-to-year. With regards to evaluating how sensitive these two mass balance metrics are to a single or few climate inputs, two different questions are addressed: *1) How well does the single (or few) climate input(s) do at producing the magnitude of variability in the metric as compared to when forced with all climate inputs?* and *2) How well does this single (or few) climate input(s) do at producing the timing of variability in the metric as compared to when forced with all climate inputs?*.

Figure 2.8 illustrates the timing and magnitude of net mass balance (NMB) anomalies that would be produced using different combinations of climate inputs. For all three glaciers, the climate input combination that produces the closest magnitude and timing to what is produced in Section 2.3.1 is when both temperature and precipitation are allowed to time evolve. For the simulation where both temperature and precipitation time evolve, the magnitude of NMB variability (quantified as the 1-σ value) for Volcán Antisana is 93.3% the value it is when all climate inputs are allowed to time evolve. For the Quelccaya Ice Cap, the magnitude of NMB variability is 105.8% the value when all inputs are allowed to time evolve. For the dry tropical glaciers, Nevado Sajama, NMB variability for this simulation is 85.6% the value from when all inputs time evolve. For all three glaciers, the temperature and precipitation simulation also has the closest timing of mass balance variability as determined by the root mean square difference (RSMD) between the time series where all variables time evolve from year-to-year and the simulation where only temperature and precipitation time evolve from year-to-year (see Figure 2.8). The second best simulation at producing the magnitude and timing of NMB anomalies differs for the wet and dry tropical glaciers.

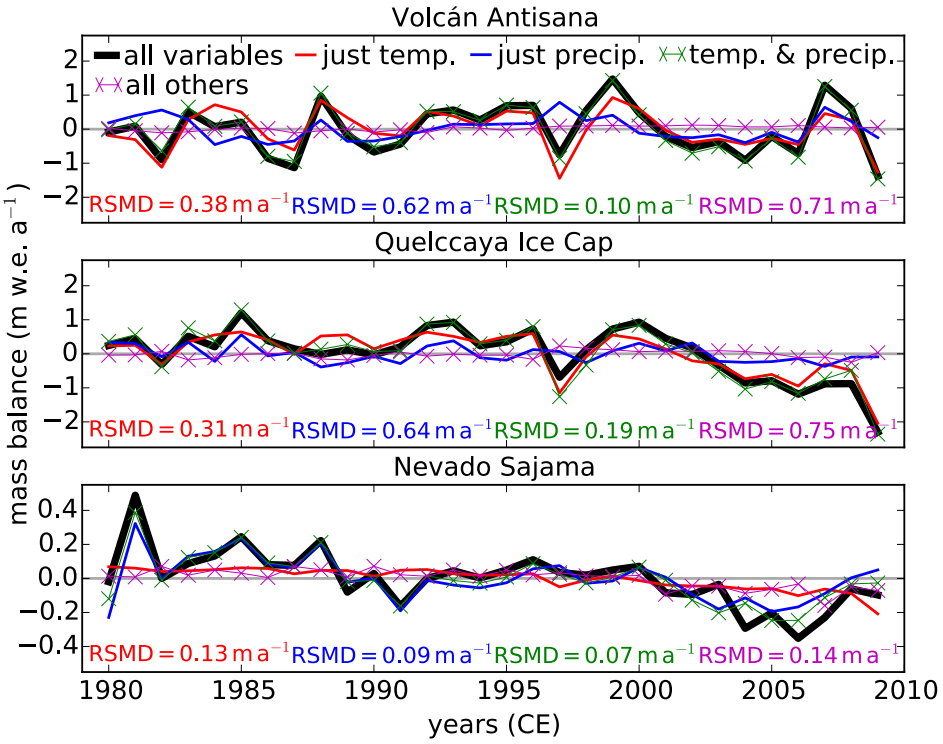

Figure 2.8: 30-year simulated net mass anomalies for different combinations of climate inputs. The root mean square difference (RSMD) between the simulation from Section 2.3.3 (black) and each combination of climate inputs (colored curves) is indicated.

For the two wet tropical glaciers, Volcán Antisana and the Quelccaya Ice Cap, the simulation where only the temperature input evolves from model year to model year is the next closest (after the temperature and precipitation simulation) in terms of both magnitude and timing of NMB variability (see Figure 2.8). For Volcán Antisana, the magnitude of NMB variability in this simulation is 82.3% the magnitude of variability as when all inputs time evolve, and for the Quelccaya Ice Cap it is 84.1%. For both these glaciers, the simulation where just precipitation time-evolve produces less than half the magnitude of variability as in the simulation when all inputs were allowed to vary (47.5% for Volcán Antisana and 33.9% for the Quelccaya Ice Cap), and timing is worse than the above-mentioned simulations. The worst simulation at producing the magnitude and timing of NMB variability as compared to the simulation where all climate inputs time evolved is the one where neither temperature

or precipitation time evolve. For this simulation, the NMB variability at Volcán Antisana is only 9.9% the magnitude as when all inputs time evolved, and for the Quelccaya Ice Cap, it is 14.5%. The timing of the simulated NMB for this case is the worst for both glaciers, with the largest RMSD values (see Figure 2.8).

For Nevado Sajama, the dry tropical glacier, the simulation where precipitation is the only model climate input to time evolve is the next closest (after the temperature and precipitation simulation) at capturing the magnitude and timing of NMB variability. The precipitation-only simulation produces 79.7% the magnitude of NMB variability as when all inputs time evolve, and regarding the timing, and the RSMD-value is only slightly larger than when all inputs time evolve. The two simulations for the dry tropical glaciers where the precipitation does not evolve from year-to-year are significantly worse at producing the magnitude and timing of NMB variability. The magnitude of variability is less than 40% of its value when all inputs are allowed to evolve with time for both cases. The temperature only simulation produces a slightly larger magnitude of variability than the simulation where both temperature and precipitation are held fix at an annual climatology. For both precipitation-fixed simulations, the timing is much worse as determined by the RSMD (see Figure 2.8). These results suggest that in order to model the magnitude and timing of NMB variability that temperature is the essential input into the SEMB model for the two wet tropical glaciers, while precipitation is the essential input for the dry tropical glacier. For all three glaciers, however, the combination of both the temperature and precipitation inputs produces the closest magnitude and timing of the simulated contemporary NMB variability.

The ELA variability for these different simulations is also analyzed (see Figure 2.9), and they tell much the same story as the NMB variability, however, with a few caveats. For all three glaciers, the regionals-scale SEMB simulation where both temperature and precipitation time evolve from year-to-year produces the closest magnitude and timing for the simulated contemporary ELA variability. The magnitude of ELA variability produced in this simulation is 100.5% the value when all inputs time evolve for Volcán Antisana, 107.1%

the value for the Quelccaya Ice Cap, and 72.6% the value for Nevado Sajama. In terms of timing, this simulation also produces the best signal (see Figure 2.9). In much the same way, the two wet tropical glaciers require a time-evolving temperature input to produce either the timing or magnitude of ELA variability as in Section 2.3.3, while the dry tropical glacier requires a time-evolving precipitation signal.

A way in which the story of net mass balance anomalies and the ELA anomalies differs is that for the wet tropical glaciers, the precipitation only simulation produces an appreciable magnitude of net mass balance variability ($\sim$30 - 50%), while the two simulations without temperature variability produce negligible ELA variability ($<$15% for Volcán Antisana and $<$6% for the Quelccaya Ice Cap). Also, in the two simulation without temperature variability for the wet tropical glaciers, there is no difference between the mean ELA and net ELA, suggesting that this mass balance asymmetry somehow relates to temperature. For Nevado Sajama, the dry tropical glacier, there are differences between the mean ELA and the net ELA for all four simulations. The two simulations where the precipitation input time evolves produce a mean ELA at a higher elevation than the net ELA (same as in Chapter 2.3.3). For the temperature only simulation and the simulation where all inputs except for temperature and precipitation are allowed to time evolved, however, the mean ELA is lower than the net ELA. Including in the insights from the ELA variability further supports the results that suggest that for the two wet tropical glaciers, temperature is the vital component of the story while for the dry tropical glaciers precipitation is the vital component. The ELA results, however, illustrate the importance of different climate variables in producing ELA asymmetries observed in Chapter 2.3.3, which warrants further exploration.

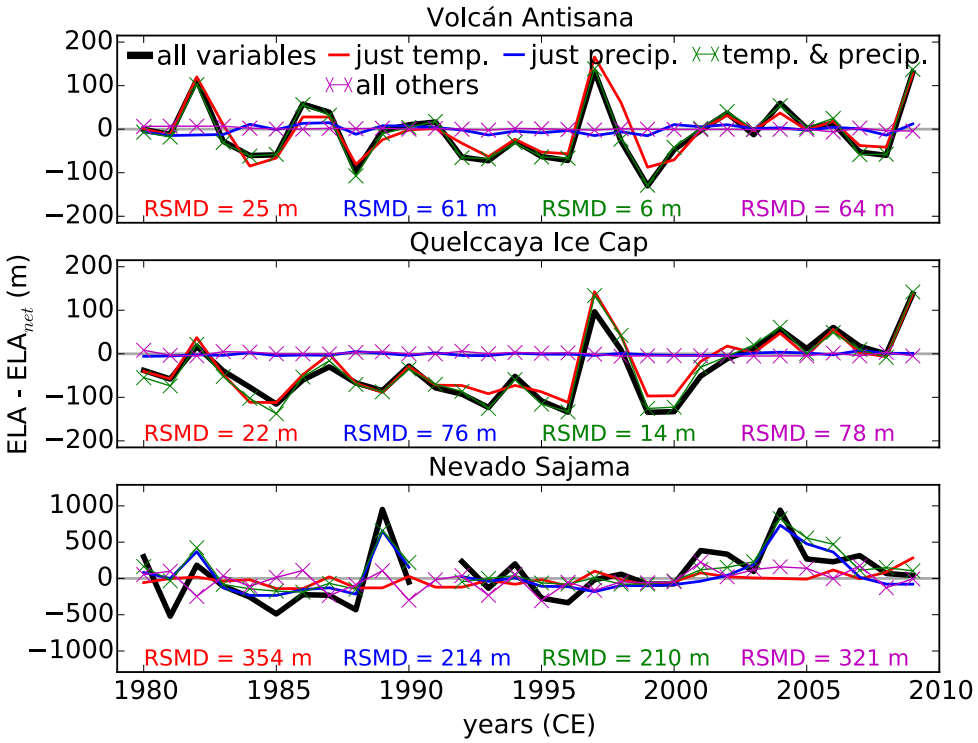

Figure 2.9: 30-year simulated ELA anomalies for different combinations of climate inputs. The root mean square difference (RSMD) between the simulation from Section 2.3.3 (black) and each combination of climate inputs (colored curves) is indicated.

These simulations also provide useful metrics: the mass balance and ELA sensitivity to interannual anomalies in temperature and precipitation, i.e. how sensitive the the mass balance (or ELA) is to a warm year or a wet year (in the absence of changes in the other climate inputs). These results are shown in Table 2.1, and these values can be compared to the literature. These parameters are determined through a least-squares linear regression between each sensitivity metric and the annual average temperature anomalies or net annual precipitation anomalies. In all instances the linear regressions are statistically significant ($p<0.05$). In the case of the net mass balance sensitivities parameters, the regression correlations are very strong statistically ($p < 0.001$) for all three glaciers and both temperature and precipitation. In the case of the ELA sensitivity parameters, five of the six values have a very strong statistical correlation ($p < 0.001$), except for the correlation between ELA anomalies

and annual net precipitation anomalies at Nevado Sajama, where the correlation is only strong (p = 0.01). In terms of the explanatory power between annual average/net climate anomalies and anomalies in the mass balance metrics, for either metric, the two wet tropical glaciers have larger coefficients of determination as compared to the dry tropical glacier. Also, between ELA and net mass balance anomalies, the coefficients of determination are larger for the net mass balance than ELA.

Table 2.1: Mass Balance and ELA Sensitivity Parameters for Three Case Study Glaciers

	Volcan Antisána	Quelccaya Ice Cap	Nevado Sajama
$\frac{d}{dT}$b (m w.e. a^{-1} per °C)	-1.54	-1.33	-0.1
$\frac{d}{dT}$ELA (m per °C)	149	138	145
$\frac{d}{dp}$b (m w.e. a^{-1} per 20%)	0.33	0.26	0.05
$\frac{d}{dp}$ELA (m per 20%)	-7	-3	-57

2.3.5 Day-To-Day and Year-To-Year Melt Variability at Different Elevations and Associated Energy Fluxes and Climate Inputs

'Virtual' point-scale studies are conducted by quantifying the relationship between melt variability and variability in the climate inputs or energy fluxes at three different elevations on the glacier: 100 m below the ELA (ablation zone), at the ELA, and 100 m above the ELA (accumulation zone). These results can be compared to previous point-scale studies that quantify the relationship between melt and climate variables or energy fluxes (e.g. citewagnon1999annual; Favier et al. (2004a); Favier et al. (2004b); Francou et al. (2004); Sicart et al. (2008)). Day-to-day correlations are presented for a single year, and interannual correlations are presented for the full 30-year period. Results are only presented for the two wet tropical glaciers: Volcán Antisana and the Quelccaya Ice Cap.

At Nevado Sajama, the dry tropical glacier, results are not presented in a figure because there are only a few statistically significant and notable correlations ($r^2 > 0.5$) between daily melt and a single climate variable or energy flux. The only energy flux with a statically sig-

nificant and a notable coefficient of determination is daily all-wave radiation, with r^2 values between 0.4 and 0.5. Temperature does not have any statistically significant correlation with daily melt at any elevation, and the relationships with solid or liquid precipitation, although significant, are minimal ($r^2 < 0.1$).

For the two wet tropical glaciers, the correlations between daily melt variability and the climate inputs and net all-wave radiation are found in Table 2.3. Additional statistically significant correlations exist, but the strength of the correlations are secondary to the ones presented in this section. For both glaciers, the strongest correlation is with net all-wave radiation (i.e. sum of net shortwave and net longwave radiation). At and below the ELA, the correlation is very strong ($r^2 > 0.85$), suggesting that melt variability in the ablation zone and near the ELA of wet tropical glaciers primarily reflects variability in the radiative fluxes. In the accumulation zone, the correlation is smaller, albeit still strong ($r^2 > 0.75$). All other correlations between melt and an energy flux pale in comparison, with coefficients of determination (r^2-values) less than 0.2. These results for both wet inner and outer tropical glaciers are consistent with previous point-scale studies in the Andes (e.g. Sicart et al. (2008)).

Table 2.2: Daily Correlation Between Melt and Climate Variables and All-wave Radiation At The Two Wet Tropical Glaciers (Volcán Antisana and the Quelccaya Ice Cap)†

		Antisana			QIC		
	distance to ELA_{net}	-100 (m)	0 (m)	100 (m)	-100 (m)	0 (m)	100 (m)
temperature							
	a (mm w.e. d^{-1} / °C)	**7.317**	**4.873**	**1.359**	**7.45**	*0.844*	0.066
	r^2	**0.28**	**0.35**	**0.13**	**0.30**	*0.02*	<0.01
precipitation rate							
	a (mm w.e. d^{-1} / mm w.e. d^{-1})	*-0.139*	-0.005	-0.016	0.251	**-0.193**	**-0.191**
	r^2	*0.03*	<0.01	<0.01	0.01	**0.04**	**0.06**
solid accumulation rate							
	a (mm w.e. d^{-1} / mm w.e. d^{-1})	**-1.296**	**-0.252**	*-0.043*	**-1.366**	**-0.287**	**-0.199**
	r^2	**0.25**	**0.10**	*0.03*	**0.14**	**0.07**	**0.06**
net all-wave radiation							
	a (mm w.e. d^{-1} / W m^{-2})	**0.274**	**0.238**	**0.183**	**0.270**	**0.198**	**0.168**
	r^2	**0.97**	**0.93**	**0.78**	**0.97**	**0.85**	**0.77**

† **bold** text indicates a p-value <0.001. *italics* indicates a p-value <0.05.

The strongest correlation between daily melt and a climate input is with temperature (see Table 2.3). In the ablation zones of both glaciers, coefficients of determination (r^2-values) are

>0.25, although none exceed 0.4. These correlations are similar to those found for both wet inner and outer tropical glaciers (e.g. Sicart et al. (2008)). Correlations between precipitation rate variability and melting are negligible. Looking at just solid precipitation, however, illustrates a stronger correlation and highlights the important of the phase of precipitation (solid versus liquid) as compared to the absolute amount. The stronger correlation with solid precipitation than total precipitation illustrates an important component of temperature in determining melt variability – dictating the phase of precipitation. At the ELA in the accumulation zone of the Quelccaya Ice Cap, a wet outer tropical glacier, the most significant climate variable switches from temperature to precipitation, in either the solid or liquid form. At a yearly timescale, the climate input most responsible for interannual mass balance variability at any of the elevations is temperature, similar to the results presented in Chapter 2.3.3 for the glacier-wide mass balance. Precipitation does not have a significant correlation with year-to-year variability with melt, but solid precipitation has a very strong statistical correlation and large coefficient of determination (r^2-value), albeit smaller than the values for temperature.

Table 2.3: Yearly Correlation Between Melt and Climate Variables At The Two Wet Tropical Glaciers (Volcán Antisana and the Quelccaya Ice Cap) †

		Antisana			QIC		
	distance to ELA_{net}	-100	0	100	-100	0	100
temperature							
	a (m w.e. a^{-1} / °C)	**5.229**	**2.432**	**0.917**	**5.557**	**2.171**	**0.363**
	r^2	**0.84**	**0.68**	**0.74**	**0.61**	**0.53**	**0.58**
precipitation rate							
	a (m w.e. a^{-1} / m w.e. a^{-1})	-0.842	0.271	0.289	-3.999	-0.991	-0.166
	r^2	0.03	0.01	0.08	0.09	0.03	0.03
solid accumulation rate							
	a (m w.e. a^{-1} / m w.e. a^{-1})	**-3.892**	**-1.311**	**-0.533**	**-5.814**	*-2.268*	*-0.397*
	r^2	**0.71**	**0.42**	**0.38**	**0.50**	*0.34*	*0.15*

bold text indicates a p-value <0.001. *italics* indicates a p-value <0.05.

In addition to finding correlations between climate inputs, energy fluxes, and melting, the magnitude of the relationship can be evaluated through the regression coefficient (a-value) (see Table 2.3). At the daily timescale, the size of the regression coefficient is greater in the ablation zone than the accumulation zone, suggesting that the climate variable or energy flux

with which melting is correlated plays a stronger role in the ablation zone. The amount of reduction in the regression coefficient varies, depending on the climate variable or energy flux. The regression coefficient for the relationship between melt and all-wave radiation decreases by <40% when moving from 100 m below the ELA to 100 m above the ELA. In contrast, the regression coefficient between temperature and melt decreases by more than 80% for the same 200-m change in elevation. At the interannual timescale (see Table 2.3), a similar trend emerges, with temperature and solid accumulation having much larger regression coefficients in the ablation zone than the accumulation zone. Previous studies have tried to link climate drivers of tropical glacier change by determining both the statistic significance and the magnitude of the relationship (e.g. Mölg and Hardy (2004); Mölg et al. (2008)). The results of this chapter suggest that the magnitude of these relationships could be very sensitive to where the point-scale study is conducted on the glacier.

2.4 Discussion

2.4.1 Wet-Dry Contrast

An emergent pattern from the analyses of the model output is that the two wet tropical glaciers, Volcán Antisana and the Quelccaya Ice Cap, tell a similar story, while the dry tropical glacier, Nevado Sajama, is an outlier. The two wet tropical glaciers have a similar modeled (and adjusted) ELA while the dry tropical glacier has a significantly higher (>500 m) ELA. Both the Volcán Antisana and Quelccaya Ice Cap have a similar magnitude of simulated contemporary mass balance and ELA variability, while Nevado Sajama has a significantly smaller mass balance variability and surprisingly larger ELA variability. All three glaciers have an asymmetry between the mean ELA and net ELA, but for the two wet tropical glaciers it is in one direction (higher net ELA than average ELA) while for the dry tropical glacier it is in the other direction (lower net ELA than average ELA). Finally, when looking at the climate drivers of glacier variability, inferred from either the mass

balance or ELA anomalies, the glacier-climate interactions at the two wet tropical glaciers strongly depend on temperature anomalies, while the single most important variable for the dry tropical glacier variability is precipitation. These results suggest that the amount of precipitation that a glacier receives is paramount in defining its glacier-climate interactions.

The wet-dry contrast in terms of glacier-climate interactions is not surprising. The amount of precipitation that a glacier received has long been associated with the relative sensitivity of that glacier to temperature or precipitation changes (e.g. Meier (1984); Oerlemans and Fortuin (1992)), with wetter glaciers having greater temperature sensitivity. The relative contribution of melt and sublimation to the overall ablation at the ELA provides a useful framework to explore how the wetness of a glacier helps to determine its glacier-climate interactions (e.g. Rupper and Roe (2008) and Figure 2.10). As illustrated in Section 1.1, melt is $\sim$8.5x more effective (watt-per-watt) at ablating mass than sublimation. As such, in low accumulation regions, glaciers need to be situated in ways that minimize melt, for example, at high elevations. Figure 2.10 illustrates that at low accumulation rates, the primary mechanism for mass loss is sublimation, while at high accumulation rates, the primary mass loss mechanism is melt. Nevado Sajama, a dry tropical glacier, presents a nice test case since in one year it receives anomalously high precipitation, pushing it out of the clumping of points with low accumulation rates into the clumping with higher accumulation rates. That anomalous year's melt fraction seems to follow the overall trend for the two wet tropical glaciers. The shape of Figure 2.10 agrees well with a similar figure from Rupper and Roe (2008), and the key conclusions are the same: at low accumulation rates, the majority of mass loss is achieved through sublimation, while at higher accumulation rates, the majority of mass loss is accomplished by melting. In this chapter, the exact transitions from melt-dominant to sublimation-dominant regimes differ slightly from Rupper and Roe (2008), who find that sublimation dominates at precipitation rates $<$0.25 m w.e. a^{-1} and that melt dominates at precipitation rates $>$0.50 m w.e. a^{-1}, albeit they do not define what it means for one ablation mode to 'dominate'. For the three case-study tropical glaciers, sublimation

dominates at the ELA (>75% of net ablation) when the net accumulation at the ELA is <0.30 m w.e. a^{-1}, while melt dominates at the ELA (>75% of net ablation) when the net accumulation at the ELA is >0.75 m w.e. a^{-1}. The slight differences between the results in this chapter and Rupper and Roe (2008) may relate to differences in the climate settings of the three tropical glaciers in this study and glaciers in the Himalaya from Rupper and Roe (2008). Despite these slight differences in accumulation/precipitation values, the general conclusions remain the same.

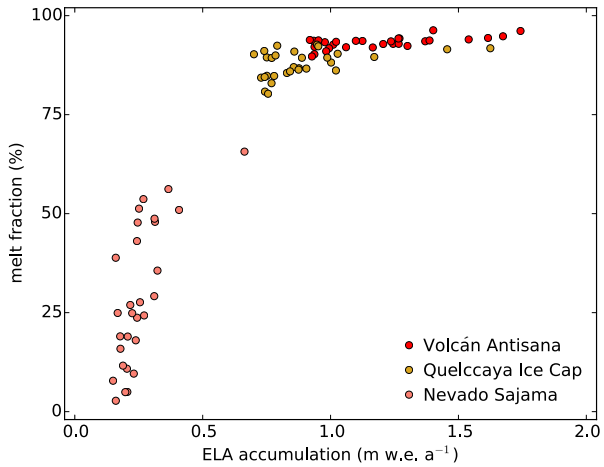

Figure 2.10: Melt fraction versus accumulation rate for the three case study glaciers. The melt fraction is the percentage of total ablation that is achieved through melting. The ELA accumulation rate is the sum of the solid precipitation and the deposition at the ELA. The various circle for each glacier represent different modeled years. At accumulation rates above a threshold (∼0.75 m w.e. a^{-1}), melt accounts for more than 75% of the total mass loss. At accumulation rates below a threshold (∼0.30 m w.e. a^{-1}), sublimation accounts for more than 75% of the total mass loss. Glaciers in the sublimation-dominated regime need to be at high elevations, where air temperature are cold enough to make melt an infrequent occurrence. Glaciers in the melt-dominated regime, are generally situated such that at the lowest elevations of the glacier spend a significant portion of the year near or above the freezing point.

The notion that tropical Andean glaciers might respond differently to similar climate changes depending on the wetness of the glacier setting is explored in Sagredo et al. (2014), where both the temperature and precipitation sensitivity of the ELA (i.e. $\frac{d}{dT}$ELA and $\frac{d}{dp}$ELA) are quantified. For the regions corresponding to the three tropical glaciers in this

chapter, Sagredo et al. (2014) find that wet inner tropical glaciers have the highest ELA sensitivity to temperature (>200 m per °C), followed by the wet outer tropical glaciers (∼175 m per °C), and finally the dry tropical glaciers (∼165 m per °C). Looking at precipitation, Sagredo et al. (2014) find that dry inner outer tropical glaciers have the greatest ELA sensitivity to precipitation ($\gtrsim$50 m per 25%), followed by the wet outer tropical glaciers (∼50 m per %), and the least sensitivity is the wet inner tropical glaciers (<50 m per 25%). Sagredo et al. (2014) ultimately concluded that in wetter regions temperature plays a comparably larger role in glacier change while in drier regions, precipitation plays a comparably larger role, a conclusion consistent with the results in this chapter.

Though the results from this chapter agree with the conclusions from Sagredo et al. (2014), the values of the sensitivity parameters differ significantly, except for the ELA sensitivity to precipitation at Nevado Sajama (see Table 2.1). For the two wet tropical glaciers, the results presented in this chapter show virtually no ELA sensitivity to precipitation, whereas Sagredo et al. (2014) find less than a factor of two difference between the wet inner tropics and the dry outer tropics. These large differences likely reflect the differences in the models. Sagredo et al. (2014) use the Rupper and Roe (2008) model, which has a monthly time-step, a different atmospheric emissivity parameterization, and a fixed albedo. The model developed and implemented for this chapter is run at a daily time-step, includes an atmospheric emissivity parameterization accounting for the effects of cloud cover, and implements a dynamic albedo model. At tropical glaciers, variations in net longwave radiation stemming from changes in cloud cover and net shortwave radiation stemming from albedo modification have been long been linked to variations in melting (Wagnon et al. (1999); Francou et al. (2003); Favier et al. (2004a); Favier et al. (2004b); Mölg and Hardy (2004); Mölg et al. (2008)). It is not surprising that the simulated melt and corresponding ELA variability would differ between models. Some of the differences in temperature sensitivity between the results presented here and Sagredo et al. (2014) are also likely due to the different models, but some also likely reflect different climate inputs. Sagredo et al. (2014) use output from

the NCEP-NCAR Reanalysis I (NCEP-NCAR R1) product, while here, the NCEP/DOE R2 product is used. Sagredo et al. (2014) find that the ELA sensitivity to temperature is inversely proportional to the lapse rate. From previous explorations of the similarities and differences between the NCEP-NCAR R1 and NCEP-DOE R2 reanalysis products, the lapse rates at the elevations of Andean glaciers are generally shallower in the NCEP-NCAR R1 product than the NCEP-DOE R2 product, possibly accounting for the smaller ELA temperature sensitivities in this chapter. At Zongo Glacier, a wet outer tropical glacier in Bolivia, the ELA sensitivity to temperature is estimated at 150 +/- 30 m per °C (Réveillet et al. (2015)), which has a mean slightly higher than the values found in the chapter, but the values from this chapter are within the error bars from the Réveillet et al. (2015) study. The results presented in this chapter highlight the importance of the amount of precipitation that a tropical glacier receives in defining its sensitivity to climate changes. Consideration of the wetness must be taken into account before trying to compare or generalize conclusions about tropical glacier-climate interactions.

2.4.2 Drivers of Wet Tropical Glacier Change Across Temporal And Spatial Scales

The results presented in this chapter illustrate that for wet tropical glaciers year-to-year mass balance variability primarily reflects temperature changes. This result would suggest that temperature has driven past changes and is driving current changes. At the day-to-day timescale and at any point on the glacier, however, temperature is only weakly correlated with melt ($r^2 < 0.4$). At a single point on the glacier and at the daily timescale, variations in all-wave radiation accounts for the vast majority of mass balance variability. These model results are consistent with previous studies about both the longer term variability (e.g. Rabatel et al. (2008); Sicart et al. (2008); Rabatel et al. (2013); López-Moreno et al. (2014)) and the day-to-day variability (e.g. Wagnon et al. (1999); Francou et al. (2003); Favier et al. (2004a); Favier et al. (2004b); Sicart et al. (2008)). This apparent discrepancy between

the drivers of wet tropical glaciers change across temporal and spatial scales has presented challenges to the field, and the results of this chapter can partially resolve these challenges.

Various hypotheses regarding how temperature impacts longer-term and glacier-wide mass balance variability have been proposed. One hypothesis attributes the strong interannual correlation between glacier-wide melt and temperature to co-variations of the different climate variables with temperature (Francou et al. (2003); Sicart et al. (2008). This hypothesis is consistent with observations about the strong impact of ENSO events on glacier mass balance (e.g. Wagnon et al. (2001); Francou et al. (2004); Favier et al. (2004b); Vuille et al. (2008b); Maussion et al. (2015)). Another hypothesis focuses on the role that temperature plays in determining the phase of precipitation (Favier et al. (2004b)) and has been suggested as the mechanism linking interannual mass variability at the Volcán Antisana to temperature. It has been suggested, however, that because zero degree isotherms tend to be below or at only the lowest elevations of wet outer tropical glaciers that this mechanism would play less of a role (Favier et al. (2004b)). A third hypothesis suggests that the processes at the lowest elevations of tropical glaciers are able to dictate glacier-wide mass balance and that these processes are most sensitive to temperature (Sicart et al. (2011); Gurgiser et al. (2013)). This third hypothesis has been put forth in light of new studies at the wet outer tropics using models that can simulate the mass balance processes glacier-wide. These studies, however, are limited to two glaciers and only a few years of analysis. The results presented in this chapter provide perspectives to address these various hypotheses.

The first hypothesis can be evaluated against the results in Chapter 2.3.4. In the simulation where only temperature evolves from year-to-year, >80% of the modeled contemporary interannual glacier-wide mass balance variability is able to be produced. These results indicate that temperature variability alone is able to produce the majority of the simulated mass balance variability, indicating that co-variation in climate inputs are not a necessary condition. The simulation driven with only temperature variability, however, is unable to produce all the mass balance variability, suggesting that co-variation of climate variables

may play at least some role.

The co-variation of variables likely contributes in part to the second hypothesis: temperature dictating the phase of precipitation and thus the glacier surface albedo. In Chapter 2.3.4, the simulation that is able to produce the closest output to the modeled contemporary glacier-wide mass balance (or ELA) variability is the one where the model is forced with both time-evolving temperature and precipitation inputs. This simulation is able to produce within 7% of the simulated contemporary glacier-wide mass balance variability, suggesting that the co-variation of temperature and precipitation is needed to more accurately simulate interannual mass balance variability. The interplay between changes in freezing-level-height and melt at wet inner tropical glaciers proposed by Favier et al. (2004b) can be observed in the results from Chapter 2.3.5 for both Volcán Antisana (wet inner tropics) and the Quelccaya Ice Cap (wet outer tropics). In the ablation zone of the both glaciers, precipitation has no effect on day-to-day variability in melt, but there are strong, statistically significant ($p < 0.001$) and at least moderate ($r^2 \sim 0.2$) correlations between day-to-day melt and solid accumulation, i.e. precipitation when air temperature is below the freezing point. In the ablation zone, daily all-wave radiation variable has a nearly one-to-one correlation with melt variability. Variations in all-wave radiation substantially reflect the surface albedo, and albedo variations reflect the frequency and phase of precipitation (e.g. Favier et al. (2004b); Sicart et al. (2008)). For wet outer tropical glaciers, in particular, it has been often assumed that the freezing-level-height and albedo interplay would play a less significant role, but the results from this chapter challenge that assumption.

The third hypothesis, that processes at the lowest extents of the glacier dictate glacier-wide mass balance, are consistent with the results from this chapter. The processes in play are the same as in the second hypothesis – the freezing-level-height and impact on surface albedo interplay. This hypothesis results from recent work moving beyond point-scale studies to modeling glacier-wide mass loss and gain through distributed surface energy and mass balance models. The results from Chapter 2.3.5 support this third hypothesis.

The regression coefficients (a-values) between temperature and melt and solid accumulation and melt are significantly larger in the ablation zone than at the ELA or the accumulation zone at both the daily and yearly timescales. These large regression coefficients support the suggestions by Sicart et al. (2011) and Gurgiser et al. (2013) that variability in wet tropical glacier mass balance reflect temperature at yearly timescales due to the strength to the freezing-level-height and albedo interplay in the lowest parts of the ablation zone.

The results from this chapter also highlight the challenges of extrapolating results and conclusions from studies at a single location on a glacier to glacier-wide mass loss and gain processes. Hopefully future field studies will begin to incorporate studies using multiple meteorological stations and distributed surface energy mass balance modeling. Regional-scale modeling such as that conduced in this chapter helps to provide perspective in extrapolating results from a single location to glacier wide responses and may aid in future planning of field studies.

2.4.3 Tropical Glaciers and Mass Balance Asymmetries

A third feature from this study is that all three glaciers have a different mean ELA than net ELA. The net ELA is the elevation where there is zero net mass loss or gain over the 30-year period, while the mean ELA is the average of the ELA time series. (note: the vertical mass balance profiles are adjusted such that the entire glacier will be in equilibrium with the net profile from the 30-year period). The difference in these two descriptions of the long-term ELA suggests that years with an anomalous climate in one direction produce a different magnitude response than years with the same magnitude anomalous climate but opposite sign, introducing a nonlinearity into the system. Also, these nonlinearities may stem from different processes at the wet and dry tropical glaciers, since the two wet tropical glaciers have lower mean ELAs than net ELAs while the dry tropical glacier has a higher mean ELA than net ELA.

In the tropical Andes, El Niño Southern Oscillation (ENSO) is one of the major modes of

climate variability, causing a large percentage of the anomalies in rainfall and temperature (Garreaud et al. (2009)). Tropical Andean glacier mass balance variability is also reflective of anomalies stemming from modes of ENSO in both the wet inner (Francou et al. (2004); Favier et al. (2004b)) and wet outer (Wagnon et al. (2001); Favier et al. (2004b); Vuille et al. (2008b); Maussion et al. (2015)) tropics. In the dry outer tropics as well, there are correlations between snowline altitude and ENSO (Arnaud et al. (2001)). The results from this chapter for both the simulated NMB and ELA anomalies have significant statistical correlations with the NINO 3.4 index, which quantifies tropical Pacific sea surface temperature anomalies in the region 5°N - 5°S, 120°W - 170°W, for all three glaciers (not shown). El Niño events tend to coincide with large negative mass balances, which are attributed to a combination of both hotter and drier years (Francou et al. (2004); Favier et al. (2004b)). The combination of anomalous warmth and dryness would produce a strong feedback on the albedo, amplifying the mass loss during El Niño events, and possibly providing a mechanism for the discrepancies in the mean and net ELAs at the wet tropical glaciers observed in this chapter. This co-variation of warmth and dryness, however, is not a necessary condition for the discrepancies. As seen in Chapter 2.3.4, the lower mean ELA than net ELA for the two wet tropical glaciers can be produced even in the simulation where only temperature time-evolves from year-to-year. Nevado Sajama also experiences a lower mean ELA than net ELA in the simulation where only temperature time-evolves from year-to-year, suggesting that temperature alone may be the culprit in producing a lower mean ELA than net ELA.

To explore the mechanisms for the discrepancies between the mean and net ELAs, statistics on the mass balance at the mean ELA (Figure 2.11) are analyzed. The two wet tropical glaciers have larger excursions to negative mass balances, and the aggregated mass balance at the mean ELA for the full 30 years is negative. Looking at how mass balance and temperature correlate at the mean ELA, it is strong but not purely linear, especially at the Quelccaya Ice Cap. The regression line in Figure 2.11 (center column) is the correlation between positive temperature anomalies and the mass balance at the mean ELA. The shape of

the mass balance versus temperature output is similar to the proposed *curvilinear* relationship between temperature and mass balance (Bradley and England (1978)), where negative mass balance anomalies can grow almost limitlessly on warm years, but there is hard and fast limit to the size of a positive anomaly on a cold year – the net annual precipitation. In essence, on a cold year, you cannot anti-melt.

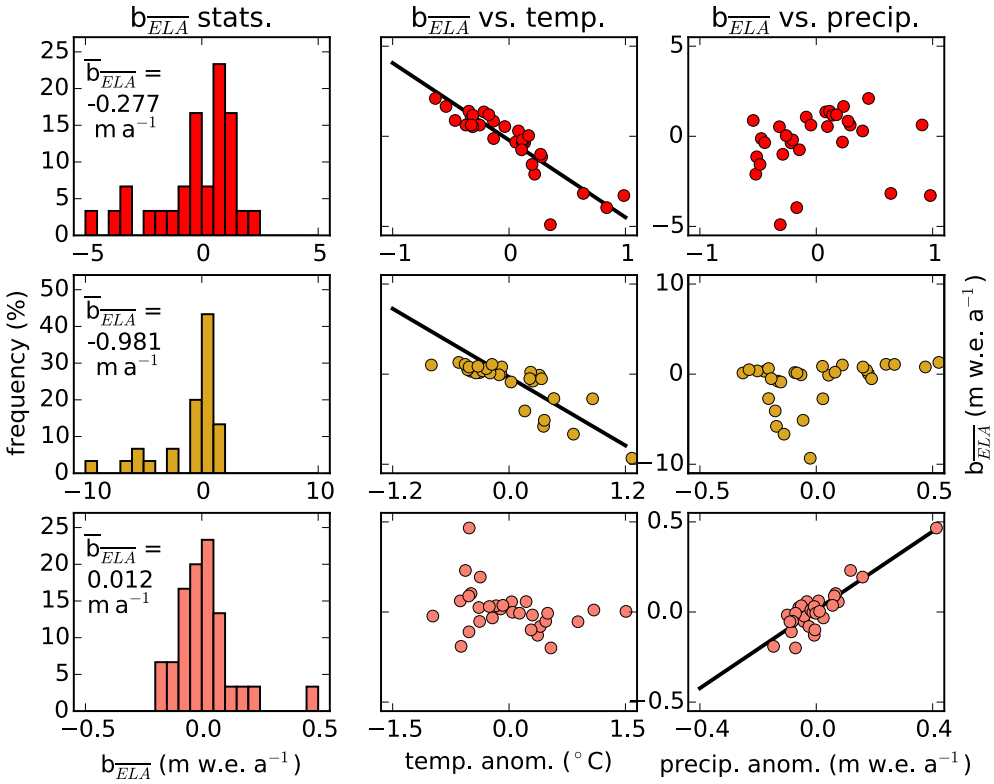

Figure 2.11: Histograms of the mass balance at the mean ELA ($B_{\overline{ELA}}$) (left column), correlation of that mass balance at the mean ELA to temperature anomalies (middle column), and correlation of that mass balance at the mean ELA to the precipitation anomalies (right column). In the first column, the aggregate mass balance (over the 30-year period) at the ELA is displayed ($\bar{b}_{\overline{ELA}}$). When correlating mass balance to temperature or precipitation, the linear regression line is drawn only if the correlation is strongly significant ($p<0.01$). For linear regressions with temperature, the line reflects correlation between only the positive temperature anomalies and mass balance at the mean ELA. (note: there are no instances where p is <0.05 but >0.01.)

Figure 2.11 also garners insight into why Nevado Sajama has a lower net ELA than mean ELA. There is a large positive mass balance balance anomaly, and the aggregate mass

balance at the mean ELA is positive. Looking at the correlation between precipitation and mass balance at the mean ELA, the relationship appears purely linear, requiring some other mechanism for the nonlinearity. An asymmetry in ELA excursions can be well observed in Figure 2.5, with large jumps to higher elevations above the mean (or net) ELA but much smaller jumps to lower elevations. This asymmetry between jumps to high and low ELAs likely reflects the two major ablation regimes (Figure 2.10). In the dry regime, the ELA can fluctuate wildly as slight differences in precipitation require drastic shifts in the ELA to balance sublimation with precipitation. In the wet regime, however, slight changes in elevation result in drastic changes in the melt rate (Table 2.3), and the magnitude of ELA variability for the two wet tropical glaciers is significantly smaller than for Nevado Sajama. As a result, Nevado Sajama can have different ELA responses to the same magnitude but different sign climate forcing, if the forcing requires the ablation regimes to switch. On dry years, the glacier remains in the sublimation-dominated regime with high ELA variability, but on wetter years the glacier tries to enter into a melt-dominated regime with low ELA variability.

For all three glaciers there is one drastic excursion in the mass balance at the mean ELA that could be the culprit for the difference between the net and mean ELAs. It has been shown that long-term trends in mass balance can be erased by a one-off year (Bradley and England (1978)). For Nevado Sajama, if the largest positive anomaly is removed, then the net 29-year aggregate mass balance at the mean ELA is zero, suggesting that the lower net ELA than mean ELA reflects that one anomalously wet year. That one anomalously wet year, however, is also the year that Nevado Sajama jumps into the melt-dominated ablation regime, consistent with the hypothesis that switching ablation regimes is a mechanism for the discrepancy between the mean and net ELA at the dry tropical glacier. For both wet tropical glaciers, however, if the largest negative anomaly at the mean ELA is removed, then the 29-year aggregate mass balances at the mean ELA are still negative, albeit with a smaller value. The mechanisms producing the discrepancy between the mean and net

ELA at the wet tropical glaciers seem robust and are likely related to the curvilinear nature of anomalous melt with anomalous temperature. The nonlinear mass balance response to climate anomalies at tropical glaciers warrant further exploration.

2.5 Concluding Remarks

In this chapter, a regional-scale surface energy and mass balance (SEMB) model is developed to address the question *what climate variables are important in defining the glacier-climate interactions at low latitudes?* The model is run for three case study glaciers that span the breadth in diversity of tropical Andean glaciers: 1) the Volcán Antisana, Ecuador, 2) the Quelccaya Ice Cap, Peru, and 3) Nevado Sajama, Bolivia. The key results are the following:

1. Differences in glacier-climate interactions primarily reflect the rate of (solid) precipitation at the glacier, a similar framework to that found for mid and high latitude glaciers (Meier (1984); Oerlemans and Fortuin (1992); Rupper and Roe (2008)).

2. The two wet tropical Andean glaciers (Volcán Antisana and the Quelccaya Ice Cap) are most sensitive to temperature, while the dry tropical Andean glacier (Nevado Sajama) is most sensitive to precipitation.

3. At wet tropical glaciers, the connection between temperature and net mass balance stems from an indirect effect, where the temperature determines the phase of precipitation, which ultimately affects the surface albedo. Since shortwave radiation determines the available melt energy, processes that alter the absorbed shortwave radiation have a large impact on the net mass balance. This connection occurs most strongly at the lowest elevations of the glacier but can dictate glacier-wide mass balance.

4. Wet tropical glaciers and the dry tropical glaciers appear to respond asymmetrically to similar magnitude but opposite sign climate anomalies, suggesting that mass balance nonlinearities exist. Preliminary explanations are provided for each type of glacier, but

further exploration is warranted.

5. The model presented here furthers previous regional-scale SEMB models, by explicitly solving for mass loss and gain processes at all elevations of the glacier, utilizing additional physical processes, and implementing data from the Randolph Glacier Inventory. It allows for quantification of the glacier-wide mass balance and exploration of mass balance processes at different elevations along the glacier.

CHAPTER 3

RECONSTRUCTIONS OF TROPICAL PALEOCLIMATES

The objective of this chapter is to quantify past tropical climate change by implementing coupled numerical models for how glaciers relate to the climate system and how they flow. As seen in Chapter 2, glacier-climate interactions at tropical glaciers can be simulated using a surface energy and mass balance model, and the dominate driver for interannual mass balance variability for wet tropical is temperature. The ability to simulate short-term and interannual mass balance variability enables explorations of tropical glacier length responses to climate change and climate variability, an important step towards using tropical glacier change as a paleoclimate proxy. Records of past glacier changes have provided a powerful tool to quantitatively reconstruct and evaluate past climate changes (e.g. Rind and Peteet (1985); Huber et al. (2006); Anderson and Mackintosh (2006); Doughty et al. (2013)), given their ability to sculpt the landscape. The lack of terrestrial paleoclimate proxies at low and southern latitudes impedes our understanding of the mechanisms for and extents of climate changes on sub-Milankovitch timescales, and ultimately general climate dynamics (Seager and Battisti (2007)). Observed changes in low latitude glacier lengths, since the Last Glacial Maximum (LGM) (26,000 - 19,500 years ago or 26.5 - 19.5 ka), coupled with numerical modeling of glacier-climate interactions and ice dynamics can help improve this limited paleoclimate proxy record.

If past changes in tropical glaciers lengths primarily reflect temperature changes, as is the case in the mid and high latitudes (Anderson and Mackintosh (2006)) and might be expected by extrapolating the results from Chapter 2, then paleoclimate reconstructions from tropical mountain glaciers would provide constraints on past regional temperature changes. In the tropics, high-altitude surface and free atmosphere temperatures deviate only sightly (Seidel and Free (2003); Bradley et al. (2006)), linking temperature change at tropical glaciers to changes in the free atmosphere. Also, low latitude horizontal free atmosphere temperature gradients are relatively homogeneous due to the weak Coriolis Force in low latitudes, which

allows for internal waves to dampen out temperature gradients (i.e. the Weak Temperature Gradient (WTG) approximation) (Pierrehumbert (1995); Sobel et al. (2001)). By the WTG approximation, changes in free atmosphere temperatures at a specific location can be related to broader regional changes at elevation. In addition, low latitude free atmosphere temperature profiles are dictated by moist convection and the Hadley and Walker circulations, and these dynamical processes link changes in sea surface temperatures (SSTs) to free atmosphere temperature changes according to the moist adiabat curve (Xu and Emanuel (1989); Pierrehumbert (1999); Williams et al. (2009)). Figure 3.1 illustrates the very strong correlation between tropical SSTs and free atmosphere temperatures at the elevation, latitude, longitude to the Quelccaya Ice Cap, Peru. Consistent with the nonlinear lapse rate structure of the tropical atmosphere, temperature changes at elevation are enhanced relative to the corresponding SST changes (by a factor of almost 2). These structures of the tropical atmosphere allow paleotemperature reconstructions for a specific tropical glacier to provide paleotemperature information for other regional glaciers and regional paleo-SSTs.

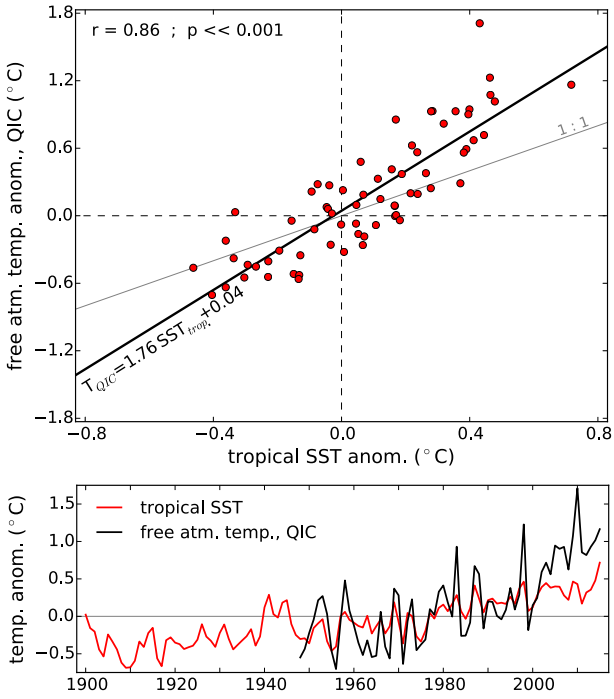

Figure 3.1: Relationship between tropical SSTs (red) and 500 mbar air temperatures (black) at the grid cell closest to the Quelccaya Ice Cap. Correlation between SST anomalies and free atmosphere anomalies (top) and the time series of both (bottom). Tropical SSTs are from 20°N to 20°S. Data: SSTs: NOAA ERSST.v4 (Huang et al. (2015)); atmospheric temperature: NCEP-NCAR Reanalysis I (Kalnay et al. (1996)).

Before conducting such paleoclimate reconstructions, some outstanding questions must be addressed. First, the climate drivers of tropical glacier length changes are poorly understood. The relative importance of temperature versus precipitation in driving tropical length changes is hotly debated (Kaser et al. (2004); Taylor et al. (2006); Thompson et al. (2006); Vuille et al. (2008b); Licciardi et al. (2009); Jomelli et al. (2011); Thompson et al. (2013); Stroup et al. (2014); Jomelli et al. (2014)). Minimal publications, however, have tried to address this question using numerical models to determine drivers of tropical glacier length changes. Second, the climate interpretation of glacial geomorphic features is not fully understood. Glacier landscape features, such as terminal and lateral moraines, are often associated with the equilibrium glacier position, which is determined by the climate (Oerlemans (2001)). Glacier length fluctuations in modeling studies, however, can occur as a

result of mass balance anomalies stemming from interannual climate variability within an unchanging mean climate state (Oerlemans (2000); Roe and O'Neal (2009); Huybers and Roe (2009); Roe (2011); Roe and Baker (2014)). A downslope excursion beyond the equilibrium length forced by interannual climate variability may remove the features outlining the equilibrium position or move those features further down-slope (e.g. push moraine), thus detaching the glacial geomorphic record from the climate signal. In a study of LGM features in the Rocky Mountains, the mean glacier length ranged between 3% to 50% up-valley from the furthest downslope excursion, and any climate reconstructions from moraines would overestimate LGM climate change (Anderson et al. (2014)). In order to utilize the moraine record at the QIC as a paleoclimate proxy, the climatic drivers of length changes and response to interannual climate variability must be assessed .

This chapter presents results from three experiments for the Huancané outlet glacier of the Quelccaya Ice Cap (QIC), Peru, using a 1-D numerical flow-line model to address the above questions above and provide paleoclimate reconstructions for the Little Ice Age (LIA) ($\sim$ 1330 - 1850 CE) and Younger Dryas (YD) ($\sim$12.8 - 11.5 thousand years ago (ka)). In Experiment 1, the equilibrium glacier length sensitivity of the Huancané glacier to temperature, precipitation rate, and summit accumulation rate changes is investigated. In Experiment 2, the glacier length response to interannual climate variability is determined. In Experiment 3, temperature and precipitation rate changes that can produce the LIA and YD glacier lengths are quantified.

3.0.1 Quelccaya Ice Cap Setting and Glacial Chronology

The QIC, located in the Cordillera Oriental of the Andes [13.9°S; 70.9°W; 55 km^2; summit altitude 5670 m a.s.l.; Figure 3.2], sits atop an ignimbrite plateau with multiple valleys connecting the plateau to the surrounding landscape that contain glacial features (Mercer et al. (1975); Mercer and Palacios (1977); Goodman et al. (2001); Mark et al. (2002); Kelly et al. (2012); Stroup et al. (2014); Kelly et al. (2015)). The Rio Huancané valley, on the southwest

side of the ice cap (Figure 3.2), contains three prominent moraine belts: 1) Huancané I (Hu-I) (∼ 1 km downslope); 2) Huancané II (Hu-II) (∼ 4 km downslope); and 3) Huancané III (Hu-III) (∼ 8 km downslope) (Mercer et al. (1975); Mercer and Palacios (1977)). The Hu-I moraines date to the LIA ((Mercer et al. (1975); Mercer and Palacios (1977); Stroup et al. (2014)) and may mark the the maximum Holocene glacier extent (Stroup et al. (2014)). The Hu-II moraines mark a readvance of the glacier at the end of the Lateglacial Period (Mercer and Palacios (1977); Goodman et al. (2001); Kelly et al. (2012); Kelly et al. (2015)) and have been constrained to 12.35 +0.2, -0.02 ka, indicating an ice advance during the early to middle YD (Kelly et al. (2012); Kelly et al. (2015)). The Hu-III moraines are attributed to the LGM or a standstill in the early part of the retreat from the LGM (Mercer and Palacios (1977); Goodman et al. (2001); Kelly et al. (2015)) and are not studied here.

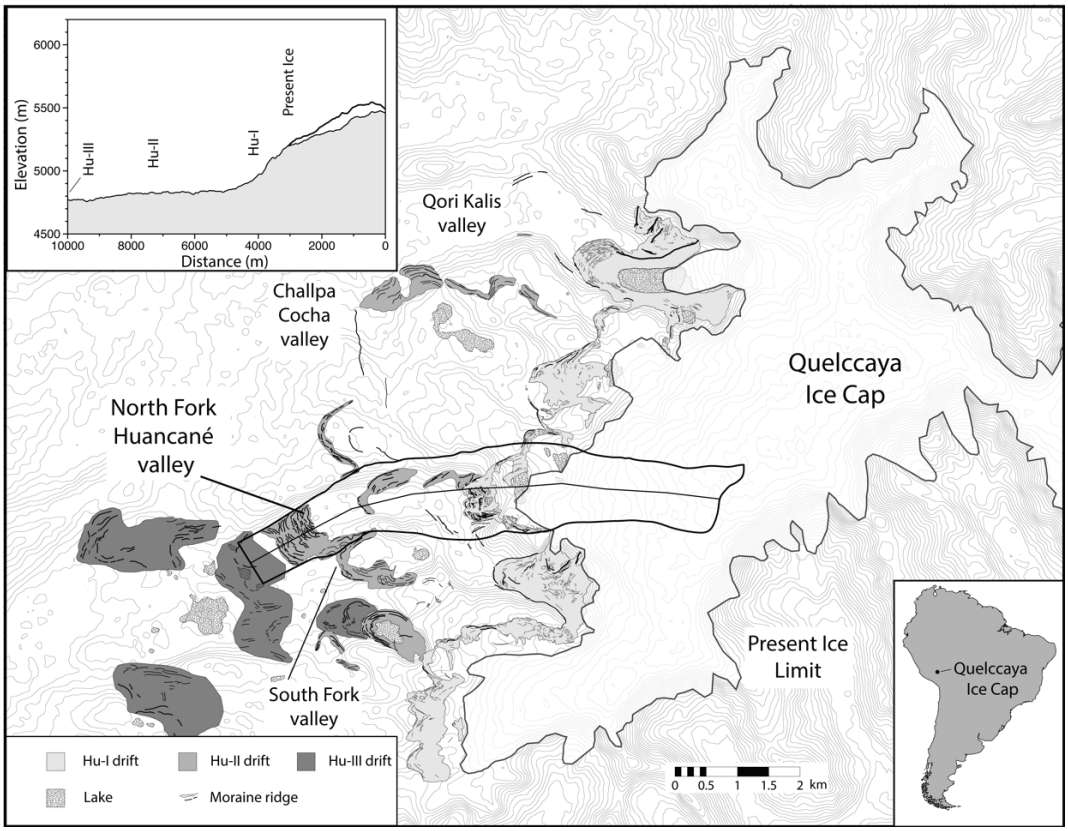

Figure 3.2: Glacier geologic map of the three outlet glaciers on the west side of the Quelccaya Ice Cap. The outlined area indicates the North Fork of the Rio Huancané Valley (focus area). The flowline along the valley is indicated by the line in the middle of the outline. The insert in the top left is the characteristic bedrock profile of the valley. Adapted: Kelly et al. (2012).

3.1 Methods

A shallow-ice 1-D glacier flowline model is coupled to a surface energy and mass balance (see Chapter 2.2.1) model to simulate the surface mass loss and gain and interior mass transport. From this coupled modeled, the glacier length for a given set of climate conditions can be calculated. Both equilibrium and transient simulations are conducted. Similar methods have been used (although ablation schemes have varied) to quantify glacier length sensitivity to different types of climate change, make predictions about future glacier glacier length changes, and reconstruct paleoclimates associated with glacial geomorphic features (e.g. Oerlemans (1986); Oerlemans (1997a); Oerlemans (1997b); Oerlemans (2000); Roe and O'Neal (2009)).

3.1.1 Glacier Flow Model

The shallow-ice 1-D flowline model has been shown to capture the dynamics of mountain glacier flow (Oerlemans (1986)). The governing equation is the 1-D mass continuity equation for a constant density fluid:

$$\frac{\partial}{\partial t}H = -\frac{1}{w}\frac{\partial}{\partial x}(u\ H\ w) + b \tag{3.1}$$

where H is the ice thickness, t is time, w is the valley width, x is the position along the flowline, u is the sum of the vertically averaged deformation velocity (u_d) and sliding velocity (u_s) in the direction of the flowline, and b is the surface mass balance (see Chapter 3.1.2). The trapezoidal approximation is used for w (see Oerlemans (1997a)). Velocity relationships follow Oerlemans (1997a) and Oerlemans (2001):

$$u_d = f_d H \tau^3 \tag{3.2}$$

and

$$u_s = f_s H^{-1} \tau^3 \tag{3.3}$$

where τ is the local driving stress (-ρ g H $\frac{\partial H}{\partial x}$), g is the acceleration of gravity, ρ is the ice density (900 kg m^{-3}), H is the ice thickness, $\frac{\partial H}{\partial x}$ is the the slope of the glacier surface, f_d is the deformation parameter, and f_s is the sliding parameter. $f_d = 1.9 \times 10^{-24}$ Pa^{-3} s^{-1} and $f_s = 5.7 \times 10^{-20}$ Pa^{-3} m^2 s^{-1} (Oerlemans (1997a)). Shuttle Radar Topography Mission (http://www2.jpl.nasa.gov/srtm/) data are used to construct the flowline geometry. The spatial resolution is 50 m and the model domain extends 250 m beyond the characteristic position of the Hu-II moraines. Eq. 3.1 is solved using the Crank-Nicholson method with a time-step of one model month.

3.1.2 Surface Energy and Mass Balance Model

The surface mass balance, b, is the difference between the solid precipitation and the ablation at each position, x, along the flow. The mass loss from melting and sublimation is described by Eq. 1.1 and Eq. 1.2. where the available melt energy is described by Eq. 1.3. Extensive details about surface energy and mass balance modeling can be found in Chapter 2.2.1. The model parameters and variables are constrained using monthly mean data from the meteorological station on the ice cap summit managed by the University of Massachusetts (correspondence with Dr. Doug Hardy). Monthly mean rainfall data from the Tropical Rainfall Measuring Mission (TRMM) (Bookhagen and Strecker (2008)) are used to determine the contemporary precipitation rate and seasonality. TRMM data, however, produce less net annual precipitation than the typical annual accumulation found towards the top of the summit ice core (Thompson et al. (2013)), and as such, the TRMM data are scaled up to a precipitation rate of 1.34 m w.e. a^{-1}, which can produce the observed recent summit accumulation rate while producing the modern terminus position. The valley air temperature profile is assumed to be linear over the range of the glacier, with a lapse rate of 5.4°C km^{-1}, which is the value for the ice cap from Bradley et al. (2009). Experiments are also conducted with a temperature-dependent lapse rate.

3.1.3 Equilibrium Glacier Length Simulations (Experiments 1 & 3)

In Experiments 1 and 3, the equilibrium glacier length and accumulation rate along the flowline are determined for a given temperature and precipitation pairing. The model is initiated with a zero-height profile and run until it reaches an equilibrium profile. To perturb the climate, the mean summit temperature is varied from -2.50°C to 1.15°C around the contemporary value in increments of 0.05°C and the precipitation rate is varied from -90% to +225% times the contemporary value in increments of 5%. In Experiment 1, the temperature or precipitation rate is fixed at the contemporary signal while the the other climate forcing is varied, running the model to equilibrium each time. In Experiment 3, the model is run to equilibrium with each pairing of temperature and precipitation rate changes (n = 4,864), and the combinations of perturbations that can produce an equilibrium glacier length that reaches the characteristic position along the flowline of the Hu-I or Hu-II moraines are determined . For the Hu-I moraines (LIA-aged), the decadal-average summit accumulation record (Thompson et al. (2013)) is utilized to determine the combinations of temperature and precipitation rate changes that can both advance the glacier to the Hu-I position and produce the observed summit accumulation rate at the time of moraine deposition. Temperature and precipitation pairings that could have advanced the glacier downslope to the Hu-I and Hu-II moraines are determined, because these features are within the same valley basin. The Hu-III moraine features cannot be reconstructed, since the glacier likely extended above the current valley basin, requiring methods beyond the scope of this chapter.

In Experiment 3, the method from Pierrehumbert (1999) is utilized to relate temperature changes at the elevation of the ice cap to their corresponding temperature changes at sea level, by extrapolating along the saturated moist adiabatic temperature profile. For this method to be appropriate, both the WTG approximation and the assumption that the atmospheric temperature follows the saturated moist adiabatic curve must hold true. The

WTG approximation is validated by calculating the 500 mbar free atmosphere temperature at the QIC latitude using NCEP-NCAR R1 output (Kalnay et al. (1996)), finding that the temperature varies by less than $\pm 1^{\circ}$C along a longitudinal sweep, which is consistent with the WTG approximation (Pierrehumbert (1995)). The assumption about the tropical temperature structure is validated by calculating the locally linear lapse rate at the QIC summit station for the moist adiabat curve that produces the observed summit temperature at the elevation of the meteorological station, finding it to be $\sim 5.4^{\circ}$C km^{-1}, which agrees with previously published values (Bradley et al. (2009)). Also, as illustrated in Figure 3.1, the free atmosphere temperatures near the Quelccaya Ice Cap agree well with the assumption that the temperature profile follows the saturated moist adiabatic. Although the moist adiabat curve is nonlinear, it is linear to first order over the elevation range of the QIC, allowing for a constant lapse rate to be used in the surface energy and mass balance model. Over greater elevation ranges, however, this non-linear structure is important. The locally linear lapse rate of the moist adiabat curve steepens with height, which amplifies temperature changes in the free atmosphere at the hight elevations of Peruvian Andes glaciers relative to the corresponding SST changes (also see Figure 3.1).

In both Experiments 1 and 3, two different lapse rate schemes are used, In the first scheme, the lapse rate is held fixed at the contemporary value (5.4°C km^{-1}). For the second scheme, the locally linear lapse rate in the valley varies with changes in the mean temperature. Since the temperature profiles follow the moist adiabat curve, which has a curvature that is dependent on regional temperatures, the slope of the linear lapse rate varies as the mean temperature changes. As regional temperatures increase, the lapse rate at the elevation of the QIC decreases, and as regional temperatures decrease, the locally linear lapse rate increases. For a one degree cooling, the locally linear lapse rate increases from 5.4°C to 5.52°C, and for a one degree warming, the locally linear lapse rate decreases to 5.28°. These changes, although small in magnitude, may be important in quantifying glacier length sensitivity to climate change and the specifics for paleo-SST reconstructions.

3.1.4 Transient Glacier Length Simulations (Experiment 2)

In Experiment 2, interannual temperature and precipitation rate variability are added to the climate signal while not changing the mean state. The model is spun-up to equilibrium without climate variability, and once the equilibrium length is reached, stochastic noise is added to both the temperature and precipitation signals. Once noise is added, the model is run for 11,000 years. The stochastic noise term is produced by a Gaussian random number generator with a prescribed standard deviation (1-σ value). The climate perturbations are uncorrelated from one model-year to the next but persist for the entire model year. The time duration of these perturbations affects the magnitude of the glacier response, with a one time-step duration (one model-month) perturbation producing a smaller magnitude glacier length response than a perturbation that persists for an entire year. For consistency with previous studies (e.g. Roe and O'Neal (2009); Huybers and Roe (2009); Roe (2011); Roe and Baker (2014); Anderson et al. (2014)), the correlation is one model year. Also for consistency, the temperature and precipitation rate anomalies are uncorrelated with each other. For the temperature variability, the annual mean but not the seasonal cycle is perturbed, and for the precipitation rate variability, only the net annual precipitation is perturbed. Simulations are run with a 1-σ value for the mean annual temperature time series ranging from 0.0°C to 0.75°C, in intervals of 0.05°C and a 1-σ value of the net annual precipitation rate time series ranging from 0% to 50%, in increments of 5%. Simulations are conducted for each pairing of temperature and precipitation variability (n = 176). For statistics, the first 1,000 years of output are discarded, and only the last 10,000 years are used.

3.2 Results

3.2.1 Equilibrium Glacier Length Response

The glacier responds differently to summit air temperature changes than to precipitation rate changes (Figure 3.3a). The rate of glacier length change due to air temperature changes varies across the valley, depending on the valley slope and to a lesser degree the lapse rate scheme. In contrast, the rate of length change due to precipitation rate changes is constant for most of the valley. The slope of the Huancané valley steepens along the flowline from the top of the ice cap to the base of the plateau (∼4,700 m along the flowline) at which point the slope becomes negligible (<1°) (see insert of Figure 3.2). Along the steepest section (from roughly the current ice margin past the Hu-I moraines to the base of the plateau), the length changes due to air temperature changes are the smallest, with a rate of ∼1,000 m per °C for the contemporary lapse rate scheme and ∼900 m per °C for the temperature-dependent lapse rate scheme. Upslope from the current ice margin to ∼2,000 m along the flowline, the valley slope is shallower, and the rate of length change increases, with a rate of ∼1,750 m per °C (contemporary lapse rate) or ∼1,700 m per °C (temperature dependent lapse rate). The topmost ∼2000 m of the valley has the shallowest bedrock slope (until the base of the plateau), and the rate of change is even larger, with a rate of ∼4,200 m per °C (contemporary lapse rate) and ∼4,250 m per °C (temperature dependent lapse rate). The length change due to a precipitation rate change is constant from the point of deglaciation to the base of the plateau, with a rate of ∼1,000 m per doubling in the precipitation rate. When the terminus reaches the base of the plateau, slight changes in either temperature of precipitation rate result in large length changes.

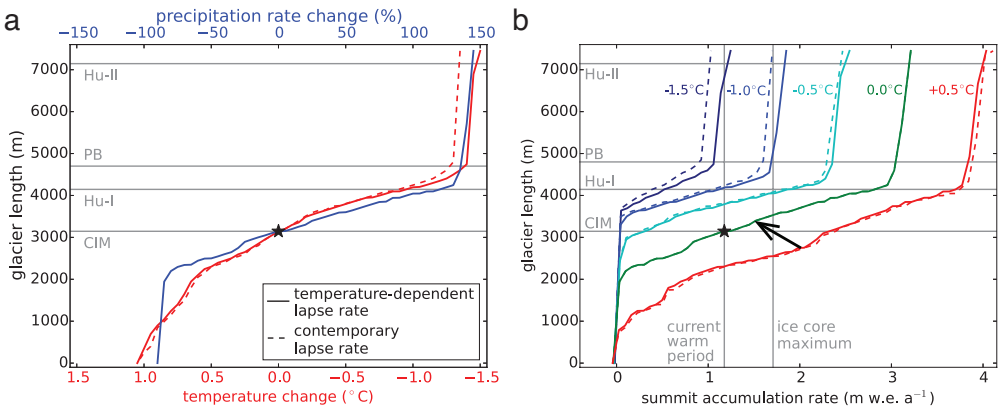

Figure 3.3: Climate drivers of Huancané glacier length changes. a) Glacier length sensitivity to precipitation rate changes and temperature changes. Notice the difference in scale of the x-axes. b) Glacier length sensitivity to summit accumulation rate changes along different summit isotherms ranging from -1.5° (dark blue curve) to +0.5°C (red curve). The black arrow indicates a 600 m glacier advance as a result of a 0.50 m w.e. a^{-1} reduction in the summit accumulation rate and a 0.50°C cooling. The current accumulation rate and maximum decadal-average accumulation rate from the QIC ice core record (Thompson et al. (2013)) are plotted. In both figures, the current climatology is indicated by the black star, and the location of the current ice margin (CIM), Hu-I moraines (Hu-I), Hu-II moraines (Hu-II), and plateau base (PB) are indicated.

The summit accumulation rate record also provides information about glacier length change but must be interpreted with knowledge of the ice cap air temperature (Figure 3.3b). For a fixed summit air temperature, the glacier will advance with increased summit accumulation and retreat with decreased summit accumulation. Significant glacier length advances, however, can occur at a fixed or even decreasing summit accumulation rate because of air temperature cooling at the summit (black arrow in Figure 3.3b). For most of the valley, air temperature changes produce greater length changes than those produced by changes in the summit accumulation rate, but once the terminus reaches the plateau base, the glacier becomes highly sensitive to any climate change.

To compare the importance of each climate forcing, the temperature or precipitation rate change required to advance the glacier to nearest moraine location is determined. An advance to the Hu-I moraine location (∼1 km downslope), in the absence of an air temperature cooling, requires a precipitation rate increase of 120% (1.60 m w.e. a^{-1} increase) or summit

accumulation rate increase of 140% (1.64 m w.e. a^{-1} increase). The largest observed increase in the decadal-average accumulation rate from the QIC ice core record is ∼45% (0.53 m w.e. a^{-1}) relative to the Current Warm Period (Thompson et al. (2013)), which in the absence of a cooling would only produce a ∼400 m length advance if sustained long enough for the glacier to reach a new equilibrium position. In contrast, an advance to the Hu-I moraines due to only air temperature changes, requires only a cooling of 0.90°C (contemporary lapse rate) or 0.95°C (temperature dependent lapse rate). Experiment 1 highlights the strong relationship between temperature changes and glacier length changes and the weaker relationships between glacier length changes and precipitation rate or accumulation rate changes. It also highlights the importance of cooling in the formation of observed glacial features in the Huancané valley.

3.2.2 Interannual Climate Variability Response

To quantify the expected glacier length fluctuations from contemporary climate variability at the QIC, contemporary temperature and precipitation rate variability is determined using the CRU Ts v3.22 monthly mean observational data product (Harris et al. (2014)). The 1-σ value for the detrended annual mean temperature time series is 0.52°C, and for the annual precipitation time series, it is 15% (Figure 3.4a). The two anomalies are uncorrelated (r = -0.10), consistent with the methodology. For these climate variabilities, the 1-σ value of the glacier length time series (magnitude of the glacier length fluctuations) is 134 m (Figure 3.4b). Assuming that the 3-σ value of the glacier length time series is the maximum excursion that could produce an observable feature, glacial features within ∼400 m of the terminus may be accounted for by glacier fluctuations due to interannual climate variability, which is far less than the advance necessary to the produce the closest moraine features (∼1 km downslope). In simulations with the observed climate noise, however, the mean glacier terminus position also retreats 300 m upslope, reducing any downslope excursions of the glacier beyond the equilibrium terminus position in simulations without climate variability.

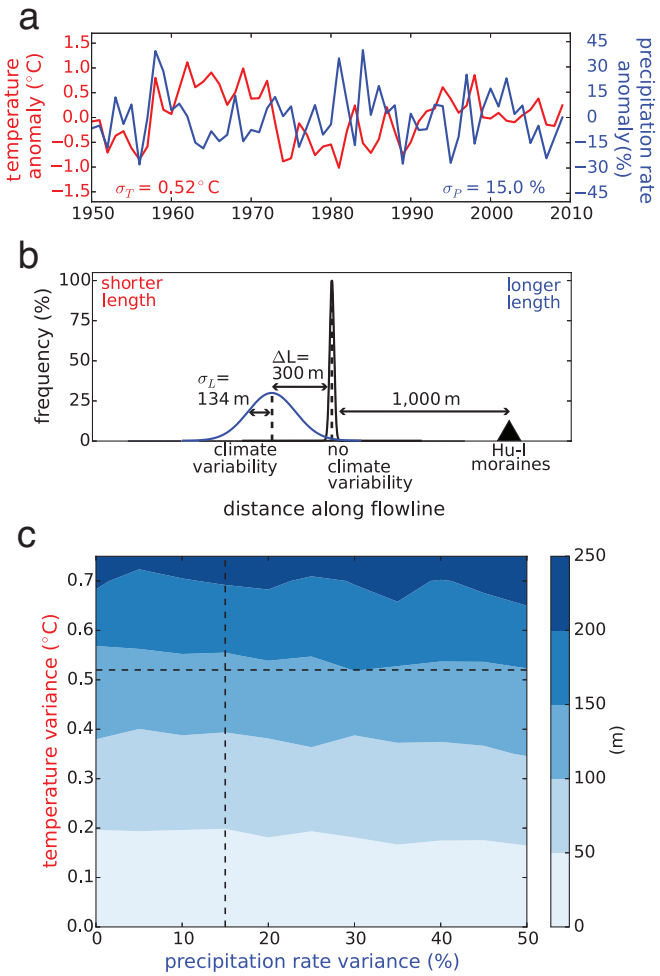

Figure 3.4: Climate variability and glacier response to variability. a) Detrended mean annual temperature anomalies and net annual precipitation anomalies from (01/1950 - 12/2009) The magnitudes of temperature and precipitation rate variability are included (1-σ values) and the correlation coefficient between the two time series is r=-0.10, indicating minimal covariance in climate signals. Data: CRU-TS v.322 (Harris et al. (2014)). b) Huancané glacier response to observed climate variability. Without climate variability, the terminus remains constant (black delta function), but with climate variability, the terminus both fluctuates around a mean position and retreats upslope to a new mean position (blue normal distribution). The magnitude of the upslope retreat is indicated (ΔL) as well as the magnitude of glacier length fluctuations (σ_L) are included. c) Magnitude of glacier length fluctuations (σ_L) due to a range of climate variabilities. The observed precipitation rate (vertical dashed line) and temperature (horizontal dashed line) variability is indicated. Glacier length fluctuations depend primarily on temperature variability and are mostly independent of precipitation rate variability.

The Huancané glacier also responds differently to noise in the temperature signal (tem-

perature variability) than to noise in the precipitation rate signal (precipitation variability) (Figure 3.4c). The magnitude of glacier length fluctuations increases with greater temperature variability but is mostly invariant to the amount of precipitation variability. The maximum 1-σ value of the glacier length fluctuations is 244 m and occurs when the temperature variability is the largest (1-σ value of the temperature series is 0.75°C). When the temperature variability is <0.2°C, the 1-σ value of the glacier length fluctuations is less than 50 m (i.e. smaller than the model spatial resolution). The upslope retreat of the mean glacier terminus position in simulations with climate noise also depends on the amount of temperature variability and is mostly insensitive to the amount of precipitation variability. The maximum upslope retreat is 700 m and corresponds with the largest temperature variability (0.75°C). Experiment 2 highlights different responses of the glacier to temperature and precipitation rate variability and also illustrates that downslope excursions of the glacier due to interannual climate variability cannot produce the glacier features in the Huancané valley without there also being a change in the mean climate state, which likely includes a temperature cooling (Experiment 1).

3.2.3 Paleoclimate Reconstructions

Combinations of temperature and precipitation rate changes that can produce an equilibrium glacier length at the position of the Hu-I moraines (LIA-age) and Hu-II moraines (YD-age) are found (Figure 3.5). Further constraints are placed on the LIA changes by utilizing the the QIC ice core record (Thompson et al. (2013)) and assuming that the Huancané valley LIA glacier chronology matches that chronology for the QIC's adjacent Qori Kalis valley. In the Qori Kalis valley, the glacier retreated from its maximum LIA extent ∼1490 CE ± 60 years and readvanced to a lesser extent between 1660 CE and 1710 CE (Stroup et al. (2014)). The climate forcing associated with the earlier moraine age must have predated the reconstructed age, placing the climate forcing during a period of decreased summit accumulation (∼13% decrease) (Thompson et al. (2013)). The age of the readvance (younger

LIA age) is concurrent with the tail end of a period of increased summit accumulation (∼27% increase) (Thompson et al. (2013)), and the climate forcing associated with the readvance most likely includes increased accumulation.

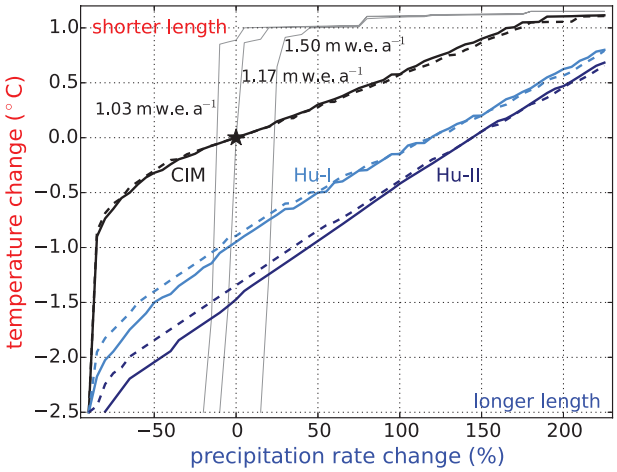

Figure 3.5: Air temperature and precipitation rate changes that can produce a glacier length at the current ice margin (CIM), Hu-I moraines (Hu-I), or Hu-II moraines (Hu-II) for the contemporary lapse rate (dashed curves) and temperature-dependent lapse rate (solid curves). The summit accumulation rate is calculated for each temperature and precipitation rate change, and the thin grey curves indicate the accumulation rate for the current period (1.17 m w.e. a^{-1}), the earlier LIA period (1.03 m w.e. a^{-1}), and the later LIA period (1.50 m w.e. a^{-1}) (Thompson et al. (2013)). The black start indicates the current climatology.

For the earlier LIA moraine age (∼1490 CE ± 60), an air temperature cooling of 1.03°C for the contemporary lapse rate scheme or 1.13°C for the temperature-dependent lapse rate scheme and a precipitation rate decrease of ∼14% (0.19 m w.e. a^{-1}) produce an equilibrium glacier length at the Hu-I moraine position and a summit accumulation rate (1.03 m w.e. a^{-1}) for the period just before the earlier age. For the later LIA moraine age (1660 CE - 1710 CE), a cooling of 0.69°C (contemporary lapse rate) or 0.74° (temperature-dependent lapse rate) and a precipitation rate increase of 21% (0.28 m w.e. a^{-1}) produce an equilibrium length at the Hu-I moraines and the summit accumulation rate for the period before the later age (1.50 m w.e. a^{-1}). Extrapolating these summit air temperature coolings along the moist adiabat curve to sea level, they correspond to SST coolings of between 0.56°C and

0.62°C for the earlier period and between 0.38°C and 0.41°C for the later period.

The QIC ice core record does not extend into the late-Pleistocene, but constraints on the possible climate changes responsible for the Hu-II moraines can be made by exploring two types of precipitation rate changes. For the first, regional circulation is assumed not to change, and the precipitation rate scales with Clausius-Clapeyron, where a 1°C cooling results in a ∼7% decrease in the precipitation rate. For the second type, there is assumed to be changes in the regional circulation resulting in increased precipitation in the southern tropical Andes. GCM simulations suggest that increased northern hemisphere sea ice during the YD forced the intertropical convergence zone (ITCZ) southward (Chiang and Bitz (2005)), providing a mechanism for increased precipitation in the southern Tropical Andes during this time. Dynamic GCM simulations for the last 22,000 years indicate increased precipitation for the grid cells near the QIC during the YD (output from the TraCE 21k simulation; Liu et al. (2009); He (2011); He et al. (2013)). Also, geologic evidence supports increased regional precipitation during the late-Pleistocene, with higher lake levels at Lake Titicaca (Baker et al. (2001)), large paleolakes in southern Bolivia (Placzek et al. (2006)), and increased net accumulation at nearby Nevado Sajama (Bolivia) (Thompson et al. (1998)).

For the first type of precipitation rate change (Clausius-Clapeyron scaling), a greater cooling is required than for the second type (increased precipitation rate). For the first type, a summit cooling of 1.45°C (contemporary lapse rate) or 1.59°C (temperature-dependent lapse rate), corresponding to a precipitation rate decrease of ∼10% (0.14 m w.e. a^{-1}), produces an equilibrium glacier length at the Hu-II moraines. These summit air temperature coolings correspond to SST coolings of between 0.79°C and 0.87°C. For the second type of precipitation rate change, a 20% increase in the precipitation rate (consistent with output from the TraCE simulation; Liu et al. (2009); He (2011); He et al. (2013)), and a summit cooling of 1.14°C (contemporary lapse rate) or 1.24°C (temperature-dependent lapse rate) produce an equilibrium glacier length at the Hu-II moraines. These summit air temperature coolings correspond with SST coolings of 0.63°C and 0.68°C. For an upper extreme on YD

precipitation rate increases (and lower extreme on YD cooling), the precipitation rate is increased to 40%. With this drastically increased precipitation, summit coolings of 0.94°C (contemporary lapse rate) and 1.04°C (temperature-dependent lapse rate) produce an equilibrium glacier length at the position of the Hu-II moraines. These summit air temperature coolings correspond to SST coolings of between 0.52°C and 0.57°C.

3.3 Discussion

3.3.1 Climate Drivers of Glacier Length Change

Air temperature change is the major climate driver for length changes at the Huancané glacier of the QIC. The glacier advance for a 1°C cooling is between one and four times greater than the advance from a doubling in the precipitation rate. Air temperature changes have been shown to be the dominant mechanism for length changes for mid and high latitude glaciers (Anderson and Mackintosh (2006)), and this situation also seems to be true for tropical glaciers. Sagredo et al. (2014) show that wet tropical glaciers have a greater sensitivity in their equilibrium line altitude (ELA) to temperature changes than to precipitation rate changes and that many low-latitude glaciers have a greater temperature sensitivity than mid and high latitude glaciers. Furthermore, Sagredo et al. (2014) find that low-latitude glaciers require a precipitation rate increase of between ∼100% and ∼300% to balance the ELA change from a 1°C warming while mid latitude South American glaciers only require precipitation rate increases of ∼30%. For mid and high latitude glaciers, values of ∼25% have been more broadly used (Braithwaite and Zhang (2000); Oerlemans (2001)). For the QIC, a precipitation rate increase of ∼170% is needed to offset the retreat from a 1°C warming.

Climatology may account for why changes in tropical glaciers lengths are dominated by air temperature changes. Mild temperature seasonality in the tropics creates a relatively constant snowline (Kaser (1995)), limiting solid accumulation on tropical glaciers and thus restricting the size of the accumulation area. In addition, 70-80% of the QIC precipitation

falls during the austral summer (Thompson et al. (2013)), when the zero degree isotherm is the highest, and glaciers with maximum summer precipitation are especially sensitive to temperature changes (Fujita (2008b); Fujita (2008a)). Additionally, the shallow low latitude lapse rate causes larger vertical displacements of freezing level heights for a given temperature change than for glaciers with steeper lapse rates, further amplifying ELA changes (Sagredo et al. (2014)). Recent work finds that high-altitude mountain regions (where all tropical glaciers are found) have experienced amplified warming, which may further increase the sensitivity of tropical glaciers to regional air temperature changes (Pepin et al. (2015)). The especially high sensitivity of the Huancané glacier length to air temperature changes may also be due to the hypsometry of the ice cap (see insert in Figure 3.2). The accumulation area is a flat plateau, making the ice cap especially vulnerable to shifts in the freezing level height (Mark et al. (2002)). The large response of the Huancané glacier length to temperature changes should also be realized at other low-latitude glaciers, due to the constraints placed by climatology.

The results of this chapter illustrate that the observed glacier features in the Huancané valley could only have been formed during past cooler climates. To reproduce the Hu-I or Hu-II moraines in the absence of regional cooling requires a more than doubling of the precipitation rate, which far exceeds any long-term anomalies in the ice core accumulation record (Thompson et al. (2013)) or precipitation rate increases realized in GCM simulations of the late Pleistocene (Liu et al. (2009); He (2011); He et al. (2013)) and Holocene (González-Rouco et al. (2006)) (see Figure 3.6b and Figure 3.7b). Significant glacier advances, however, can occur during periods of unchanged or even decreased summit accumulation due to air temperature coolings (Figure 3.3b). The modeling results are consistent with interpretations from Stroup et al. (2014)), who suggest that regional cooling during a period of decreased summit accumulation provided the climate forcing for the maximum late Holocene glacier extent of the QIC's Qori Kalis glacier. Finally, the magnitude of glacier length fluctuations in response to climate variability is far less than what would be needed to form the downs-

lope glacial features in the Huancané valley. Glacier features within ∼400 m of the current ice margin could be accounted for by fluctuations of the glacier in response to interannual climate variability, but the closest downslope moraines require an advance of ∼1,000 m.

The response of the Huancané glacier differs from previous studies of mid latitude glaciers (e.g. Oerlemans (2000); Roe and O'Neal (2009); Huybers and Roe (2009); Roe (2011); Anderson et al. (2014); Roe and Baker (2014)). The magnitude of length fluctuations depends primarily on the magnitude of temperature variability and is insensitive to precipitation variability (Figure 3.4c), unlike for mid latitude glaciers where both temperature and precipitation play a role (Roe and O'Neal (2009); Roe and Baker (2014)). This strong dependence on temperature but minimal dependence on precipitation mirrors the trend for length sensitivity (Figure 3.3) and is likely also due to the climatology. Since the accumulation season is during the austral summer, the net precipitation that falls as snow is limited, thus decreasing the net mass balance response to precipitation variability. Temperature variability not only affects the melt rate in the ablation zone, but also the elevation of the freezing line, which in turn affects the positive mass balance side as well. In addition to producing length fluctuations, climate variability also causes changes in the mean length of the glacier. Increased temperature variability results in an upslope retreat of the glacier, suggesting that a glacier will retreat more from a few warm years than advance from a few cold ones. Some of this asymmetry between advance and retreat may also reflect variations in the slope of the bedrock (see insert in Figure 3.2). The upslope retreat of the mean terminus position with increased temperature variability suggests that the mean state of the glacier may be dependent on more than just the mean climate state (mean annual temperature and net annual precipitation). Fujita (2008b), Fujita (2008a), Vacco et al. (2009), and Sagredo et al. (2014) have shown that seasonality plays an important role in the glacier mass balance, length, and ELA, and the results from this chapter suggest that climate variability may also play a role in determining the mean glacier length.

3.3.2 Little Ice Age (LIA) Tropical Climate Change

Paleo-SST changes are reconstructed for two periods during the LIA based on the chronology at the Qori Kalis valley of the QIC. These two periods are concurrent with Northern Hemisphere temperature depressions (Mann et al. (2009)). Also late Holocene glacier fluctuations in the tropical Andes are concurrent with those in the Northern Hemisphere (Licciardi et al. (2009); Jomelli et al. (2009)). For the earlier period (1490 CE $\pm$ 60 years), a precipitation decrease of $\sim$14% and a regional SST cooling of between 0.56°C and 0.62°C is found. For the latter period (1660 - 1710 CE), a precipitation increase of $\sim$21% and a regional SST cooling of between 0.38 and 0.41°C is found. The González-Rouco et al. (2006) GCM simulation (GR) of the last millennium, forced with greenhouse gas reconstructions from ice cores, short-term solar variations, and volcanic aerosols, finds a cooling during these periods in the global and northern hemisphere surface temperatures and tropical SSTs (Figure 3.6a). During the earlier period, the GR output is 0.1°C to 0.15°C warmer than the reconstructions from flowline model. During the latter period, the GR output is 0.1°C to 0.15°C cooler. Discrepancies between flowline model reconstructions and the GR output may indicate uncertainties in the external forcings in the GR model (Zorita et al. (2004)). The TraCE-21 ka GCM simulation (TraCE) from the LGM to the present (Liu et al. (2009); He (2011); He et al. (2013)), in contrast, is only forced during the last millennium with greenhouse gas changes and Milankovitch forcings on insulation (correspondence with Dr. Feng He). TraCE output does not exhibit a LIA temperature signal in the global or northern hemisphere surface temperatures, and similarly does not show a LIA signal in tropical SSTs (Figure 3.6a). Neither GCM captures precipitation rate variability similar to that in the summit accumulation record (Figure 3.6b), suggesting that these GCMs are unable to capture QIC precipitation rate variability. Proxy reconstructions of SSTs in the NINO4 region (5°N to 5°S; 160°E to 150°W) from the QIC ice core record of $\delta^{18}0$ (Thompson et al. (2011)) find mild cooling during the later LIA period (readvance of the Qori Kalis valley (1660 - 1710

CE)) but no real trend during the earlier period (maximum glacier extent in the Qori Kalis valley (1490 CE ± 60 years)) (Figure 3.6a). Tropical SST reconstructions from Andean ice core δ^{18}O records, however, differ in magnitude and trend (e.g. Thompson et al. (1998); Pierrehumbert (1999); Thompson et al. (2011)).

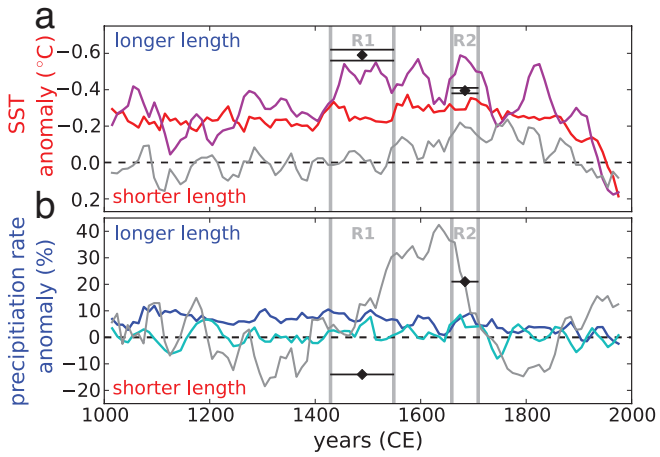

Figure 3.6: Little Ice Age paleoclimate reconstructions of a) SST anomalies from the TraCE GCM simulation (Liu et al. (2009); He (2011); He et al. (2013)) (red curve), the González-Rouco et al. (2006) GCM simulation (magenta curve), reconstructions for the NINO4 region from the Thompson et al. (2013) ice core record (grey curve), and this study (black diamonds with error bars) and b) precipitation rate anomalies from the TraCE simulation (blue), González-Rouco et al. (2006) GCM simulation (cyan), accumulation rate anomaly from the Thompson et al. (2013) ice core record (grey curve), and this study (black diamonds with error bars). R1 indicates the age-range of the earlier LIA period, and R2 indicates the age-range of the latter LIA period. SST anomalies from GCM outputs are for the region 1.8°S to 20.4°S; 108.7°W to 18.7°W. Precipitation rate anomalies from GCM output are for the grid cells adjacent to the QIC. All curves are decadal-average anomalies relative to the 1900 - 1990 CE mean and smoothed with a 30-year running mean.

The paleoclimate reconstructions from the flowline model agree well with the GCM simulation that includes climate forcing mechanisms believed to have been important in producing LIA climate changes. SST reconstructions from the modeling work at the QIC agree well with SST coolings realized in the GR simulation (González-Rouco et al. (2006)), which includes short-term insulation and volcanic aerosol forcings. Both the SST reconstructions from the glacier modeling and the GR simulation, however, disagree with the TraCE simulation (Liu et al. (2009); He (2011); He et al. (2013)), which does not include these forcings and does not

illustrate a LIA-like climate change. This disagreement and lack of a LIA signature in the TraCE simulation possibly highlights the importance of short-term insolation and volcanic aerosol forcings in producing the temperature trends over the last millennium. This analysis also supports the viability of using tropical moraine records and glacier flowline modeling to evaluate forcing mechanisms for past climate change events.

3.3.3 Younger Dryas (YD) Tropical Climate Change

YD paleo-SST changes are reconstructed and range between a cooling of 0.52°C and 0.87°C, with the lower bound corresponding to a 40% increase in precipitation and the upper bound corresponding to a scaling with Clausius-Clapeyron. For a ∼20% increase in the precipitation rate, which agrees with changes realized in the TraCE simulation during the YD (Liu et al. (2009); He (2011); He et al. (2013)), a SST cooling of between 0.63°C and 0.68°C could advance the glacier to the YD position. The TraCE simulation, which is forced with changes in sea ice extent, continental configurations, meltwater fluxes, and Milankovitch forcing on insulation, suggests that the early YD (12.8 - 12.4 ka) at the QIC was both colder (∼ 0.84°C tropical SST cooling) and wetter (∼20%) than present (Figure 3.7). The TraCE simulation, however, also shows a slight tropical SST warming (∼0.2°C) going from the Antarctic Cold Reversal (ACR) (13.5 - 12.8 ka) to the early YD, but this warming corresponds with ∼10% increase in precipitation at the QIC. The TraCE temperature anomalies agree with the results in the limit where the precipitation rate scales with Clausius-Clapeyron. For a 20% increase in precipitation, however, the reconstructed SST cooling is ∼0.20°C less than the TraCE simulation. The proxy record from tropical marine cores in similar regions is conflicting. The Lea et al. (2003) reconstruction for the Cariaco Basin core (10.7°N; 64.9°W) finds significant cooling (3°C - 4°C) from the late ACR to the YD, while the Hüls and Zahn (2000) core for the Tobago Basin (12.1°N; 61.2°W) finds mild warming from the ACR to the YD. Wan et al. (2009) illustrate how marine sediment core records capture local trends, which can differ from regional trends due to changes in sea level, ocean circulation, and

upwelling.

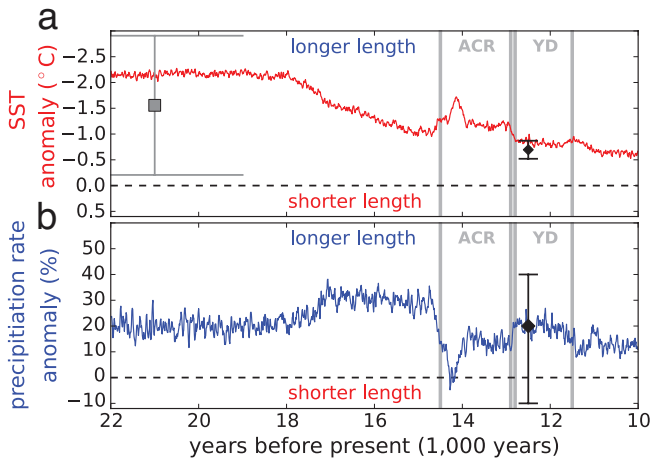

Figure 3.7: Younger Dryas paleoclimate reconstructions of a) SST anomalies from the TRaCE GCM (Liu et al. (2009); He (2011); He et al. (2013)) (red curve), MARGO SST reconstructions (Waelbroeck et al. (2009)) for the same region as the GCM (grey squares with error bars), and this study (black diamond with errors bars) and b) precipitation rate anomalies from the TraCE simulation (blue curve) and this study (black diamond with error bars). The geographic regions, averaging, and smoothing are the same as in Figure 3.6.

YD paleoclimate reconstructions using the moraine position and flowline modeling agree on a whole with climate changes realized in the TraCE simulation (Liu et al. (2009); He (2011); He et al. (2013)), which includes many of the hypothesized late Pleistocene forcing mechanisms. Both the reconstructions from the glacier record and the TraCE output indicate that the southern hemisphere tropics were colder and wetter than present. Despite the lack of tropical SST cooling going from the late ACR to the early YD in the TraCE simulation, the bedrock slope profile of the Huancané valley is such that if the terminus were near the plateau base, a slight temperature or precipitation forcing would result in a significant readvance of the glacier. Tropical SSTs in the TraCE simulation continue to gradually warm from the YD into the early Holocene, and such a warming trend would have quickly overpowered any mass imbalance that might have caused the readaveance to the Hu-II moraine, resulting in an upslope retreat. The geologic record in the Huancané valley suggests that the glacier retreated from the Hu-II moraines to almost the Hu-I position between ∼12.35 ka and 11.6

ka (Kelly et al. (2012); Kelly et al. (2015)). Such a glacier response would be the expected result for the gradual tropical SST warming realized in the TraCE simulation.

3.4 Concluding Remarks

In this chapter, a coupled surface energy mass balance and glacier flowline model is implemented to quantify the glacier length response to climate change and variability at the Huancané outlet glacier of the Quelccaya Ice Cap, Peru. This approach is able to reconstruct paleoclimates, both at the ice cap and regionally, for the Little Ice Age (LIA) and Younger Dryas (YD). The key results are the following:

1. Over the range of plausible changes in air temperature and precipitation rate, air temperature changes are the dominant climate forcing mechanism for glacier length changes. The glacier advance for a 1 °C cooling is about one to four times larger than the advance for a doubling in the precipitation rate. Also, the maximum observed decadal average accumulation rate increase from the ice core record (Thompson et al. (2013)) can not even produce half of the necessary glacier advance to form the LIA moraines, in the absence of a temperature cooling.

2. Glacier length fluctuations due to interannual climate variability are significantly smaller than the glacier advances necessary to form the Huancané valley moraines. Glacier features within ∼400 m of the current ice margin may have been produced by glacier fluctuations due to contemporary interannual climate variability, but glacier advances more than twice as great as that are needed to form the geomorphic observations.

3. The observed geomorphic features in the Huancané valley can only be explained by a change in the mean climate state and require some degree of cooling.

4. During the LIA, air temperature coolings at the ice cap are reconstructed to between ∼0.7°C and ∼1.1°C, and tropical SST coolings are reconstructed to between ∼0.4°C

and ∼0.6°C.

5. During the YD, air temperature coolings at the ice cap are bounded to between ∼0.9°C and ∼2.6°C, corresponding to tropical SST coolings between ∼0.5°C and ∼1.5°C

6. LIA and YD paleo-SST reconstructions from the Huancané geomorphic record and flowline model agree in magnitude and trend with GCM simulations that include forcing mechanisms that are believed to have been causes for the LIA and YD climate change events, indicating the viability of using moraine records from tropical glaciers in conjunction with flowline modeling to reconstruct tropical paleoclimate.

CHAPTER 4

HINDCASTS AND FORECASTS IN LIGHT OF MASS BALANCE NONLINEARITIES

The objective of this chapter is to illustrate how interannual climate variability can help to determine the mean state of a glacier, such as the long term length and net mass balance. Glacier length changes, especially for mid and high latitude glaciers, are usually attributed to changes in the mean climate state, with mean annual (or summertime) temperature changes being the main climate forcing for glacier length change (Oerlemans (2005); Anderson and Mackintosh (2006); Leclercq and Oerlemans (2012)). This relationship between temperature and length has made it possible to cite the nearly global contemporary retreat of glaciers as an indicator of anthropogenic climate change (Dyurgerov and Meier (2000); Vaughan et al. (2013)). Substantial length fluctuations, however, can also occur in an unchanged mean climate state (i.e. no change in the annual (or summertime) mean temperature or net precipitation), due to mass balance anomalies stemming from interannual climate variability (Oerlemans (2000); Roe and O'Neal (2009); Roe (2011); Roe and Baker (2014)). Changes in glacier length driven by mass balance anomalies stemming from interannual climate variability rather than from changes in the mean climate state complicate climatological interpretations of past glacier length changes or forecasts for future evolution. Previous work on interpreting glacier length fluctuations due to climate variability has linearized the mass balance anomalies stemming from interannual climate variability that drive the length fluctuations around the equilibrium state of the glacier, and thus the interannual climate variability does not affect the mean state of the glacier (e.g. Roe and O'Neal (2009); Roe (2011); Roe and Baker (2014)). Within this framework, the challenge becomes how to untangle glacier changes driven by variability from those driven by changes in the annual (or summertime) temperature and/or net annual precipitation (Anderson et al. (2014)).

A definition of the mean climate state that focuses primarily on mean temperature and

net precipitation may exclude additional aspects of the mean climate that are important for defining the mean state of a glacier. Temperature and precipitation seasonality have been identified as an additional component in the mean climate that can determine the mean glacier state (Fujita (2008b); Fujita (2008a); Sagredo et al. (2014)). Exemplifying how this additional aspect of the mean climate state can affect paleoclimate reconstructions, Vacco et al. (2009) illustrate how changes in seasonality (in addition to changing in the mean values of the climate variables) can reproduce the observed glacial moraine records in Greenland more consistently than by changing just the mean values of the climate variables. The magnitude of interannual climate variability itself may also be an important additional component of the mean climate state, as illustrated by results presented in earlier chapters. In Chapter 2, the long-term mass balance of a glacier is, in part, determined by the presence of interannual temperature variability. In Chapter 3, the mean length of the Huancané glacier can change even if the mean temperature and net precipitation remain the same because of changes in the magnitude of interannual temperature variability. Farinotti (2013) also finds that increasing the temperature variability produces significantly less ice volume and a smaller extent at Rhonegletscher, Switzerland, but his results indicate that future glacier evolution will be only minimally impacted by the expected changes in temperature variability. In some cases, additional aspects (beyond just mean annual (or summertime) temperature and net annual precipitation) of the mean climate are important for reconstructing past climates or forecasting future glacier evolution. For seasonality, Fujita (2008b) and Fujita (2008a) provide a framework for when the impacts could be substantial. A similar framework for when interannual climate variability could play a substantial role in impacting the mean state of a glacier has not been able to be located in the literature.

This chapter will accomplish two objectives. First, it will identify a mechanism through which interannual climate variability can produce changes in the mean state of a glacier. Second, it will provide a framework for when changes in interannual climate variability play a significant role in determining the mean state of the glacier. The chapter focuses on an

idealized representation of a tropical and mid latitude glacier to elucidate the fundamentals of the mechanism and compare and contrast how climate setting may impact the effects. Taken together, these objectives will improve interpretations of the climate signal embedded in records of past glacier changes and forecasts of future glacier evolution.

4.1 Methods

A shallow ice 1-D glacier flowline model (see 3.1.1 for details) is used to determine the length response of a glacier to interannual climate variability. 1-D flowline models are commonly used in the literature to determine glacier response to climate change and variability (e.g. Oerlemans (2000); Roe and O'Neal (2009); Roe and Baker (2014)). In this study, the rate mass loss and gain at the glacier surface is assumed to follow an elevational relationship, with lower elevations having net mass loss over the course of the year and higher elevations having net mass gain. A common framework to visualize this elevation dependence is a vertical mass balance profile (see Figure 4.1). In addition to serving as an input into the 1-D flowline model, vertical mass balance profiles can also be used to determine the equilibrium line altitude (ELA) and the net mass balance for the glacier. The ELA is the elevation at which the vertical mass balance profile transitions from mass loss to mass gain. The net mass balance is calculated based on a glacier's elevation-area distribution by summing the products of the rate of mass loss or gain at an elevation and the percentage of glacier area at that elevation.

Glaciers in different climate settings tend to have different vertical mass balance profiles, reflecting the specifics of the glacier-climate interactions in their climate setting (Kuhn (1981)). Tropical glaciers have particularly large mass balance gradients (i.e. the rate at which mass is lost/gained over a change in elevation) in their ablation zones and much smaller mass balance gradients in the accumulation zone (Kaser et al. (1996); Kaser (2001); Kaser and Osmaston (2002)). Mass balance gradients in the ablation zone for mid latitude glaciers tend to be smaller than for tropical glaciers (Kaser (2001)), but ablation zone mass

balance gradients still tend to be larger than those in the accumulation zone (*World Glacier Monitory Service 2015 Bulletin*). To zeroth order, the vertical mass balance profiles in the ablation and accumulation zones are linear but with different slopes, intersecting close to the equilibrium line altitude (ELA) (Benn et al. (2014)). In this chapter, modified mass balance gradients from Kaser (2001) are used. Their values are in Table 4.1.

Table 4.1: Representative mass balance gradients

	Tropical Glaciers	Mid Latitude Glaciers
$a^{\dagger}_{abla.}$	2.0 m w.e. a^{-1} per 100 m	0.5 m w.e. a^{-1} per 100 m
$a^{\dagger}_{accum.}$	1.0 m w.e. a^{-1} per 100 m	0.5 m w.e. a^{-1} per 100 m

† $a_{abla.}$ and $a_{accum.}$ are the gradients in the ablation and accumulation areas.

Before conducting transient simulations to quantify the glacier response to interannual climate variability, the glacier is spun-up to an equilibrium length for its representative vertical mass balance profile. An idealized valley geometry with a slope of 10° and a width that is twice as large at the summit than at the terminus is used to represent the topographic setting for both glaciers. Both glaciers have a length of 2 km, when in equilibrium with the representative vertical mass balance profile. Once in equilibrium, transient simulations with interannual climate variability begin.

4.1.1 Transient Glacier Length Simulations

After an equilibrium glacier length is reached for the represented vertical mass balance profile, a transient simulation is run, with interannual climate variability added to the representative vertical mass balance profiles. The mass balance response to perturbations caused by interannual climate variability is simulated by shifting the vertical mass balance profile, a common approximation for simulating how glaciers respond to climate change and variability (Meier and Tangborn (1965); Kaser et al. (2003)). Within this framework, temperature anomalies result in vertical translations of the vertical mass balance profile, with hot years moving

the profile to higher elevations and cold years moving the profile to lower elevations. The magnitude of the translation is the product of the temperature anomaly, ΔT, and the ELA sensitivity to temperature, $\frac{\partial ELA}{\partial T}$, which can be determined through field studies, modeling, or in this case is assumed to be the inverse of the atmospheric lapse rate, Γ. Precipitation anomalies cause horizontal translations of the vertical mass balance profile by the magnitude of the precipitation anomaly (ΔP). On a wet (or dry) year, the entire glacier gains that extra wetness (or dryness), and the mass balance profile is uniformly shifted to the right (or left). The net effect of temperature and precipitation anomalies is the superposition of the vertical translation (from the temperature anomaly) and the horizontal translation (from the precipitation anomaly) for each year (see Figure 4.1). 10,100 years of anomalous vertical mass balance profiles are produced and used to drive the 1-D flowline model.

The interannual temperature and precipitation anomalies that are used to perturb the vertical mass balance profiles are produced using a Gaussian random number generator with a prescribed standard deviation (1-σ value). The anomalies are uncorrelated from year-to-year and uncorrelated with each other. The magnitude of temperature variability, σ_T, is quantified by the 1-σ value of the temperature anomaly time series. The magnitude of precipitation variability, σ_P, is quantified by the 1-σ value of the precipitation anomaly time series. Both the tropical glacier and the mid latitude glacier are perturbed by the following climate anomalies: $\sigma_T = 0.75$°C and $\sigma_P = 0.50$ m w.e. a^{-1}. Additionally, simulations are conducted for both representative glaciers where only one of the types of interannual climate variability is used to perturb the mass balance profiles. For statistics on the output, the final 10,000 model years are used.

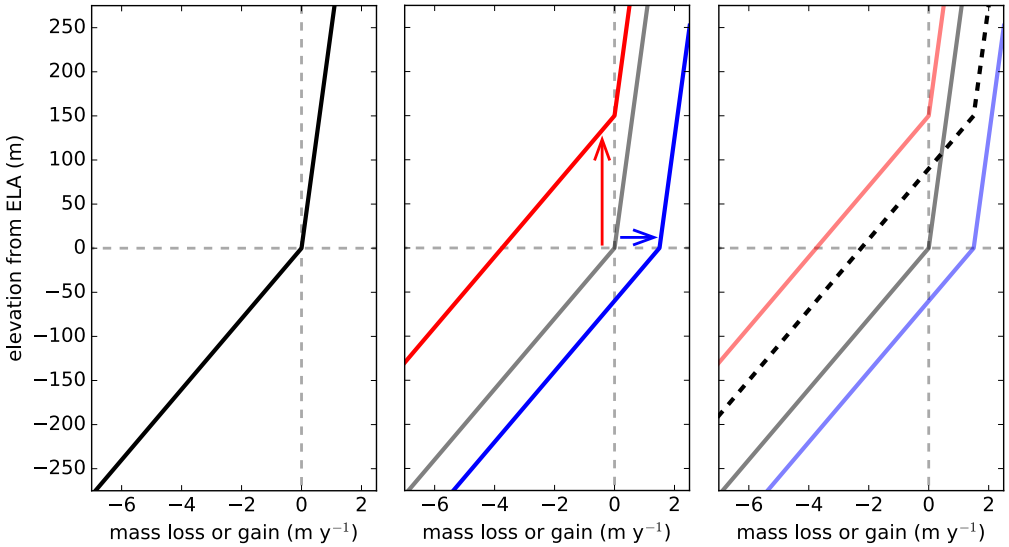

Figure 4.1: A representative vertical mass balance profile for tropical glaciers (left column) (adapted: Kaser (2001)). The vertical mass balance profile indicating a hot year (red) or a wet year (blue) (middle column). The net mass balance profile indicating a hot and wet year (dashed) (right column), which is the superposition of the vertical mass balance profile for a hot year and a wet year. These dashed lines are the anomalous mass balance profiles used to drive the numerical 1-D flowline model in the transient simulations.

4.1.2 Equilibrium Glacier Length Simulations

In addition to running transient simulations for both the representative tropical glacier and representative mid latitude glacier, the 1-D flowline model is also run to equilibrium for a series of additional vertical mass balance profiles. For both the tropical glacier and mid latitude glacier, the vertical mass balance profile representative of the climate setting, which is used in the spin-up the model, differs from the average vertical mass balance profile from the transient simulation, i.e. the aggregate vertical mass balance profile (see Figure 4.2). The flowline model is run to equilibrium with the aggregate vertical mass balance profiles.

Additionally, the equilibrium glacier length response to sustained climate change is determined. The mass balance response to climate change is simulated by translating the representative vertical mass balance profile vertically for temperature change and horizontally for precipitation change (see Chapter 4.1.1). The flowline model is run to equilibrium

with a perturbed mass balance profile that represents the response to sustained climate change.

4.2 Results

4.2.1 ELA and Net Mass Balance Variability

The equilibrium line altitude (ELA) and net mass balance provide two metrics to determine the static (i.e. no dynamic adjustment through length changes) response of a glacier to interannual climate variability. Histograms of the ELA anomalies and net mass balance anomalies, as well as the vertical mass balance profiles, are illustrated in Figure 4.2. For both the representative tropical and mid latitude glaciers, the average glacier response to the climate state that includes interannual climate variability differs from its response to the mean climate state (without variability. i.e. σ_T=0 and σ_P=0). This difference is more pronounced for the tropical glacier. The amount of anomalous mass loss and mass gain is book-kept at every elevation over the 10,000 year simulation with interannual climate variability and used to produce an aggregate vertical mass balance profile. The representative vertical mass balance profile for the climate state that does not include interannual climate variability differs from the aggregate mass balance profile. For both glaciers, the aggregate vertical mass balance profile has a higher ELA than the vertical mass balance profile without interannual climate variability, but the aggregate mass balance profile also has a smoother transition between the ablation and accumulation zones. The ELA shift to higher elevation is greater for the tropical glacier than the mid latitude glacier. For both glaciers, the 2 km spin-up length would be out of equilibrium with the aggregate vertical mass balance profile from the simulation with interannual climate variability, and this disequilibrium is negative, indicating that the glacier needs to retreat. The mass balance is calculated using the aggregate mass balance profile and the spin-up equilibrium glacier length is defined as the net mass balance anomaly, and it is more negative for the tropical glacier than the mid

latitude glacier. The addition of interannual climate variability produces a change in the mean state of the glacier that drives a dynamic glacier retreat.

The time series of ELA anomalies and mass balance anomalies in the simulation with interannual climate variability also provides insights. Both glaciers have a higher mean value of the ELA time series in the simulation with variability than in the simulation without variability, with this difference being greater for the tropical glacier. Similar to the results in Chapter 2, the mean of the ELA time series (i.e. mean ELA) for both glaciers is lower than the net ELA (i.e. the elevation at which there is no mass loss or gain over the 10,000 year simulation with interannual climate variability). The difference between the mean and net ELA is greater for the representative tropical glacier. The mid latitude glacier, however, has a slightly larger magnitude of ELA variability (as quantified by the standard deviation (1-σ value) of the ELA time series, σ_{ELA}). Looking at the net mass balance anomalies, as noted above, both glaciers have a negative net mass balance, suggesting that the spin-up glacier length is out of equilibrium with the aggregate mass balance profile and that the glacier will want to retreat upslope. Calculating the net mass balance anomaly for every year in the simulation with interannual climate variability, the mean of the mass balance time series is also negative. Unlike with the ELA anomalies, the mean and the net values are the same, as is also the case in Chapter 2. For the exact same climate forcing, the mass balance variability (as quantified by the 1-σ value of the mass balance time series, σ_b) is greater for the tropical glacier than the mid latitude glacier.

The time series also provides a means through which to explore the relative contribution of temperature and precipitation variability in producing the different responses of the glacier to the mean climate state (without variability) and the climate state with variability. The results discussed above, which include both interannual temperature and precipitation variability, are compared to simulations with only one type of interannual climate variability. In the absence of precipitation variability (i.e. only temperature variability), ELA fluctuations are normally distributed between higher and lower elevations, with a mean value that

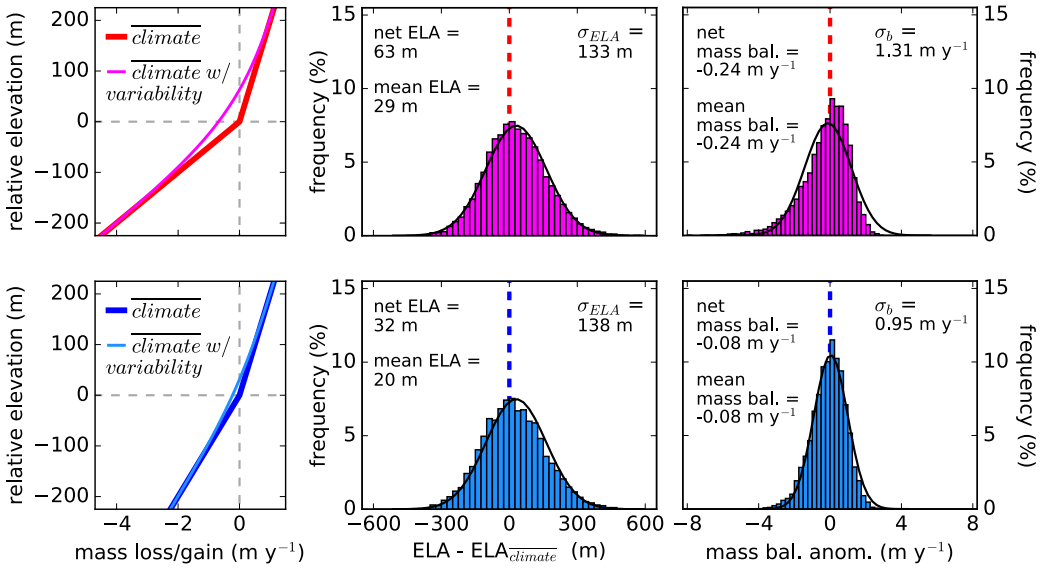

Figure 4.2: Vertical mass balance profile (left column), ELA (middle column), and mass balance (right column) response to interannual climate variability for a representative tropical glacier (upper row) and mid latitude glacier(bottom row). In the absence of variability ($\overline{climate}$), the ELA is at a relative elevation of zero and the mass balance anomaly is zero. For the two histograms, the black curves represent normal distributions with the same mean value and standard deviation as their respective time series. Net-values refer to quantities derived from the aggregate net mass balance profile from the simulation with variability ($\overline{climate}$ $w/variability$). Mean-values refer to the mean value of the time series from the simulation with variability. The dotted lines for the histograms represent the value from the simulation without climate variability. Mass balance is calculated for a static 2 km length glacier.

is the same as the ELA for the mean climate state (without variability). This ELA response is prescribed by how the vertical mass balance profile responds to temperature variability (i.e. vertical translations), and the magnitude of ELA variability (σ_{ELA}) in the simulation with only temperature variability is just the product of the ELA sensitivity to temperature ($\frac{\partial ELA}{\partial T}$) and the magnitude of the temperature variability (σ_T). With only temperature variability, however, the net ELA, i.e. the elevation at which there is zero cumulative mass loss or gain over the entire 10,000 years, is the same as it is in the simulation with both temperature and precipitation variability. Also the glacier-wide mass balance in the simulation with only temperature variability is the same value as it is in the simulation with both

types of climate variability. In the absence of temperature variability (i.e. only precipitation variability), there is an asymmetry in the ELA time series, and the mean ELA is the same as it is in the simulation with both temperature and precipitation variability. The net ELA, however, is zero, and the net (and mean) mass balance is also zero. These results indicate that any mass loss/gain asymmetries and the negative net mass balances that result from interannual climate variability are due to temperature variability.

4.2.2 Length Fluctuations and Upslope Retreat

Fluctuations in glacier length provide a metric to determine the dynamic response of the glacier to interannual climate variability. Previous studies have assumed that length fluctuations will be around an otherwise unchanged mean state (e.g. Roe and O'Neal (2009); Roe (2011); Roe and Baker (2014)). The results from the ELA and mass balance anomalies, however, suggest that the mean state of the glacier (e.g. ELA and length) changes with the addition of interannual climate variability. Figure 4.3 presents the first 1,000 years of the glacier length time series once variability is added as well as the histogram of the glacier length anomalies for the final 10,000 years of the simulation with interannual climate variability. For both glaciers, the length fluctuates once variability is added to the input, but these fluctuations are around a new and shorter length. In the first fifty years or so, the primary mode of glacier length fluctuation is towards shorter lengths, i.e. trending towards a new and smaller mean length. This upslope retreat is greater for the tropical glacier than the mid latitude glacier. After this transition phase to a new mean position, both glaciers fluctuate around this new position, and the mid latitude glacier has a slightly greater magnitude of length fluctuations (as quantified by the 1-σ value of the glacier length time series, σ_L) than the tropical glacier.

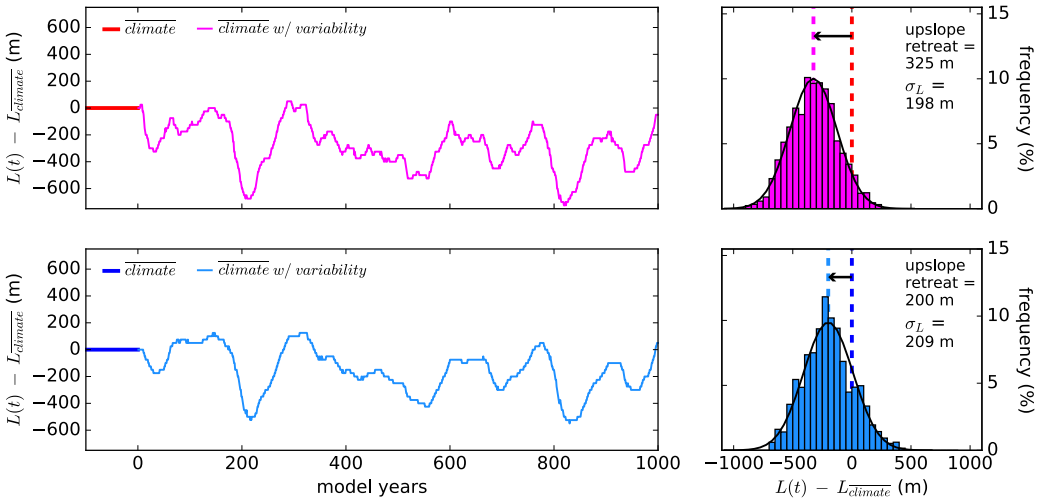

Figure 4.3: Time series of glacier length fluctuations (left column) for the end of the model spin-up (no climate variability) and the first 1,000 years of the simulation with interannual climate variability and the statistics on glacier length fluctuations (right column) for the final 10,000 years of output for the representative tropical glacier (upper row) and mid latitude glacier (bottom row). For the histograms, the black curves represent normal distributions with the same mean-value and standard deviation as their respective time series. Also, the dotted lines for the histograms represent the equilibrium lengths for either the vertical balance profile without climate variability ($\overline{climate}$) or the aggregate vertical mass balance profile for the climate with variability ($\overline{climate}\ w/\ variability$).

The upslope retreat ultimately reflects a change in the mean state of the glacier. Driving the flowline model to equilibrium with the aggregate mass balance profile from the simulation with variability (magenta or lighter blue curve in Figure 4.2), produces an equilibrium length that is the same as the mean of the glacier length time series. As seen in Chapter 4.2.1, changes in the mean (or net) mass balance due to the addition of interannual climate variability solely reflect temperature variability. In much the same way, the retreat of the mean glacier length with the addition of variability solely reflects temperature variability. In the absence of interannual temperature variability, there is no upslope retreat of the mean glacier length, and the glacier fluctuates around the same position as the climate without variability, albeit with a significantly smaller magnitude of length fluctuations (σ_L) than when both temperature and precipitation variability are included. With only temperature variability, the upslope retreat of the mean glacier length is exactly the same as when both

temperature and precipitation variability are included, and the magnitude of length fluctuations are closer to the value when both types of variability are included. These results suggest that interannual climate variability can drive glacier length fluctuations but that the mean position around which the glacier fluctuates is in part defined by the magnitude of the temperature variability.

4.3 Discussion

4.3.1 Interannual Climate Variability and Mass Balance Nonlinearities

The results of this chapter indicate that interannual climate variability does in fact influence the mean state of a glacier and that changes in temperature variability are how interannual climate variability affects the mean state. The addition of temperature variability changes the shape of the vertical mass balance profile, particularly near the inflection point at the ELA. These changes result in a higher net ELA and negative net mass balance, which drives an upslope retreat of the glacier to a new equilibrium position around which the glacier fluctuates. Precipitation variability, in contrast, does not produce changes in the mean (or net) mass balance or glacier length, and length fluctuations occur around the same equilibrium glacier length as the climate state without interannual climate variability. The change in the mean state of the glacier with the addition of temperature variability suggests an asymmetry between warm years and cold years, with warm years producing greater mass loss than can be compensated by an equal magnitude cold year. This asymmetry can be thought of as a nonlinearity – for the same forcing but opposite signs, the magnitude of response is different.

This mass balance nonlinearity emerges because vertical mass balance profiles are not straight lines. Ablation zones have larger mass balance gradients than accumulation and ablation zones, producing a point of inflection in the mass balance profile. Within the framework of climate variability producing fluctuations in mass balance by translating the

vertical mass balance profile, a hot year will shift part of the glacier that is usually in the accumulation zone into the ablation zone, and a cold year will shift part of the glacier usually in the ablation zone into the accumulation zone. Since the mass balance gradient in the ablation zone is steeper than in the accumulation zone, a hot year will ablate more mass in the anomalous ablation zone than can be build up into a surplus mass on a cold year in the anomalous accumulation zone (see Figure 4.4). Take for example the anomalous ablation at the elevation of the ELA for the mean climate without variability. For an anomalously warm year, the tropical glacier ablates 4x more mass than can accumulate from an equal magnitude but anomalously cold year. For the mid latitude glacier, the anomalous ablation would only be 2x as great. These differences between ablation and accumulation are the same as the ratio of mass balance gradients between the ablation and accumulation zones, supporting the hypothesis that the nonlinearity reflects the difference in the mass balance gradients. Glacier-wide, this story also holds. The length retreat of the tropical glacier due to the addition of interannual climate variability is over 60% larger than the length retreat of the mid latitude glacier. The net ELA increase is nearly 2x greater for the tropical glacier than the mid latitude and the net (or mean) mass balance is 3x more negative. Both the results from this chapter and the proposed mechanism for the nonlinearity suggest that the mass balance nonlinearity will be more acute for glaciers with large differences in mass balance gradients between the ablation and accumulation zones.

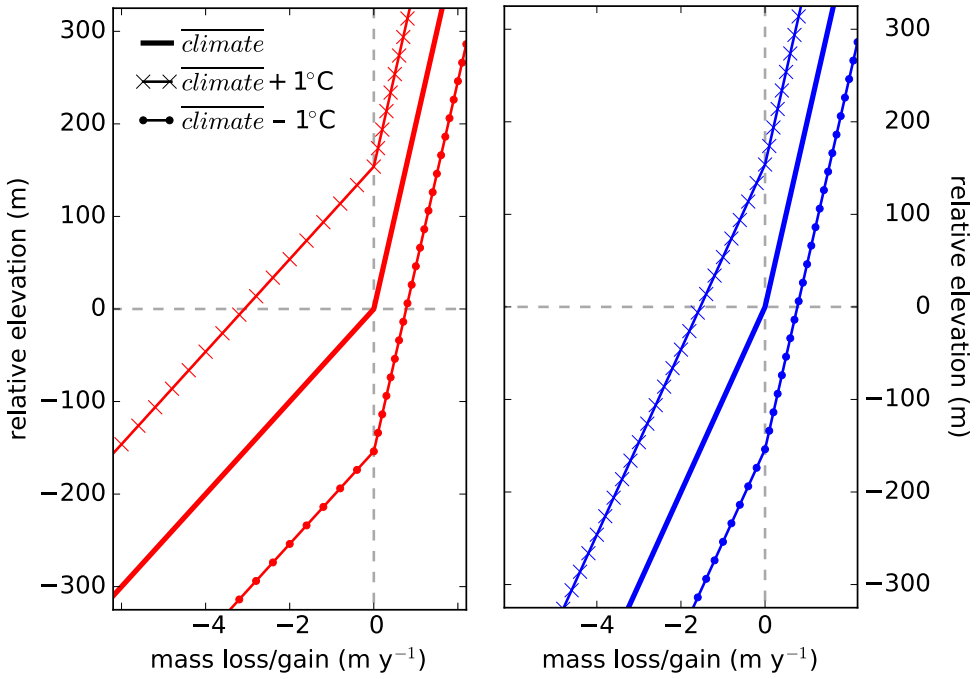

Figure 4.4: Vertical mass balance profile for the mean climate without interannual climate variability ($\overline{climate}$) for the representative tropical (top) and mid latitude (bottom) glaciers. The perturbations the mass balance gradient as a result of warming (line with x's) and cooling (line with dots) are also included. As can be seen, near the point of inflection in the mass balance gradients, the hot year produces significantly more anomalous ablation than can be compensated by anomalous accumulation on the cold year.

The mass balance nonlinearity discussed above is the logical consequence of the assumption that the mass balance response of a glacier to interannual climate variability can be simulated by translations in the vertical mass balance profile, which is a commonly made assumption (Meier and Tangborn (1965); Kaser et al. (2003)). Oerlemans and Hoogendoorn (1989) illustrate that this assumption is an oversimplification, and with a more accurate treatment of how the vertical mass balance profiles respond to climate change, glaciers in the Austrian Alps are even more sensitive to temperature changes. The subtleties presented by Oerlemans and Hoogendoorn (1989) for typical mid latitude glaciers would not decrease the nonlinearities in response to temperature but further exacerbate them. The key result that temperature variability can impact the mean (or longterm) state of a glacier has been

observed elsewhere. Bradley and Eddy (1991) find that the longterm mass balance at Devon Ice Cap, Canada can be determined by one or a few warm years. In this study, the mass balance nonlinearity is attributed to a *curvilinear* relationship between mass balance and temperature – negative mass balance anomalies can grow almost limitlessly as hotter years produce more melt, but there is a limit to positive mass balance anomalies, i.e. the net solid precipitation (Bradley and Eddy (1991)). Farinotti (2013), coupling a full Stokes ice flow model to a positive degree day (PDD) ablation model for the Rhonegletcher, Switzerland, finds that changes in the magnitude of temperature variability can drastically alter the ice volume and terminus position. In this study, the mass balance nonlinearity is attributed to the one prescribed in a PDD model – ablation can only occur if the air temperature is above some threshold (Farinotti (2013)). The emergence of a mass balance nonlinearity caused by temperature variability is not just an artifact of the simplified mass balance scheme implemented in this chapter but a result observed and modeled elsewhere. The mechanism for the nonlinearity presented in this chapter and those previously suggested are in many ways just different sides of the same coin.

4.3.2 The Universality of Mass Balance Nonlinearities

The results from this chapter suggest that glaciers with a steeper mass balance gradient in their ablation zone than in their accumulation zone will experience a mass balance nonlinearity due to interannual temperature variability. Consistent with the vertical mass balance profiles used in this chapter, many of world's monitored glaciers have steeper mass balance gradients at lower elevations (*World Glacier Monitory Service 2015 Bulletin*). Some of the largest mass balance gradients in the ablation zone are found at tropical glaciers (Kaser and Osmaston (2002)), suggesting that tropical glaciers are more susceptible to mass balance nonlinearities due to climate variability. The magnitude of mass balance nonlinearities produced in this chapter for the representative tropical glaciers may, in fact, understate that magnitude of nonlinearities for some wet outer tropical glaciers. Gurgiser et al. (2013) simu-

late an ablation zone mass balance gradient of ∼3 m w.e. a^{-1} per 100 m and accumulation zone gradient of ≤0.15 m w.e. a^{-1} per 100 m at Shallap Glacier in the Cordillera Blanca (Peru). Such a mass balance gradient difference would produce an even larger nonlinearity (for the same magnitude of temperature variability) as found in this chapter. Mid and high latitude glaciers tend to have both smaller mass balance gradients in their ablation zones than tropical glaciers and larger accumulation zone mass balance gradients than tropical glaciers (Kaser et al. (1996); Kaser (2001); Kaser and Osmaston (2002)), likely reducing the magnitude of their mass balance nonlinearities due to temperature variability. A nonlinear mass balance response to climate variability, however, should be a generally observed phenomenon for many of the world's glaciers, and the nonlinearity should be more pronounced at glaciers with large differences in their mass balance gradients, such as tropical glaciers.

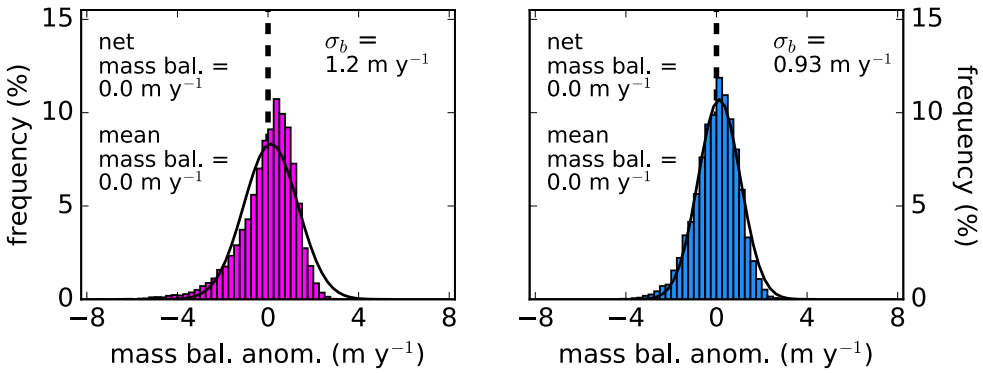

Figure 4.5: Mass balance anomalies in response to temperature and precipitation variability for a representative tropical glacier (left) and mid latitude glacier (right).The mass balance anomalies are calculated for the mean glacier length that each glacier retreats to once climate variability is introduced to the simulation. For this new length, the glacier has a net (and mean) mass balance of zero, indicating that the glacier is in equilibrium with the climate state that includes variability. Solid black lines represent normal distributions with the same mean and 1-σ value as the mass balance time series. Both mass balance distributions have a negative skew and are statistically distinguishable from a normal distribution by means of a D'Agostino and Pearson's test.

A universality of this mass balance nonlinearity, however, may appear to conflict with observations about the net mass balance variability of the world's glaciers. Medwedeff and

Roe (2016) analyze detrended net mass balance records for 130 glaciers, finding that the vast majority (>85%) of them are normally distributed. In their study, all six of the tropical glaciers analyzed pass tests for normal distributions (Medwedeff and Roe (2016)). A normally distributed mass balance record (once detrended) would conflict with a nonlinear response to climate variability, assuming that the climate anomalies (once detrended) are roughly normally distributed. In this chapter, the mass balance variability is not normally distributed, being negatively skewed with a long tail to large negative mass balance anomalies (see Figure 4.2). Some of the negative skew in Figure 4.2 may be an artifact of having calculated the mass balance for the spin-up equilibrium glacier length, which is multiple hundreds of meters longer than the mean length of either glacier once interannual climate variability is added to the simulations. Figure 4.5 illustrates a recalculated distribution using the new (shorter) mean length. Even with the shorter glacier length, however, the mass balance anomalies still lack a normal distribution, with a $p \ll 0.05$ for D'Agostino and Pearson's tests.

The negative skew in the mass balance anomalies from this study (see Figure 4.5) appears to conflict with the mass balance anomaly observations for the world's glaciers (Medwedeff and Roe (2016)), which may cast doubt on the universality of the mass balance nonlinearity presented in this chapter. Without a nonlinearity, normally distributed interannual climate variability would produce a normally distributed mass balance anomaly, but in this study, a normally distributed interannual climate variability produces a skewed mass balance response. The apparent contradiction between the shape of the mass balance nonlinearities in this study and in the observational record, however, may reflect an artifact of the limited duration of mass balance data in the observational record. For this study, 10,000 years of mass balance anomalies are produced, but data on glacier mass balance variability cover a much shorter time span, on the order of a few decades. The longest record in the Medwedeff and Roe (2016) study is only 67 years, and for tropical glaciers, the longest record is 21 years. The simulated mass balance output from this study can be used to evaluate whether

there may be nonlinearities hidden in the mass balance data that have not emerged due to the limited time span of measurements. A Shapiro-Wills test is conducted on smaller time increments of the full 10,000 model years of output from this study. Table 4.2 illustrates the percentage of times that a small increment of mass balance output would be statistically distinguishable ($p<0.05$) from a normal distribution, for increments of 10 years, 20 years, 30 years, and 50 years. If only 10 years of mass balance data are available, then the vast majority of the time, both the representative tropical glacier and mid latitude glacier mass balance anomalies would be statistically indistinguishable from a normal distribution. As the number of years of mass balance data increases, distributions of mass balance anomalies become more consistently distinguishable from a normal distribution, especially for the tropical glacier. If analyses are conducted on 50 years worth of output for the tropical glacier, then a super majority of time the distribution would be statistically distinguishable from a normal distribution. For the mid latitude glacier, however, even with 50 years worth of output, the mass balance anomalies would only be statistically distinguishable from a normal distribution <20% of the time. The apparent normally distributed mass balance data for the vast majority of the world's glaciers does not necessarily conflict with a nonlinear response of glaciers to interannual climate variability but instead highlights the challenge of trying to capture glacier mass balance dynamics from limited data. As the length of mass balance data records increases, the mass balance nonlinearity presented in this chapter should be able to be better observed.

Table 4.2: Percentage of Times During 10,000-Year Simulation That The Mass Balance Anomalies Are Distinguishable From A Normal Distribution For The Representative Glaciers

year increments	Tropical Glacier	Mid Latitude Glacier
10	16.1	6.5
20	33.3	9.7
30	47.4	13.1
50	68.0	19.9

4.3.3 Mass Balance Nonlinearities And Interpreting Glacier Length Changes

Temperature variability, through the mass balance nonlinearity presented above, drives an upslope retreat of the glacier to a mean length around which the glacier fluctuates. This upslope mean position is, unsurprisingly, the same as the equilibrium length of the glacier driven with the aggregate vertical mass balance profile. The addition of temperature variability, with a 1-σ value of 0.75°C, produces an upslope retreat of 325 m for the tropical glacier and 200 m for the mid latitude glacier. Farinotti (2013) finds that for a doubling of contemporary temperature variability at Rhonegletcher (Switzerland), the glacier length is ∼500 m shorter after only 45 years. In terms of impacting the future evolution of the glacier, however, Farinotti (2013) concludes that projected future changes in the climate variability will produce only very minimal changes to the state of the glacier (<8% in ice volume and <100 m in terminus position). Comparing the retreat due to variability from this chapter to what the retreat would be for a 0.75°C increase in the mean temperature, provides a metric through which to determine if either the tropical glacier or mid latitude glacier would have significant length changes due to changes in variability. For the representative tropical glacier, the upslope retreat is 1,300 m, and for the mid latitude glacier it is 1,550 m for a warming of 0.75°C. In both cases, the retreat introduced by the mass balance nonlinearity is less than the retreat from an equal magnitude warming, but for the tropical glacier, which experiences a greater magnitude mass balance nonlinearity, this difference is not as great. The ratio between the retreat due to variability and the retreat due to warming is 1/4 for the tropical glaciers and ∼1/10 for the midlatitude glacier, suggesting that that changes in temperature variability will not significantly impact changes in the mean glacier length for mid latitude glaciers (similar to the findings for a glacier in Switzerland by Farinotti (2013)). In the case of the representative tropical glacier, however, there is only a factor of 4 difference, and thus changes in temperature variability could produce noticeable length

changes that would need to be differentiated from length changes caused by changes in the mean climate.

4.4 Concluding Remarks

In this chapter, a flowline model from chapter 3 is implemented with an idealized representation of interannual climate variability to identify the mechanism for and quantify the impact of mass balance nonlinearities. The key results are the following:

1. For both the idealized representative tropical glacier and mid latitude glacier, the addition of interannual climate variability produces a different mean glacier state than if the model is driven with just a mean climate signal. The addition of temperature variability as opposed to precipitation variability causes the mass balance nonlinearity, which causes an increase in the ELA, a negative net mass balance, and ultimately an upslope length retreat. The change in the mean state is greater for the tropical glacier than the mid latitude glacier.

2. The mass balance nonlinearity is the result of temperature variability and originates because of the difference in mass balance gradients between the accumulation and ablation zones. Since ablation zone mass balance gradients are larger than those in accumulation zones, switching the lower portion of the accumulation zone into the ablation zone (on a hot year) will produce a greater mass loss than the mass gain from switching the upper portion of the ablation zone into the accumulation zone (on a cold year). This nonlinearity is more pronounced for larger differences between mass balance gradients. Tropical glaciers have very large ablation zone mass balance gradients, and the mass balance nonlinearity will be more pronounced at tropical glaciers.

3. Many of the world's glaciers have larger mass balance gradients in the ablation zone than accumulation zone, indicating that the nonlinearity is robust.

4. The importance of this nonlinearity for reconstructing past climate and forecasting future glacier evolution depends on the relative magnitude of the mass balance nonlinearity versus the glacier response to climate change. The larger the magnitude of the nonlinearity, the more important this nonlinearity will be for proper hindcasts and forecasts. For mid latitude glaciers, which have a smaller difference in the slope of the mass balance gradient between the two zones, the importance of this nonlinearity is negligible. For tropical glaciers, however, the nonlinearity is significantly larger and may be need to be accounted for in order to produce accurate hindcasts and forecasts.

CHAPTER 5

CONCLUSION

Tropical glaciers have long been viewed as a highly sensitive component of the environment (Kaser (1995)) and a means though which to observe past and present climate change (Thompson et al. (2006); Francou et al. (2005); Thompson et al. (2011)). They are also vital water resources for communities in their shadows (Mark et al. (2005); Soruco et al. (2015)) and play an integral spiritual role for many of these communities (Bolin et al. (2009)). Their fate looks bleak in a world of anthropogenic warming (Bradley et al. (2006); Vuille et al. (2008a); Rabatel et al. (2013)). A challenge in reconstructing past tropical climate changes through records of glacier change and in forecasting their future evolution is the incomplete understanding of the climate variables most responsible for driving their changes. This dissertation elucidates the climate drivers responsible for tropical glacier change, illustrates how records of tropical glacier change can be used as a quantitive paleoclimate proxy, and explores additional drivers of tropical glacier length, beyond just the mean annual temperature and net annual precipitation. Taken together, these efforts provide information and insight for improving hindcasts of tropical climates and forecasts of tropical glacier evolution.

How glaciers respond to climate change varies, depending in part on their climate setting (Rupper and Roe (2008); Rupper et al. (2009); Sagredo et al. (2014)). Even though this dissertation only focuses on tropical Andean glaciers, which span a relatively narrow latitude and longitude range, there are additional climate distinctions among these glaciers (Sagredo and Lowell (2012)). Chapter 2 illustrates that the dominant climate setting distinction is the amount of net annual precipitation, which defines whether a tropical glacier responds more strongly to temperature or precipitation changes. This wet-glacier/dry-glacier contrast has been noted previously, for glaciers in a variety of different climate settings (e.g. Meier (1984); Oerlemans and Fortuin (1992); Rupper et al. (2009); Sagredo et al. (2014)). Some of the past debate about which climate variables drive tropical glacier change likely stems from not fully appreciating the role that climate setting plays on how tropical glaciers respond to

climate change.

The results from Chapter 2 and Chapter 3 also illustrate that for wet tropical glaciers, which are the vast majority in the Andes, and also the most important for regional water resources, temperature is the major driver of mass balance and length changes. The importance of temperature, especially for wet outer tropical glaciers, seems to contradict previous studies (Wagnon et al. (1999); Favier et al. (2004a)) and the dominant energy source for melt (absorbed solar radiation) (Favier et al. (2004b); Sicart et al. (2008)). Previous studies suggest that the important climate variables for mass loss and gain differ depending on where on the glacier these determinations are made (Sicart et al. (2011); Gurgiser et al. (2013)). The results from Chapter 2 support the assertion by Gurgiser et al. (2013) that temperature drives mass balance variability for wet outer tropical glaciers through the dominant impact that it has on the lowest elevations of the glacier. This dominant relationship would be missed in studies that only focus at higher elevations on tropical glaciers. As the community collects more meteorological and mass balance data from more locations along a glacier, the conclusion that temperature is what is driving glacier change in the wet tropic should become more apparent.

Tropical Andean glaciers have long been viewed as a means through which to understand the timing of low latitude deglaciation from the Last Glacial Maximum (LGM) (e.g. Mercer et al. (1975)) as well as climate changes during the Late Glacial and Holocene (e.g. Kelly et al. (2012); Stroup et al. (2014)). In some cases, the magnitude of these glacier changes have been used as a way to constrain past climate change (Rind and Peteet (1985); Stansell et al. (2007)). Chapter 3 provides one of the first published attempts to use a numerical glacier model in conjunction with the geologic record of past glacier changes to quantitatively constrain past climates in the tropical Andes. For the moraines at the Quelccaya Ice Cap, Peru, which are associated with the Younger Dryas and Little Ice Age, both moraine sets require regional cooling to advance the glacier to their positions. The results from Chapter 3 also highlight the high sensitivity of wet tropical Andean glaciers to even mild temperature

changes in the tropics. Since the tropical atmosphere is well constrained by the moist adiabat (Xu and Emanuel (1989); Pierrehumbert (1999); Williams et al. (2009); see Figure 3.1), slight sea surface temperature (SST) changes are amplified at the high elevations of Andean glaciers. These results suggest that SST changes during the Younger Dryas and Little Ice Age were relatively mild, and hint that LGM tropical temperature changes may be consistent with the milder MARGO reconstructions for paleo-SSTs during the LGM (Waelbroeck et al. (2009)). This conclusion, however, depends on the assumption that atmospheric temperature profiles remain close to the moist adiabat in the past. Recent work, in the Indo-Pacific warm pool (Tripati et al. (2014)) and tropical East Africa (Loomis et al. (2017)), suggests that tropical atmospheric profiles may have been steeper during the LGM than what would be expected along the moist adiabat, which would require larger SST changes to reproduce the observed glacial features. The question of tropical atmospheric temperature profiles during the LGM is one that warrants further study, in particular in the tropical Andes.

To relate glacier changes to a climate signal, especially for tropical glaciers, may require looking beyond just the mean state of the climate, i.e. annual mean temperature and net annual precipitation. As seen in Chapter 3 and Chapter 4, interannual climate variability, i.e. weather, can drive mass balance anomalies that can produce fluctuations around a mean, but the variability itself can also change the mean state of the glacier. Previous studies have looked at how interannual climate variability can cause length fluctuations and how to interpret the climate signal embedded within records of length fluctuations (Oerlemans (2000); Roe and O'Neal (2009); Roe (2011); Roe and Baker (2014)). These studies, however, assume that variability does not affect the mean state of the glacier (Roe and O'Neal (2009); Roe and Baker (2014)). In Chapter 3, the Huancané outlet glacier of the Quelccaya Ice Cap retreats upslope as the amount of interannual temperature variability increases, and in Chapter 4, both the representative mid latitude and tropical glacier retreat upslope with increased interannual temperature variability. The upslope retreat in response to changes in the amount of interannual climate variability indicates a change in the mean state of

the glacier, which is driven not by changes in the mean climate variables but by just the interannual variability in these variables.

The mean glacier state changes in response to changes in the amount of interannual climate variability because warm years produce more anomalous ablation than can be compensated by anomalous accumulation on cold years, thus introducing a mass balance nonlinearity into the system. In Chapter 4, this mass balance nonlinearity is explored and attributed to the difference in mass balance gradients between ablation zones and accumulation zones. The larger the mass balance gradient difference, the more significant the mass balance nonlinearity and the further upslope the retreat. Tropical glaciers have especially large ablation zone mass balance gradients (Kaser (2001); Kaser and Osmaston (2002)), making the nonlinearity more acute. In Chapter 4, for the representative mid latitude glacier, the retreat due to changes in interannual temperature variability is small compared to retreat due to a similar magnitude warming. Similarly, at Rhonegletcher (Switzerland), Farinotti (2013) finds that future changes in temperature variability will have a minimal impact on the future evolution of the glacier as compared to changes in the mean temperature. For tropical glaciers, which have larger ablation zone mass balance gradients, glacier length changes due to changes in interannual temperature variability can be larger.

This dissertation contributes to the community's understanding of the climatological signal behind tropical glacier changes. For the vast majority of Andean tropical glaciers, temperature is the primary variable for mass balance and length changes. Thus geologic records of past length changes make for promising paleo-thermometers for both local and regional temperature change. In making such a climate inversion, some caution may be needed to separate the mean climate signal from length changes driven by variability. Chapter 4 provides a framework for when variability might play an important role. The strong relationship between temperature change and glacier change also poses concern for the long-term fate of the majority of tropical Andean glaciers. Tropical Andean glaciers are retreating at an alarming rate (Vuille et al. (2008a); Rabatel et al. (2013)), and air temperatures are

warming fastest at high elevations (Pepin et al. (2015)), which is where all tropical glaciers are found. In light of the findings of this dissertation, the extinction of tropical Andean glaciers looks even more certain.

APPENDIX A

SURFACE ENERGY AND MASS BALANCE MODEL VARIABLES AND PARAMETERS

Table A.1: Climate Variables

	name	units	source
T_s	surface temperature	K	iterative process
T_a	2-meter air temperature	K	reanalysis
P	precipitation rate	$m\ (w.e.)\ s^{-1}$	data & reanalysis
S_{down}	incoming solar radiation	$W\ m^{-2}$	reanalysis
$p(z)$	atmospheric pressure	*unitless*	reanalysis
U	2-meter windspeed	$m\ s^{-1}$	reanalysis
n	cloud cover	*unitless*	reanalysis
RH_a	2-m relative humidity	*unitless*	reanalysis
Γ	lapse rate	$^{\circ}C\ m^{-1}$	reanalysis

Table A.2: Climate Parameters: Radiative Fluxes

	name	value	units
α	surface albedo	eq. 2.2	*unitless*
α_{snow}	snow albedo	eq. 2.3	*unitless*
$\alpha_{fresh\ snow}$	fresh snow albedo	0.90	*unitless*
α_{firn}	firn albedo	0.53	*unitless*
α_{ice}	ice albedo	0.34	*unitless*
t^*	firnification timescale	1.70	*days*
d^*	snow depth scale	11	*mm*
ϵ_{eff}	effective atmospheric emissivity	eq. 2.7	*unitless*
ϵ_{cs}	clear-sky emissivity	eq. 2.8	*unitless*
ϵ_{cs0}	baseline clear-sky emissivity	0.125	*unitless*
ϵ_{oc}	complete cloud cover emissivity	1.00	*unitless*
C_{vap}	emissivity water vapor adjustment	0.242	$(\frac{Pa}{K})^{\frac{1}{8}}$
b	cloud fraction exponent parameter	1.00	*unitless*

Table A.3: Climate Parameters: Turbulent & Other Fluxes

	name	value	units
C_H	exchange coefficient, heat	Eq. 2.12	*unitless*
C_E	exchange coefficient, water vapor	Eq. 2.12	*unitless*
Ri	Richardson Number	Eq. 2.11	*unitless*
Ri_c	critical Richardson Number	0.2	*unitless*
k	von Kármán constant	0.4	*unitless*
z	atmospheric measurement elevation	2	m
z_0	roughness length, momentum	0.5	mm
z_{0_H}	roughness length, heat	0.5	mm
z_{0_E}	roughness length, water vapor	0.5	mm
RH_i	glacier surface relative humidity	1.0	*unitless*
A	vapor pressure fitting parameter, 1	17.67	*unitless*
B	vapor pressure fitting parameter, 2	243.5	°C

Table A.4: Physical Constants

	name	value	units
σ	Stefan-Boltzmann constant	5.67×10^{-8}	$W^2\ m^{-2}\ K^{-4}$
c_p	heat capacity, air	1.010	$kJ\ kg^{-1}\ K^{-1}$
ρ_0	density of air, STP	1.29	$kg\ m^{-3}$
p_0	sea-surface pressure	1013	hPa
p_{sat_0}	triple point saturation vapor pressure	6.112	hPa
c_{p_w}	heat capacity of water, STP	4.180	$kJ\ kg^{-1}\ K^{-1}$
ρ_w	density of water, STP	1000	$kg\ m^{-3}$
g	acceleration from gravity	9.81	$m\ s^{-1}$
L_f	latent heat of fusion	0.334	$MJ\ kg^{-1}$
L_v	latent heat of vaporization	2.501	$MJ\ kg^{-1}$
L_s	latent heat of sublimation	2.834	$MJ\ kg^{-1}$

APPENDIX B

STATISTICS BETWEEN GLACIER-CLIMATE INTERACTION METRICS AND CLIMATE INPUTS

Table B.1: Statistics between Mass Balance and Temperature (T), Lapse Rate (LR), Shortwave Radiation (SW), Longwave Radiation (LW), Windspeed (U), Precipitation (precip.), Relative Humidity (RH), and Cloud Cover (CC) at the Annual Average (AA), June, July, and August (JJA) Average, September, October, and November (SON) Average. December, January, and March (DJM) Average, and March, April, and May (MAM) Average Timescales

	Volcán	Antisana		Quelccaya	Ice Cap		Nevado	Sajama
	a	r^2		a	r^2		a	r^2
T	m w.e. a^{-1} per (deg C)							
AA	-1.64	0.75		-1.42	0.73		-0.15	0.26
JJA	-1.81	0.49		-0.93	0.52		-0.1	0.21
SON	-1.46	0.45		-1.3	0.57		-0.1	0.13
DJF	-1.04	0.71		-1.05	0.57		-0.1	0.13
MAM	-1.19	0.68		-0.99	0.51		-0.14	0.3
LR	m w.e. a^{-1} per (0.1 deg per km)							
AA	0.34	0.24		0.4	0.34		-0.1	0.25
JJA	0.1	0.06		0.15	0.16		-0.03	0.06
SON	0.19	0.1		0.26	0.3		-0.03	0.02
DJF	0.31	0.2		0.3	0.27		-0.06	0.15
MAM	0.41	0.39		0.12	0.05		-0.07	0.26
SW	m w.e. a^{-1} per (10 W m^{-2})							
AA	-0.38	0.28		-0.29	0.11		-0.04	0.06
JJA	-0.12	0.03		-0.12	0.02		-0.01	<0.01
SON	-0.33	0.32		0.02	<0.01		0	<0.01
DJF	-0.28	0.34		-0.23	0.21		-0.02	0.06
MAM	-0.18	0.08		-0.23	0.1		-0.08	0.23
U	m w.e. a^{-1} per (0.5 m s^{-1})							
AA	0.7	0.05		0.84	0.2		0.05	0.01
JJA	-0.12	0.01		0.62	0.17		-0.08	0.17
SON	0.9	0.1		0.41	0.08		0.08	0.11
DJF	1.06	0.22		0.57	0.14		0.04	0.07
MAM	0.19	0.01		0.68	0.16		0.02	¡0.01
precip.	m w.e. a^{-1} per (20%)							
AA	0.32	0.2		0.4	0.26		0.06	0.64
JJA	0.05	0.03		0.03	0.03		0.02	0.12
SON	0.13	0.07		0.14	0.09		0.01	0.06
DJF	0.22	0.23		0.21	0.11		0.04	0.53
MAM	0.08	0.04		0.22	0.21		0.04	0.12
RH	m w.e. a^{-1} per (10%)							
AA	0.98	0.04		-0.81	0.21		-0.07	0.15
JJA	0.07	¡0.01		-0.66	0.25		-0.07	0.22
SON	0.73	0.04		-0.59	0.16		-0.05	0.17
DJF	2.25	0.14		-0.56	0.1		-0.05	0.06
MAM	1.29	0.04		-1.04	0.21		-0.05	0.08
CC	m w.e. a^{-1} per (10%)							
AA	0.87	0.19		0.44	0.07		0.06	0.03
JJA	0.13	0.01		0.28	0.07		-0.01	<0.01
SON	0.75	0.2		-0.2	0.03		0.01	<0.01
DJF	0.8	0.33		0.52	0.2		0.04	0.04
MAM	0.43	0.08		0.15	0.01		0.06	0.03

Table B.2: ELA statistics with same climate variables and timescales as Table B.1

	Volcán	Antisana		Quelccaya	Ice Cap		Nevado	Sajama
	a	r^2		a	r^2		a	r^2
T	m per (deg C)							
AA	160	0.93		138	0.81		188	0.09
JJA	184	0.66		81	0.47		52	0.01
SON	148	0.6		125	0.62		143	0.06
DJF	101	0.86		106	0.68		129	0.05
MAM	114	0.82		103	0.66		267	0.23
LR	m per (0.1 deg per km)							
AA	-35	0.32		-39	0.39		199	0.19
JJA	-10	0.09		-12	0.12		57	0.05
SON	-24	0.21		-27	0.37		-6	¡0.01
DJF	-27	0.2		-29	0.3		117	0.12
MAM	-40	0.47		-16	0.1		158	0.33
SW	m per (10 W m^{-2})							
AA	37	0.34		24	0.09		91	0.06
JJA	21	0.11		13	0.03		-106	0.02
SON	30	0.35		0	¡0.01		30	0.02
DJF	26	0.39		17	0.15		38	0.04
MAM	15	0.08		16	0.06		168	0.18
U	m per (0.5 m s^{-1})							
AA	-23	0.01		-41	0.06		-49	¡0.01
JJA	15	0.02		-24	0.03		153	0.13
SON	-27	0.01		-23	0.03		-110	0.05
DJF	-66	0.11		-29	0.04		-40	0.01
MAM	-17	0.01		-36	0.05		-128	0.04
precip.	m per (20%)							
AA	-3	<0.01		-23	0.1		-106	0.38
JJA	-3	0.01		-1	¡0.01		-37	0.14
SON	-5	0.01		-6	0.02		-41	0.11
DJF	-9	0.05		-11	0.04		-63	0.29
MAM	7	0.03		-16	0.13		-35	0.05
RH	m per (10%)							
AA	-141	0.1		58	0.12		72	0.04
JJA	-24	0.01		45	0.14		110	0.11
SON	-120	0.14		37	0.07		54	0.04
DJF	-284	0.29		44	0.07		37	0.01
MAM	-105	0.03		86	0.17		27	¡0.01
CC	m per (10%)							
AA	-86	0.24		-40	0.06		-51	¡0.01
JJA	-33	0.05		-29	0.09		71	0.01
SON	-72	0.24		10	0.01		-23	¡0.01
DJF	-74	0.36		-39	0.14		-34	0.01
MAM	-32	0.06		-8	¡0.01		-99	0.02
freezing level heigth	m per (m)							
AA	0.9	0.93		0.85	0.8		1.36	0.12
JJA	1.05	0.64		0.53	0.49		0.43	0.02
SON	0.86	0.6		0.77	0.57		0.91	0.06
DJF	0.56	0.86		0.65	0.67		0.96	0.7
MAM	0.64	0.82		0.6	0.66		1.85	0.31

REFERENCES

Anderson, B. and Mackintosh, A. (2006). Temperature change is the major driver of late-glacial and Holocene glacier fluctuations in New Zealand. *Geology*, 34(2):121–124.

Anderson, L. S., Roe, G. H., and Anderson, R. S. (2014). The effects of interannual climate variability on the moraine record. *Geology*, 42(1):55–58.

Andreassen, L. M., Elvehøy, H., Kjøllmoen, B., Engeset, R. V., and Haakensen, N. (2005). Glacier mass-balance and length variation in Norway. *Annals of Glaciology*, 42(1):317–325.

Arnaud, Y., Muller, F., Vuille, M., and Ribstein, P. (2001). El Niño-Southern Oscillation (enso) influence on a Sajama volcano glacier (Bolivia) from 1963 to 1998 as seen from Landsat data and aerial photography. *Journal of Geophysical Research: Atmospheres*, 106(D16):17773–17784.

Baker, P. A., Seltzer, G. O., Fritz, S. C., Dunbar, R. B., Grove, M. J., Tapia, P. M., Cross, S. L., Rowe, H. D., and Broda, J. P. (2001). The history of South American tropical precipitation for the past 25,000 years. *Science*, 291(5504):640–643.

Balco, G. (2009). The geographic footprint of glacier change. *Science*, 324(5927):599–600.

Benn, D., Evans, D. J., et al. (2014). *Glaciers And Glaciation*. Routledge.

Bolin, I., Crate, S., and Nuttall, M. (2009). *The Glaciers of the Andes are Melting. Indigenous and Anthropological Knowledge Merge in Restoring Water Resources*. Left Coast Press Walnut Creek, CA.

Bolton, D. (1980). The computation of equivalent potential temperature. *Monthly weather review*, 108(7):1046–1053.

Bookhagen, B. and Strecker, M. R. (2008). Orographic barriers, high-resolution TRMM rainfall, and relief variations along the eastern Andes. *Geophysical Research Letters*, 35(6).

Braconnot, P., Harrison, S. P., Kageyama, M., Bartlein, P. J., Masson-Delmotte, V., Abe-Ouchi, A., Otto-Bliesner, B., and Zhao, Y. (2012). Evaluation of climate models using palaeoclimatic data. *Nature Climate Change*, 2(6):417–424.

Bradley, R. and Eddy, J. (1991). Records of past global changes. *Global changes of the past*, pages 5–9.

Bradley, R. S. (1999). *Paleoclimatology: Reconstructing Climates of the Quaternary*, volume 68. Academic Press.

Bradley, R. S. and England, J. (1978). Recent climatic fluctuations of the Canadian high arctic and their significance for glaciology. *Arctic and Alpine Research*, pages 715–731.

Bradley, R. S., Keimig, F. T., Diaz, H. F., and Hardy, D. R. (2009). Recent changes in freezing level heights in the tropics with implications for the deglacierization of high mountain regions. *Geophysical Research Letters*, 36(17).

Bradley, R. S., Vuille, M., Diaz, H. F., and Vergara, W. (2006). Threats to water supplies in the tropical Andes. *Science*, 312(5781):1755–1756.

Braithwaite, R. J. (1981). On glacier energy balance, ablation, and air temperature. *Journal of Glaciology*, 27(97):381–391.

Braithwaite, R. J. and Olesen, O. B. (1989). Calculation of glacier ablation from air temperature, West Greenland. In *Glacier fluctuations and climatic change*, pages 219–233. Springer.

Braithwaite, R. J. and Zhang, Y. (2000). Sensitivity of mass balance of five Swiss glaciers to temperature changes assessed by tuning a degree-day model. *Journal of Glaciology*, 46(152):7–14.

Bury, J., Mark, B. G., Carey, M., Young, K. R., McKenzie, J. M., Baraer, M., French, A., and Polk, M. H. (2013). New geographies of water and climate change in Peru: Coupled natural and social transformations in the Santa River watershed. *Annals of the Association of American Geographers*, 103(2):363–374.

Casassa, G., Haeberli, W., Jones, G., Kaser, G., Ribstein, P., Rivera, A., and Schneider, C. (2007). Current status of Andean glaciers. *Global and Planetary Change*, 1(59):1–9.

Chiang, J. C. and Bitz, C. M. (2005). Influence of high latitude ice cover on the marine Intertropical Convergence Zone. *Climate Dynamics*, 25(5):477–496.

Cogley, J., Hock, R., Rasmussen, L., Arendt, A., Bauder, A., Braithwaite, R., Jansson, P., Kaser, G., Möller, M., Nicholson, L., et al. (2011). Glossary of glacier mass balance and related terms. *IHP-VII technical documents in hydrology*, 86:965.

Cuffey, K. M. and Paterson, W. S. B. (2010). *The Physics of Glaciers*. Academic Press.

Doughty, A. M., Anderson, B. M., Mackintosh, A. N., Kaplan, M. R., Vandergoes, M. J., Barrell, D. J., Denton, G. H., Schaefer, J. M., Chinn, T. J., and Putnam, A. E. (2013). Evaluation of lateglacial temperatures in the Southern Alps of New Zealand based on glacier modelling at Irishman Stream, Ben Ohau Range. *Quaternary Science Reviews*, 74:160–169.

Dyurgerov, M. B. and Meier, M. F. (2000). Twentieth century climate change: evidence from small glaciers. *Proceedings of the National Academy of Sciences*, 97(4):1406–1411.

Farinotti, D. (2013). On the effect of short-term climate variability on mountain glaciers: insights from a case study. *Journal of Glaciology*, 59(217):992–1006.

Favier, V., Wagnon, P., Chazarin, J.-P., Maisincho, L., and Coudrain, A. (2004a). One-year measurements of surface heat budget on the ablation zone of Antizana Glacier 15, Ecuadorian Andes. *Journal of Geophysical Research: Atmospheres*, 109(D18).

Favier, V., Wagnon, P., and Ribstein, P. (2004b). Glaciers of the outer and inner tropics: A different behaviour but a common response to climatic forcing. *Geophysical Research Letters*, 31(16).

Fernández, A. and Mark, B. G. (2016). Modeling modern glacier response to climate changes along the Andes Cordillera: A multiscale review. *Journal of Advances in Modeling Earth Systems*.

Fountain, A. G., Krimmel, R. M., and Trabant, D. C. (1997). A strategy for monitoring glaciers. *US Geological Survey Circular; 1132*.

Francou, B., Ribstein, P., Wagnon, P., Ramirez, E., and Pouyaud, B. (2005). Glaciers of the tropical Andes: indicators of global climate variability. In *Global change and mountain regions*, pages 197–204. Springer.

Francou, B., Vuille, M., Favier, V., and Cáceres, B. (2004). New evidence for an ENSO impact on low-latitude glaciers: Antizana 15, Andes of Ecuador, 0 28 S. *Journal of Geophysical Research: Atmospheres*, 109(D18).

Francou, B., Vuille, M., Wagnon, P., Mendoza, J., and Sicart, J.-E. (2003). Tropical climate change recorded by a glacier in the central Andes during the last decades of the twentieth century: Chacaltaya, Bolivia, 16 S. *Journal of Geophysical Research: Atmospheres*, 108(D5).

Fujita, K. (2008a). Effect of precipitation seasonality on climatic sensitivity of glacier mass balance. *Earth and Planetary Science Letters*, 276(1):14–19.

Fujita, K. (2008b). Influence of precipitation seasonality on glacier mass balance and its sensitivity to climate change. *Annals of Glaciology*, 48(1):88–92.

Gardner, A. S., Moholdt, G., Cogley, J. G., Wouters, B., Arendt, A. A., Wahr, J., Berthier, E., Hock, R., Pfeffer, W. T., Kaser, G., et al. (2013). A reconciled estimate of glacier contributions to sea level rise: 2003 to 2009. *science*, 340(6134):852–857.

Garreaud, R. (2009). The Andes climate and weather. *Advances in Geosciences*, 22:3.

Garreaud, R. D., Vuille, M., Compagnucci, R., and Marengo, J. (2009). Present-day South American climate. *Palaeogeography, Palaeoclimatology, Palaeoecology*, 281(3):180–195.

González-Rouco, J. F., Beltrami, H., Zorita, E., and Von Storch, H. (2006). Simulation and inversion of borehole temperature profiles in surrogate climates: Spatial distribution and surface coupling. *Geophysical Research Letters*, 33(1).

Goodman, A. Y., Rodbell, D. T., Seltzer, G. O., and Mark, B. G. (2001). Subdivision of glacial deposits in southeastern Peru based on pedogenic development and radiometric ages. *Quaternary Research*, 56(1):31–50.

Gurgiser, W., Marzeion, B., Nicholson, L., Ortner, M., and Kaser, G. (2013). Modeling energy and mass balance of Shallap Glacier, Peru. *The Cryosphere*, 7(6):1787.

Hanshaw, M. and Bookhagen, B. (2014). Glacial areas, lake areas, and snow lines from 1975 to 2012: status of the Cordillera Vilcanota, including the Quelccaya Ice Cap, northern central Andes, Peru. *The Cryosphere*, 8(2):359–376.

Hardy, D., Vuille, M., and Bradley, R. S. (2003). Variability of snow accumulation and isotopic composition on Nevado Sajama, Bolivia. *Journal of Geophysical Research: Atmospheres*, 108(D22).

Hardy, D. R., Vuille, M., Braun, C., Keimig, F., and Bradley, R. S. (1998). Annual and daily meteorological cycles at high altitude on a tropical mountain. *Bulletin of the American Meteorological Society*, 79(9):1899.

Harris, I., Jones, P., Osborn, T., and Lister, D. (2014). Updated high-resolution grids of monthly climatic observations–the CRU TS3.10 Dataset. *International Journal of Climatology*, 34(3):623–642.

Hastenrath, S. (1978). Heat-budget measurements on the Quelccaya Ice Cap, Peruvian Andes. *Journal of Glaciology*, 20(82):85–97.

Hastenrath, S. (1984). *The Glaciers of Equatorial East Africa*, volume 2. Springer Science & Business Media.

Hays, J., Imbrie, J., and Shackleton, N. (1976). Variations in the Earths Orbit: Pacemaker of the Ice Ages. *Science*, 194(4270):11211132.

He, F. (2011). *Simulating transient climate evolution of the last deglaciation with CCSM3*. PhD thesis, University of Wisconsin-Madison.

He, F., Shakun, J. D., Clark, P. U., Carlson, A. E., Liu, Z., Otto-Bliesner, B. L., and Kutzbach, J. E. (2013). Northern Hemisphere forcing of Southern Hemisphere climate during the last deglaciation. *Nature*, 494(7435):81–85.

Hock, R. (2005). Glacier melt: a review of processes and their modeling. *Progress in physical geography*, 29(3):362–391.

Hoffman, P. F., Kaufman, A. J., Halverson, G. P., and Schrag, D. P. (1998). A Neoproterozoic Snowball Earth. *Science*, 281(5381):1342–1346.

Huang, B., Banzon, V. F., Freeman, E., Lawrimore, J., Liu, W., Peterson, T. C., Smith, T. M., Thorne, P. W., Woodruff, S. D., and Zhang, H.-M. (2015). Extended reconstructed sea surface temperature version 4 (ERSST v4). Part I: Upgrades and intercomparisons. *Journal of climate*, 28(3):911–930.

Huber, U. M., Bugmann, H. K., and Reasoner, M. A. (2006). *Global Change and Mountain Regions: An Overview of Current Knowledge*, volume 23. Springer Science & Business Media.

Hüls, M. and Zahn, R. (2000). Millennial-scale sea surface temperature variability in the western tropical North Atlantic from planktonic foraminiferal census counts. *Paleoceanography*, 15(6):659–678.

Huybers, K. and Roe, G. H. (2009). Spatial patterns of glaciers in response to spatial patterns in regional climate. *Journal of Climate*, 22(17):4606–4620.

Imbrie, J. and Imbrie, K. P. (1986). *Ice Ages: Solving the Mystery*. Harvard University Press.

Jomelli, V., Favier, V., Rabatel, A., Brunstein, D., Hoffmann, G., and Francou, B. (2009). Fluctuations of glaciers in the tropical Andes over the last millennium and palaeoclimatic implications: A review. *Palaeogeography, Palaeoclimatology, Palaeoecology*, 281(3):269–282.

Jomelli, V., Favier, V., Vuille, M., Braucher, R., Martin, L., Blard, P.-H., Colose, C., Brunstein, D., He, F., Khodri, M., et al. (2014). A major advance of tropical Andean glaciers during the Antarctic Cold Reversal. *Nature*, 513(7517):224–228.

Jomelli, V., Khodri, M., Favier, V., Brunstein, D., Ledru, M.-P., Wagnon, P., Blard, P.-H., Sicart, J.-E., Braucher, R., Grancher, D., et al. (2011). Irregular tropical glacier retreat over the holocene epoch driven by progressive warming. *Nature*, 474(7350):196–199.

Kalnay, E., Kanamitsu, M., Kistler, R., Collins, W., Deaven, D., Gandin, L., Iredell, M., Saha, S., White, G., Woollen, J., et al. (1996). The NCEP/NCAR 40-year Reanalysis Project. *Bulletin of the American meteorological Society*, 77(3):437–471.

Kanamitsu, M., Ebisuzaki, W., Woollen, J., Yang, S.-K., Hnilo, J., Fiorino, M., and Potter, G. (2002). Ncepdoe amip-ii Reanalysis (R-2). *Bulletin of the American Meteorological Society*, 83(11):1631–1643.

Kaser, G. (1995). Some NOTES ON THE BEHAVIOUR OF TROPICAL GLACIERS. *Bull. Inst. fr. études andines*, 24(3):671–681.

Kaser, G. (1999). A review of the modern fluctuations of tropical glaciers. *Global and Planetary Change*, 22(1):93–103.

Kaser, G. (2001). Glacier-climate interaction at low latitudes. *Journal of Glaciology*, 47(157):195–204.

Kaser, G., Fountain, A., Jansson, P., et al. (2003). *A Manual For Monitoring The Mass Balance of Mountain Glaciers*. Unesco Paris.

Kaser, G., Georges, C., Juen, I., and Mölg, T. (2005). Low latitude glaciers: unique global climate indicators and essential contributors to regional fresh water supply. a conceptual approach. In *Global Change and Mountain Regions*, pages 185–195. Springer.

Kaser, G., Großhauser, M., and Marzeion, B. (2010). Contribution potential of glaciers to water availability in different climate regimes. *Proceedings of the National Academy of Sciences*, 107(47):20223–20227.

Kaser, G., Hardy, D. R., Mölg, T., Bradley, R. S., and Hyera, T. M. (2004). Modern glacier retreat on Kilimanjaro as evidence of climate change: observations and facts. *international Journal of Climatology*, 24(3):329–339.

Kaser, G., Hastenrath, S., and Ames, A. (1996). Mass balance profiles on tropical glaciers. *Zeitschrift für Gletscherkunde und Glazialgeologie*, 32:75–81.

Kaser, G. and Osmaston, H. (2002). *Tropical Glaciers*. Cambridge University Press.

Kelly, M. A., Lowell, T. V., Applegate, P. J., Phillips, F. M., Schaefer, J. M., Smith, C. A., Kim, H., Leonard, K. C., and Hudson, A. M. (2015). A locally calibrated, late glacial 10be production rate from a low-latitude, high-altitude site in the Peruvian Andes. *Quaternary Geochronology*, 26:70–85.

Kelly, M. A., Lowell, T. V., Applegate, P. J., Smith, C. A., Phillips, F. M., and Hudson, A. M. (2012). Late glacial fluctuations of Quelccaya Ice Cap, southeastern Peru. *Geology*, 40(11):991–994.

Konzelmann, T., van de Wal, R. S., Greuell, W., Bintanja, R., Henneken, E. A., and Abe-Ouchi, A. (1994). Parameterization of global and longwave incoming radiation for the Greenland Ice Sheet. *Global and Planetary change*, 9(1):143–164.

Kuhn, M. (1981). Climate and Glaciers. *International Association of Hydrological Sciences Publication*, 131:3–20.

Lea, D. W., Pak, D. K., Peterson, L. C., and Hughen, K. A. (2003). Synchroneity of tropical and high-latitude Atlantic temperatures over the last glacial termination. *Science*, 301(5638):1361–1364.

Leclercq, P. W. and Oerlemans, J. (2012). Global and hemispheric temperature reconstruction from glacier length fluctuations. *Climate Dynamics*, 38(5-6):1065–1079.

Licciardi, J. M., Schaefer, J. M., Taggart, J. R., and Lund, D. C. (2009). Holocene glacier fluctuations in the Peruvian Andes indicate northern climate linkages. *Science*, 325(5948):1677–1679.

Liniger, H., Weingartner, R., Grosjean, M., Kull, C., MacMillan, L., Messerli, B., Bisaz, A., and Lutz, U. (1998). *Mountains of the World: Water Towers for the 21st Century*. Mountain Agenda c/o Institute of geography University of Berne.

Liu, Z., Otto-Bliesner, B., He, F., Brady, E., Tomas, R., Clark, P., Carlson, A., Lynch-Stieglitz, J., Curry, W., Brook, E., et al. (2009). Transient simulation of last deglaciation with a new mechanism for Bølling-Allerød warming. *Science*, 325(5938):310–314.

Loomis, S. E., Russell, J. M., Verschuren, D., Morrill, C., De Cort, G., Damsté, J. S. S., Olago, D., Eggermont, H., Street-Perrott, F. A., and Kelly, M. A. (2017). The tropical lapse rate steepened during the Last Glacial Maximum. *Science Advances*, 3(1):e1600815.

López-Moreno, J. I., Fontaneda, S., Bazo, J., Revuelto, J., Azorin-Molina, C., Valero-Garcés, B., Morán-Tejeda, E., Vicente-Serrano, S. M., Zubieta, R., and Alejo-Cochachín, J. (2014). Recent glacier retreat and climate trends in Cordillera Huaytapallana, Peru. *Global and Planetary Change*, 112:1–11.

Malone, A. G., Pierrehumbert, R. T., Lowell, T. V., Kelly, M. A., and Stroup, J. S. (2015). Constraints on southern hemisphere tropical climate change during the Little Ice Age and Younger Dryas based on glacier modeling of the Quelccaya Ice Cap, Peru. *Quaternary Science Reviews*, 125:106–116.

Manciati, C., Villacís, M., Taupin, J.-D., Cadier, E., Galárraga-Sánchez, R., and Cáceres, B. (2014). Empirical mass balance modeling of South American tropical glaciers: case study of Antisana volcano, Ecuador. *Hydrological Sciences Journal*, 59(8):1519–1535.

Mann, M. E., Zhang, Z., Rutherford, S., Bradley, R. S., Hughes, M. K., Shindell, D., Ammann, C., Faluvegi, G., and Ni, F. (2009). Global signatures and dynamical origins of the Little Ice Age and Medieval Climate Anomaly. *Science*, 326(5957):1256–1260.

Mark, B. G., McKenzie, J. M., and Gomez, J. (2005). Hydrochemical evaluation of changing glacier meltwater contribution to stream discharge: Callejon de Huaylas, Peru. *Hydrological Sciences Journal*, 50(6).

Mark, B. G., Seltzer, G. O., Rodbell, D. T., and Goodman, A. Y. (2002). Rates of deglaciation during the Last Glaciation and Holocene in the Cordillera Vilcanota-Quelccaya Ice Cap region, southeastern Peru. *Quaternary Research*, 57(3):287–298.

Masson-Delmotte, V., Schulz, M., Abe-Ouchi, A., Beer, J., Ganopolski, A., Gonzalez Rouco, J., Jansen, E., Lambeck, K., Luterbacher, J., Naish, T., Osborn, T., Otto-Bliesner, B., Quinn, T., Ramesh, R., Rojas, M., Shao, X., and Timmermann, A. (2013). *Information from Paleoclimate Archives*, book section 5, page 383464. Cambridge University Press, Cambridge, United Kingdom and New York, NY, USA.

Maussion, F., Gurgiser, W., Großhauser, M., Kaser, G., and Marzeion, B. (2015). Enso influence on surface energy and mass balance at Shallap Glacier, Cordillera Blanca, Peru. *The Cryosphere*, 9(4):1663–1683.

Medwedeff, W. G. and Roe, G. H. (2016). Trends and variability in the global dataset of glacier mass balance. *Climate Dynamics*, pages 1–13.

Meier, M. F. (1984). Contribution of small glaciers to global sea level. *Science*, 226:1418–1422.

Meier, M. F. and Tangborn, W. V. (1965). Net budget and flow of South Cascade Glacier, Washington. *Journal of Glaciology*, 5(41):547–566.

Mercer, J. and Palacios, O. (1977). Radiocarbon dating of the Last Glaciation in Peru. *Geology*, 5(10):600–604.

Mercer, J. H., Thompson, L. G., Marangunic, C., and Ricker, J. (1975). Peru's Quelccaya Ice Cap: glaciological and glacial geological studies, 1974. *Antarctic Journal of the United States*, 10(1):19–24.

Milankovič, M. (1998). *Canon of Insolation And The Ice-Age Problem*. Zavod za udžbenike i nastavna sredstva.

Mölg, T., Cullen, N. J., Hardy, D. R., Kaser, G., and Klok, L. (2008). Mass balance of a slope glacier on Kilimanjaro and its sensitivity to climate. *International Journal of Climatology*, 28(7):881–892.

Mölg, T. and Hardy, D. R. (2004). Ablation and associated energy balance of a horizontal glacier surface on Kilimanjaro. *Journal of Geophysical Research: Atmospheres*, 109(D16).

Oerlemans, J. (1986). An attempt to simulate historic front variations of Nigardsbreen, Norway. *Theoretical and Applied Climatology*, 37(3):126–135.

Oerlemans, J. (1997a). Climate sensitivity of Franz Josef Glacier, New Zealand, as revealed by numerical modeling. *Arctic and Alpine Research*, pages 233–239.

Oerlemans, J. (1997b). A flowline model for Nigardsbreen, Norway: projection of future glacier length based on dynamic calibration with the historic record. *Journal of glaciology*, 24:382–389.

Oerlemans, J. (2000). Holocene glacier fluctuations: is the current rate of retreat exceptional? *Annals of Glaciology*, 31(1):39–44.

Oerlemans, J. (2001). *Glaciers and Climate Change*. CRC Press.

Oerlemans, J. (2005). Extracting a climate signal from 169 glacier records. *Science*, 308(5722):675–677.

Oerlemans, J. and Fortuin, J. (1992). Sensitivity of Glaciers and Small Ice Caps to Greenhouse Warming. *Science*, 258(5079):115–117.

Oerlemans, J. and Hoogendoorn, N. (1989). Mass-balance gradients and climatic change. *Journal of Glaciology*, 35(121):399–405.

Oerlemans, J. and Knap, W. (1998). A 1 year record of global radiation and albedo in the ablation zone of Morteratschgletscher, Switzerland. *Journal of Glaciology*, 44(147):231–238.

Ohmura, A. (2001). Physical basis for the temperature-based melt-index method. *Journal of applied Meteorology*, 40(4):753–761.

Pachauri, R., Allen, M., Barros, V., Broome, J., Cramer, W., Christ, R., Church, J., Clarke, L., Dahe, Q., Dasgupta, P., Dubash, N., Edenhofer, O., Elgizouli, I., Field, C., Foster, P., Priedlingstein, P., Fuglestvedt, J., Gomez-Echeverri, L., Hallegatte, S., Hegerl, G., Howden, M., Jiang, K., Cisneros, B., Kattsov, V., Lee, H., Mach, K., Marotzke, J., Mastrandrea, M., Meyer, L., Minx, J., Mulugetta, Y., OBrien, K., Oppenheimer, M., J., P., Pichs-Madruga, R., Plattner, G., Portner, H., Power, S., Preston, B., Ravindranath, N., Reisinger, A., Riahi, K., Rusticucci, M., Scholes, R., Seyboth, K., Sokona, Y., Stavins, R., Stocker, T., Tschakert, P., van Vuuren, D., and van Ypersele, J. (2015). *Future Climate Change, Risk and Impacts*, book section 2, page 5673. Cambridge University Press, Cambridge, United Kingdom and New York, NY, USA.

Pepin, N., Bradley, R., Diaz, H., Baraer, M., Caceres, E., Forsythe, N., Fowler, H., Greenwood, G., Hashmi, M., Liu, X., et al. (2015). Elevation-dependent warming in mountain regions of the world. *Nature climate change*, 5(5):424–430.

Pfeffer, W. T., Arendt, A. A., Bliss, A., Bolch, T., Cogley, J. G., Gardner, A. S., Hagen, J.-O., Hock, R., Kaser, G., Kienholz, C., et al. (2014). The Randolph Glacier Inventory: A globally complete inventory of glaciers. *Journal of Glaciology*, 60(221):537–552.

Pierrehumbert, R., Abbot, D., Voigt, A., and Koll, D. (2011). Climate of the Neoproterozoic. *Annual Review of Earth and Planetary Sciences*, 39:417–460.

Pierrehumbert, R. T. (1995). Thermostats, Radiator Fins, and the Local Runaway Greenhouse. *Journal of the atmospheric sciences*, 52(10):1784–1806.

Pierrehumbert, R. T. (1999). Huascaran δ18o as an indicator of tropical climate during the last glacial maximum. *Geophysical Research Letters*, 26(9):1345–1348.

Placzek, C., Quade, J., and Patchett, P. J. (2006). Geochronology and stratigraphy of late Pleistocene lake cycles on the southern Bolivian Altiplano: Implications for causes of tropical climate change. *Geological Society of America Bulletin*, 118(5-6):515–532.

Rabatel, A., Bermejo, A., Loarte, E., Soruco, A., Gomez, J., Leonardini, G., Vincent, C., and Sicart, J. E. (2012). Can the snowline be used as an indicator of the equilibrium line and mass balance for glaciers in the outer tropics? *Journal of Glaciology*, 58(212):1027–1036.

Rabatel, A., Francou, B., Jomelli, V., Naveau, P., and Grancher, D. (2008). A chronology of the Little Ice Age in the tropical Andes of Bolivia (16 s) and its implications for climate reconstruction. *Quaternary Research*, 70(2):198–212.

Rabatel, A., Francou, B., Soruco, A., Gomez, J., Cáceres, B., Ceballos, J., Basantes, R., Vuille, M., Sicart, J.-E., Huggel, C., et al. (2013). Current state of glaciers in the tropical Andes: A multi-century perspective on glacier evolution and climate change. *The Cryosphere*, 7(1):81.

Réveillet, M., Rabatel, A., Gillet-Chaulet, F., and Soruco, A. (2015). Simulations of changes to Glacier Zongo, Bolivia (16 s), over the 21st century using a 3-d full-Stokes model and CMIP5 climate projections. *Annals of Glaciology*, 56(70):89–97.

Rind, D. and Peteet, D. (1985). Terrestrial conditions at the last glacial maximum and CLIMAP sea-surface temperature estimates: Are they consistent? *Quaternary Research*, 24(1):1–22.

Roe, G. H. (2011). What do glaciers tell us about climate variability and climate change? *Journal of Glaciology*, 57(203):567–578.

Roe, G. H. and Baker, M. B. (2014). Glacier response to climate perturbations: An accurate linear geometric model. *Journal of Glaciology*, 60(222):670–684.

Roe, G. H. and O'Neal, M. A. (2009). The response of glaciers to intrinsic climate variability: observations and models of late-Holocene variations in the Pacific Northwest. *Journal of Glaciology*, 55(193):839–854.

Rupper, S. and Roe, G. (2008). Glacier changes and regional climate: A mass and energy balance approach. *Journal of Climate*, 21(20):5384–5401.

Rupper, S., Roe, G., and Gillespie, A. (2009). Spatial patterns of Holocene glacier advance and retreat in Central Asia. *Quaternary Research*, 72(3):337–346.

Sagredo, E. and Lowell, T. (2012). Climatology of Andean glaciers: A framework to understand glacier response to climate change. *Global and Planetary Change*, 86:101–109.

Sagredo, E. A., Rupper, S., and Lowell, T. V. (2014). Sensitivities of the equilibrium line altitude to temperature and precipitation changes along the Andes. *Quaternary Research*, 81(2):355–366.

Schmidt, G. A. (2010). Enhancing the relevance of palaeoclimate model/data comparisons for assessments of future climate change. *Journal of Quaternary Science*, 25(1):79–87.

Seager, R. and Battisti, D. S. (2007). Challenges to our understanding of the general circulation: Abrupt climate change. *Global Circulation of the Atmosphere*, pages 331–371.

Seidel, D. J. and Free, M. (2003). Comparison of lower-tropospheric temperature climatologies and trends at low and high elevation radiosonde sites. In *Climate Variability and Change in High Elevation Regions: Past, Present & Future*, pages 53–74. Springer.

Sicart, J. E., Hock, R., Ribstein, P., and Chazarin, J. P. (2010). Sky longwave radiation on tropical Andean glaciers: Parameterization and sensitivity to atmospheric variables. *Journal of Glaciology*, 56(199):854–860.

Sicart, J. E., Hock, R., Ribstein, P., Litt, M., and Ramirez, E. (2011). Analysis of seasonal variations in mass balance and meltwater discharge of the tropical Zongo Glacier by application of a distributed energy balance model. *Journal of Geophysical Research: Atmospheres*, 116(D13).

Sicart, J. E., Hock, R., and Six, D. (2008). Glacier melt, air temperature, and energy balance in different climates: The Bolivian Tropics, the French Alps, and northern Sweden. *Journal of Geophysical Research: Atmospheres*, 113(D24).

Sicart, J. E., Wagnon, P., and Ribstein, P. (2005). Atmospheric controls of the heat balance of Zongo Glacier (16 s, Bolivia). *Journal of Geophysical Research: Atmospheres*, 110(D12).

Smith, C. A., Lowell, T. V., and Caffee, M. W. (2009). Lateglacial and holocene cosmogenic surface exposure age glacial chronology and geomorphological evidence for the presence of cold-based glaciers at Nevado Sajama, Bolivia. *Journal of Quaternary Science*, 24(4):360–372.

Sobel, A. H., Nilsson, J., and Polvani, L. M. (2001). The weak temperature gradient approximation and balanced tropical moisture waves. *Journal of the atmospheric sciences*, 58(23):3650–3665.

Soruco, A., Vincent, C., Rabatel, A., Francou, B., Thibert, E., Sicart, J. E., and Condom, T. (2015). Contribution of glacier runoff to water resources of La Paz City, Bolivia (16 S). *Annals of Glaciology*, 56(70):147–154.

Stansell, N. D., Polissar, P. J., and Abbott, M. B. (2007). Last Glacial Maximum equilibrium-line altitude and paleo-temperature reconstructions for the Cordillera de mérida, Venezuelan Andes. *Quaternary Research*, 67(1):115–127.

Stroup, J. S., Kelly, M. A., Lowell, T. V., Applegate, P. J., and Howley, J. A. (2014). Late holocene fluctuations of Qori Kalis outlet glacier, Quelccaya Ice Cap, Peruvian Andes. *Geology*, 42(4):347–350.

Sumner, D., Kirschvink, J., and Runnegar, B. (1987). Soft-sediment paleomagnetic fold tests of late Precambrian glaciogenic sediments. *Eos*, 68(1251):1251.

Taylor, R. G., Mileham, L., Tindimugaya, C., Majugu, A., Muwanga, A., and Nakileza, B. (2006). Recent glacial recession in the Rwenzori Mountains of East Africa due to rising air temperature. *Geophysical Research Letters*, 33(10).

Thompson, L., Mosley-Thompson, E., Davis, M., Zagorodnov, V., Howat, I., Mikhalenko, V., and Lin, P.-N. (2013). Annually resolved ice core records of tropical climate variability over the past˜ 1800 years. *Science*, 340(6135):945–950.

Thompson, L. G. (1980). Glaciological investigations of the tropical Quelccaya Ice Cap, Peru. *Journal of Glaciology*, 25(91):69–84.

Thompson, L. G. (2000). Ice core evidence for climate change in the Tropics: Implications for our future. *Quaternary Science Reviews*, 19(1):19–35.

Thompson, L. G., Davis, M. E., Mosley-Thompson, E., Sowers, T., Henderson, K. A., Zagorodnov, V. S., Lin, P.-N., Mikhalenko, V. N., Campen, R. K., Bolzan, J. F., et al. (1998). A 25,000-year tropical climate history from Bolivian ice cores. *Science*, 282(5395):1858–1864.

Thompson, L. G., Mosley-Thompson, E., Brecher, H., Davis, M., León, B., Les, D., Lin, P.-N., Mashiotta, T., and Mountain, K. (2006). Abrupt tropical climate change: Past and present. *Proceedings of the National Academy of Sciences*, 103(28):10536–10543.

Thompson, L. G., Mosley-Thompson, E., Dansgaard, W., and Grootes, P. M. (1986). The Little Ice Age as Recorded in the Stratigraphy of the Tropical Quelccaya Ice Cap. *Science*, 234(4774):361–365.

Thompson, L. G., Mosley-Thompson, E., Davis, M. E., and Brecher, H. H. (2011). Tropical glaciers, recorders and indicators of climate change, are disappearing globally. *Annals of Glaciology*, 52(59):23–34.

Tripati, A. K., Sahany, S., Pittman, D., Eagle, R. A., Neelin, J. D., Mitchell, J. L., and Beaufort, L. (2014). Modern and glacial tropical snowlines controlled by sea surface temperature and atmospheric mixing. *Nature Geoscience*, 7(3):205–209.

Vacco, D. A., Alley, R. B., and Pollard, D. (2009). Modeling dependence of moraine deposition on climate history: the effect of seasonality. *Quaternary Science Reviews*, 28(7):639–646.

Vaughan, D., Comiso, J., Allison, I., Carrasco, J., Kaser, G., Kwok, R., Mote, P., Murray, T., Paul, F., Ren, J., Rignot, E., Solomina, O., Steffen, K., and Zhang, T. (2013). *Observations: Cryosphere*, book section 4, pages 317–382. Cambridge University Press, Cambridge, United Kingdom and New York, NY, USA.

Viviroli, D., Dürr, H. H., Messerli, B., Meybeck, M., and Weingartner, R. (2007). Mountains of the world, water towers for humanity: Typology, mapping, and global significance. *Water resources research*, 43(7).

Vuille, M., Bradley, R. S., Werner, M., and Keimig, F. (2003). 20th century climate change in the tropical Andes: observations and model results. In *Climate variability and change in high elevation regions: past, present & future*, pages 75–99. Springer.

Vuille, M., Francou, B., Wagnon, P., Juen, I., Kaser, G., Mark, B. G., and Bradley, R. S. (2008a). Climate change and tropical Andean glaciers: Past, present and future. *Earth-science reviews*, 89(3):79–96.

Vuille, M., Hardy, D. R., Braun, C., Keimig, F., and Bradley, R. S. (1998). Atmospheric circulation anomalies associated with 1996/1997 summer precipitation events on Sajama Ice Cap, Bolivia. *Journal of Geophysical Research: Atmospheres*, 103(D10):11191–11204.

Vuille, M., Kaser, G., and Juen, I. (2008b). Glacier mass balance variability in the Cordillera Blanca, Peru and its relationship with climate and the large-scale circulation. *Global and Planetary Change*, 62(1):14–28.

Waelbroeck, C., Paul, A., Kucera, M., Rosell-Melé, A., Weinelt, M., Schneider, R., Mix, A. C., Abelmann, A., Armand, L., Bard, E., et al. (2009). Constraints on the magnitude and patterns of ocean cooling at the Last Glacial Maximum. *Nature Geoscience*, 2(2):127–132.

Wagnon, P., Ribstein, P., Francou, B., and Pouyaud, B. (1999). Annual cycle of energy balance of Zongo Glacier, Cordillera Real, Bolivia. *Journal of Geophysical Research: Atmospheres*, 104(D4):3907–3923.

Wagnon, P., Ribstein, P., Francou, B., and Sicart, J.-E. (2001). Anomalous heat and mass budget of Glacier Zongo, Bolivia, during the 1997/98 El Niño year. *Journal of Glaciology*, 47(156):21–28.

Wan, X., Chang, P., Saravanan, R., Zhang, R., and Schmidt, M. W. (2009). On the interpretation of Caribbean paleo-temperature reconstructions during the Younger Dryas. *Geophysical Research Letters*, 36(2).

Williams, I. N., Pierrehumbert, R. T., and Huber, M. (2009). Global warming, convective threshold and false thermostats. *Geophysical Research Letters*, 36(21).

Xu, K.-m. and Emanuel, K. A. (1989). Is the tropical atmosphere conditionally unstable? *Monthly Weather Review*, 117(7):1471–1479.

Zorita, E., Von Storch, H., Gonzalez-Rouco, F. J., Cubasch, U., Luterbacher, J., Legutke, S., Fischer-Bruns, I., and Schlese, U. (2004). Climate evolution in the last five centuries simulated by an atmosphere-ocean model: Global temperatures, the North Atlantic Oscillation and the Late Maunder Minimum. *Meteorologische Zeitschrift*, 13(4):271–289.